REPORT

FLOOD PROTECTION AT BRIDGE CROSSINGS

by

D.B. Simons and G.L. Lewis

Prepared for

Wyoming State Highway Department
Planning and Research Division

in cooperation with the

U.S. Department of Transportation
Federal Highway Administration
Bureau of Public Roads

1971

CER71-72DBS-GLL10

AUTHORIZATION OF PROJECT

The problems to be investigated were formulated by the staff of the State Highway Commission of Wyoming in consultation with personnel of Colorado State University and the Federal Highway Administration. The project was initiated by the signing of the agreement "Engineering Investigation Pertaining to Flood Protection of Bridges and Culverts," dated February 16, 1966. This agreement was modified in an addendum to the agreement dated October 8, 1969.

DISCLAIMER

The opinions, findings, and conclusions in this publication are those of the authors and not necessarily those of the State Highway Commission of Wyoming or the Federal Highway Administration.

ABSTRACT

FLOOD PROTECTION AT BRIDGE CROSSINGS

Techniques for the design of stable rock-riprap protection in the vicinity of bridge crossings are presented. Hydraulic properties of the crossings are computed from methods derived in other sources, and the properties are related to particle sizes for riprap protection of abutments and piers.

Design steps for prototype bridge crossings are enumerated so that the hydraulic engineer may use this report as a design manual. An example of the design of protection for a prototype bridge crossing is included to clarify the suggested design procedures.

Riprap-protected spill-through abutments were constructed in the hydraulic facilities at Colorado State University in order to test the validity of the suggested design procedures.

TABLE OF CONTENTS

TABLE OF CONTENTS (Continued)

NOTATION

SYMBOL	DEFINITION	UNITS
a	Half width or radius of a pier	ft
A	Cross-sectional area	sq ft
A_{2c}	Critical flow area at section 2	sq ft
A_c	Area at critical flow	sq ft
A_i	Flow area at section i	sq ft
A_n	Unconstricted flow area	sq ft
A_{ni}	Flow area at section i below normal stage	sq ft
A_s	Area of scour in the constriction	sq ft
b	Width of constriction	ft
b'	Top-width between spill-through abutments	ft
b_n	Net width of waterway excluding piers	ft
b_p	Width of pier on a normal to the flow	ft
b_r	Base width of trapezoid	ft
b_s	Distance between skewed abutments	ft
b_{tc}	Top width of flow between abutments at h_{2c}	ft
B	Top width of unconstricted channel	ft
C	Correction factor for backwater with scour	--
C_b	Critical flow base backwater coefficient	--
C_c	Contraction coefficient	--
C_d	Coefficient of discharge	--
d_i	Sieve size for which i(%) passes	ft or in
d_m	Effective diameter of rock mixture	ft or in
d_{se}	Equilibrium scour depth below bed	ft
D	Depth of flow	ft

NOTATION (Continued)

SYMBOL	DEFINITION	UNITS
D_b	Differential level ratio	--
ΔD_e	Differential level ratio increment-eccentricity	--
ΔD_s	Differential level ratio increment-skew	--
D_s	Mean bed particle diameter	ft
e	Eccentricity of a bridge crossing	--
e	Riprap void ratio	--
F	Fetch length	ft
F_e	Effective fetch length	ft
G	Specific weight of riprap	--
g	Acceleration of gravity	ft/sec^2
h	Height of model above flood plain	ft
Δh	Total water surface drop through bridge	ft
h_A	Depth of flow at the abutment at section 2	ft
h_b*	Backwater at normal crossing with no piers	ft
h_{bA}*	Backwater for abnormal flow excluding piers	ft
h_d*	Backwater for dual bridges	ft
h_i	Flow depth at section i	ft
h_{ic}	Critical depth at section i	ft
h_{L1-3}	Energy losses between section 1 and 3	ft
Δh_m	Measured value of Δh	ft
h_n	Normal stage at design discharge	ft
h_{nc}	Critical depth in unconstricted channel	ft
$\overline{h}_{n2}$	Depth in constriction below normal stage	ft
h_s	Safety factor for freeboard	ft
Δh_s	Value of Δh with scour	ft

NOTATION (Continued)

SYMBOL	DEFINITION	UNITS
Δh_t	Theoretical value of Δh	ft
h_u	Flow depth at section 1 for girders in flow	ft
h_u^*	Backwater for girders in the flow	ft
h_1^*	Backwater at normal crossing including piers	ft
h_{1A}^*	Backwater for abnormal stage-discharge	ft
h_{1s}^*	Backwater with scour	ft
h_3^*	Normal depth less the depth at section 3	ft
h_{3A}^*	Difference of abnormal stage and depth at section 3	ft
h_{3B}^*	Difference of normal and section 3 depths for dual bridges	ft
h_{3s}^*	Difference of normal and section 3 depths with scour	ft
H	Wave height	ft
i	Seepage hydraulic gradient	--
K	Conveyance	--
K*	Total backwater coefficient	--
K_b	Backwater coefficient for normal crossing	--
ΔK_e	Incremental backwater coefficient-eccentricity	--
ΔK_p	Incremental backwater coefficient-piers	--
ΔK_s	Incremental backwater coefficient-skew	--
L	Length of embankment requiring protection	ft
L_{1-3}	Distance between section 1 and section 3	ft
L_D	Distance between dual bridges	ft
L_e	Effective approach embankment length	ft
L*	Distance to maximum backwater	ft

NOTATION (Continued)

SYMBOL	DEFINITION	UNITS
L_w	Wave length	ft
m	Side-slope run for a unit rise	--
M	Discharge opening ratio	--
M'	Geometric opening ratio	--
n	Manning's roughness coefficient	--
Q	Discharge	cfs
Q_b	Discharge in the width b	cfs
Q_f	Failure discharge	cfs
r	Abutment nose radius	ft
R	Hydraulic radius	ft
$\overline{R}$	Pier Reynolds Number	--
S	Riprap safety factor	--
S_s	Specific gravity of sediment	--
S_m	Maximum riprap safety factor	--
S_o	Slope of channel bed	--
t	Riprap layer thickness	ft or in
u_r	Bed velocity at one rock diameter	fps
V	Velocity	fps
$\overline{V}$	Average velocity	fps
V_d	Design velocity at vena contracta	fps
V_t	Depth averaged velocity at abutment toe	fps
V_n	Average unconstricted velocity	fps
V_{n2}	Average velocity in area A_{n2}	fps
V_w	Wind velocity	fps

NOTATION (Continued)

SYMBOL	DEFINITION	UNITS
V_{wm}	Additional bottom velocity due to waves	fps
V_i	Average velocity at section i	fps
V_{2c}	Critical velocity at section 2	fps
W	Roadway width at top of abutment	ft
W_F	Fetch width	ft
W_s	Stone weight resistant to waves	lb
α, θ	Side slope angle with horizontal	deg
α_i	Velocity head correction coefficient	--
β	Angle of particle movement	deg
γ	Specific weight	lb/ft^3
δ	Angle relating β and λ	deg
η	Stability factor	--
ε	Seepage force parameter	--
θ	Abutment skew angle	deg
λ	Velocity vector angle	deg
ν	Kinematic fluid viscosity	ft^2/sec
ρ	Mass density	$lb\text{-}sec^2/ft^4$
τ	Shear stress	lb/ft^2
ϕ	Angle of repose of riprap	deg

LIST OF FIGURES

LIST OF FIGURES (Continued)

LIST OF FIGURES (Continued)

LIST OF TABLES

Chapter I

INTRODUCTION

In order to supplement the current knowledge of protection from scour at bridge crossings and other hydraulic structures, the State Highway Commission of Wyoming, in conjunction with the U.S. Federal Highway Adminstration, initiated a program of research involving the design and performance of channel stabilization techniques. The original agreement for "Engineering Investigation Pertaining to Flood Protection of Bridges and Culverts" was accepted by personnel of Colorado State University on February 16, 1966.

The agreement specified three phases of investigation including the stabilization of culvert outlets, the stabilization of bridge crossings, and the study of alternative methods and techniques of stablization when gravel or rock-riprap are not available, or where special problems arise.

Due to a later need for more extensive studies of the first two phases, the third phase was cancelled in an addendum to the original agreement on October 8, 1969, and the funds allocated for this phase were re-allocated to the first two phases. This report finalizes the second phase of the Colorado State University study.

Scope

Channel stabilization in the vicinity of bridge crossings must be designed from a knowledge of the relationships between stability of protection forms and the hydraulic properties of the crossings. Most of the research for this phase of the study involved the development of design methods for the stabilization of bridge crossings with known

or predictable hydraulic properties. A survey of the pertinent literature revealed that other investigators have defined the expected hydraulic and scour characteristics of bridge crossings. This report supplements the work of others with design techniques for protection from increased backwater and extreme flow velocities at bridge constrictions.

Application

The proposed design procedure was developed using backwater and scour information obtained from a review of the literature. Hydraulic data from model and prototype bridge crossings were found for most common bridge crossings, and the design techniques should be applicable for all these cases.

The laboratory portion of this study was comprised of tests of the proposed design methods. Verification of the design for the tested models does not imply verification for prototype crossings, and the design may be used only with engineering judgment to produce theoretically stable bridge crossings.

Protection of Bridge Crossings

Flood protection requirements vary from one bridge to another. Some bridges may need to allow the passage of livestock and farm equipment beneath the deck during periods of low flow. Others may require low embankments due to aesthetic considerations, especially in populated areas. Still other bridges may require short spans with long approaches and numerous piers for economic reasons. Labor costs and availability of protection materials vary from region to region.

All of these factors and many more contribute to the difficulty in generalizing stabilization techniques for all bridge crossings.

A classification of bridge crossings based on prominent features would help to alleviate this difficulty. Classifying the regions requiring protection of each crossing, the possible types of protection, the possible flow conditions, the possible channel shapes, the possible abutment types, and the various geometric conditions for crossings will aid the engineer in selecting the correct design for the conditions he has encountered.

Regions of Required Protection

Bridge crossings generally include earth-fill approach embankments terminated by earth-fill or concrete abutments. These structures reduce the initial cost of the bridge by shortening the reinforced concrete or steel superstructure that must span the low-flow channel between the abutments. Regions of required protection for this type of crossing not only include pier footings and the embankment and abutment slopes and toes, but also the downstream channel which is subjected to the high velocity jet from the constriction. Downstream slopes of embankments for perennial streams must also be protected from wave forces due to wind. In semi-arid regions, wave protection is required only if winds are expected during the design flood.

Types of Protection

The region near approach embankments and abutments may be protected in several ways. One method is to armor the possible scour surfaces with a more resistant material. Protection may also be accomplished by diverting the attacking water away from the abutment, or by reducing

flow velocities with retards, jetties, vegetation, spur dikes, or any other means of slowing or diverting the flood waters.

Another protection consideration includes "fuse-plug" designs which allow the loss of a section of the approach embankment during floods. The replacement of the plug takes only a few days, and the expenditures are minor compared to the cost of replacing the bridge superstructure. Relief bridges, or secondary bridges spanning portions of the flood plains, accomplish this same purpose.

Another protection possibility is the "sagged-roadway design" which uses the construction of approach roadways at grade on the flood plains, with the bridge spanning the low water channel. This allows the flood waters to pass over the roadway, but the roadway will occasionally be inundated leaving the bridge standing in the flow with interruptions in traffic. Hazardous vertical curves may also be present with this design.

These alternative designs are only mentioned herein, and more thorough discussions are given by Posey (61), Bradley (12), Laursen (48), and the State of California (16).

Armoring a surface with more resistant materials involves several possible types of protection which must also be classified and considered in each design. The designs herein are based only on the use of loose rock riprap placed by conventional means. Other forms such as sacked concrete, pneumatically applied concrete mortar, grouted rock, asphalt paving, concrete slabs, broken concrete, precast concrete blocks, rock and wire mattresses, rock and wire sausages, willow mattresses, tetrapods, sheet piles, or even sea-shells, have been successfully used and should not be excluded from economic

consideration, especially in areas where rock riprap is scarce. Design methods and construction techniques for all of these forms of protection have been published by private and governmental agencies such as "Shore Protection Planning and Design," by the Corps of Engineers (80), "Bank and Shore Protection in California Highway Practice," by the State of California (16), and "Use of Riprap For Bank Protection," by the Bureau of Public Roads (69).

Rock riprap for channel stabilization has several advantages over other forms whenever it is available. The State of California lists the advantages as:

1. It is flexible and is therefore not weakened by slight movements of the settling embankments.

2. Local damage is easily repaired.

3. Construction involving its use is not complicated by special equipment.

4. The appearance is natural and adds to the aesthetics of the design.

5. Vegetation will grow through the voids and increase the structural strength with time.

6. The thickness can be varied to provide more protection in critical zones.

7. Wave runup on sloping surfaces is less (as much as 70 percent) than the runup on smooth surfaces.

8. It may be stockpiled and re-used.

9. It is usually the most economical whenever stones of sufficient size and quantity are available.

Flow Conditions

Five possible types of flow conditions at bridge crossings based on non-scouring or equilibrium scour conditions are shown in Figure 1. They include:

(a) Subcritical - the flow depth remains above critical depth upstream, through, and downstream of the crossing.

(b) Critical flow in the gap - the flow depth passes from subcritical to supercritical depth in the gap and returns to subcritical flow downstream. Critical depth in the gap is greater than critical depth for the downstream reach.

(c) Critical - the flow depth passes from subcritical to supercritical depth in the gap and continues below critical depth downstream of the crossing. A hydraulic jump then forms downstream if the resistance or some control in that reach returns the depth to normal, subcritical flow conditions.

(d) Supercritical - the flow upstream, through, and downstream of the crossing remains below critical depth at every section. The slope is classified as steep because normal depth is below critical. This condition may occur in mountain streams.

(e) Abnormal - due to some downstream control, the flow must return to a depth greater than normal.

Channel Shapes

Classification by channel shape includes the two categories shown in Figure 3. These are as follows:

(a) Wide-channel flow - the flow channel is relatively wide with no flood plain, and the flow depth remains relatively constant across the channel.

(b) Overbank flow - the channel has a wide flood plain with a central low-flow channel.

Abutment Types

Types of abutments common in prototype crossings are shown in Figure 2 and include:

(a) Vertical wall - the embankment sides and abutment nose are vertical retaining walls.

(b) Vertical wall with sloping embankments - the embankment sides are sloped, and the abutment nose is a vertical retaining wall.

(c) Spill-through - the embankment sides and abutment nose are sloped with circular or other sloping transitions between them.

(d) Wing-wall - the embankment sides are sloped, and the abutment nose is vertical with vertical wing-walls forming the transition between the sides and the nose.

Geometric Properties

Geometric properties of bridge crossings are more difficult to classify than the flow conditions, channel shapes, and abutment types. Any of the geometric properties illustrated in Figure 3 may be used depending on the conditions at the proposed site. The approaches may be skewed or normal (perpendicular) to the direction of flow, or one approach may be longer than the other, producing an eccentric crossing. Abutments used for the overbank-flow case may be set back from the low-flow channel banks to allow passage of livestock and machinery, or the abutments may extend up to the banks or even protrude over the banks, constricting the low-flow channel. Piers, dual bridges for

multi-lane freeways, channel bed conditions, and spur dikes add to the list of geometric classifications.

In the past, geometric factors have been treated with solutions for some basic or standard crossing, with additive or multiplicative coefficients for geometric variations. The coefficients have been derived from laboratory and field observations of bridge crossings, and corrections are made for the effects of skewness, eccentricity, scour, abutment setback, channel shape, submergence of the superstructure, debris, spur dikes, wind waves, ice, piers, abutment types, and flow conditions. The design procedures presented herein take advantage of the large volume of work, using the above technique, that has been done by others in describing the scour characteristics and hydraulics of bridge crossings.

Chapter II

DERIVATION OF DESIGN CRITERIA

The design presented in this chapter is derived from predictable hydraulic and scour properties of bridge crossings. The crossing geometric variables and flow conditions before the bridge constriction are used to predict the backwater produced by the crossing at design discharge. A maximum expected design velocity is derived from the knowledge of the backwater and the turbulent fluctuations in the flow field. Values of the velocity at critical points in the flow field are related to the design velocity, and a technique for relating velocity and depth to stable rock size and gradation is presented.

Verification of the design of rock riprap for the protection of spill-slopes on spill-through abutments is presented in Chapter IV. The research for this investigation, as stated in Chapter I, was concerned mainly with the verification of the design procedures. The development of the design procedures is based on engineering fundamentals and data presented by other investigators.

A team of investigators was involved with the research for this report. Contributions made by Simons, Field, and Callander are mentioned at various points in this chapter to show where each individual contributed. Additional work with the analytical and experimental results of the research is being conducted by Lewis and will be presented in a dissertation and supplemental report in 1971.

Backwater Equations

Various methods of predicting backwater at flow constrictions are found in the literature. The most recent publication, "Hydraulics of

Bridge Waterways" (14), utilizes both model and recent prototype data for predicting backwater at bridge crossings. Effects of most of the variations shown in Figures 1, 2, and 3 are presented in the publication, and the whole procedure has been programmed for the computer in another publication (83). The methods presented below are based on the backwater predicted (Appendix B) from these publications. Other methods of predicting backwater should be equally applicable as long as the definitions are consistent.

Bradley (14) presents two backwater equations for bridge crossings. The first applies to subcritical flow conditions, and the second is used for each of the critical flow conditions shown in Figure 1.

By applying the energy equation from the point of maximum backwater upstream of the bridge to the downstream point at which the flow returns to normal conditions (Figure 1a), Bradley derives the subcritical flow equation

$$h_1^* = K^* \alpha_2 \frac{V_{n2}^2}{2g} + \alpha_1 \left[\left(\frac{A_{n2}}{A_4}\right)^2 - \left(\frac{A_{n2}}{A_1}\right)^2 \right] \frac{V_{n2}^2}{2g} \quad .$$

The equation is applicable to models and prototypes, and the terms are defined as

h_1^* = total backwater (Figure 1a), or $h_1 - h_n$ (ft),

K^* = total backwater head loss coefficient,

α_1 = velocity head correction coefficient at the upstream section of maximum backwater,

α_2 = velocity head correction coefficient in the constriction,

A_{n2} = cross-sectional area in the constriction, measured below the unconstricted design stage (sq ft),

V_{n2} = average velocity in the constriction for flow at the design discharge, or Q/A_{n2} (fps),

A_4 = cross-sectional area at the downstream point where normal stage has been re-established (sq ft), and

A_1 = cross-sectional area at the upstream section of maximum backwater measured below the water surface (including h_1*).

For the critical flow conditions in Figure 1b and 1c the critical section controls the backwater. For this case

$$h_1^* = \frac{\alpha_2 V_{2c}^2}{2g}(C_b + 1) + h_{2c} - h_n - \frac{\alpha_1 V_1^2}{2g} ,$$

where h_1*, α_2, and h_n were previously defined, and

V_{2c} = critical velocity (fps) in the constriction satisfying the relationship

$$V_{2c}^2 \; b_{tc} = gA_{2c} ,$$

b_{tc} = top width between the abutments measured at critical depth (ft),

A_{2c} = the cross-sectional area in the constriction measured below critical depth (ft^2),

C_b = backwater coefficient for critical flow, similar to K* for the subcritical case,

V_1 = average velocity at the section of maximum backwater, or Q/A_1 (fps), and

h_{2c} = critical depth in the constriction (ft).

Normal stage for the subcritical and critical equations is defined as the stage at which the unconstricted river would flow for the design

discharge. The backwater, h_1*, is simply the maximum rise of the flow above normal stage.

Bradley's solutions for C_b and K* in these equations require values of the opening ratio, M, for the bridge crossing. Different investigators (10, 20, 24, 41, 44, 74, 78, 82) have used several definitions of M which are based either on the geometric or the flow conditions for the constriction. The geometric definition of M is the average distance between the abutments, b, divided by the top water surface width of the channel at normal flow, B. This is a gap-width to channel-width ratio. Flow definitions incorporate the possibility of different values of flow resistance for the flood plains and low-flow channel. For this case,

$$M = Q_b/Q \ ,$$

where

M = bridge opening ratio,

Q = design discharge, and

Q_b = the portion of the unconstricted flow that can pass unimpeded through the bridge constriction.

If the wide channel flow case of Figure 3 is encountered, the flow resistance across the channel is assumed constant, and the flow definition of M becomes

$$M = \frac{Q_b}{Q} = \frac{bh_nV_n}{Bh_nV_n} = \frac{b}{B} \ ,$$

where

b/B = the geometric definition of the opening ratio,

b = the average width between the abutments measured below h_n(ft),

B = the top width of the unconstricted channel measured at h_n(ft),

h_n = the stage in the unconstricted channel flowing at design discharge (ft), and

V_n = the velocity (fps) in the unconstricted channel flowing at design discharge.

The average width between the abutments, b, is well defined for the vertical abutments in Figure 2. For the spill-through abutment,

$$b = \frac{A_{n2}}{\overline{h}_{n2}} \quad ,$$

where A_{n2} has previously been defined, and $\overline{h}_{n2}$ is the depth shown in Figure 2 after the irregular section has been converted to a trapezoid of area A_{n2}.

For the overbank flow case of Figure 3, the resistance to flow is generally greater on the flood plains. If the abutments are set back from the low-water channel banks, then the value for Q_b is comprised of the high-velocity flow in the center of the channel and the relatively low-velocity flow on the flood plains. For this case, the differences in velocities and depths do not allow a reduction of Q_b/Q to the geometric definition of the opening ratio.

The flow definition of M therefore applies to both types of channels and is more amenable to prototype conditions. Whenever wide channel conditions are encountered, the flow definition reduces to the geometric definition.

If the distribution of normal unconstricted flow across the cross-section is known, a central section of width, b, may be selected, and the flow, Q_b, may be determined. The discharge Q, is the design discharge, and a value of M may be found from these values.

The opening ratio, M, may also be determined from conveyance curves, if available, for the bridge site cross-section. The conveyance for a cross-section is defined as

$$K = Q/S^{1/2} \quad ,$$

where

K = conveyance of the cross section,

Q = discharge (cfs) of the section, and

S = slope of the energy grade-line at the section.

For uniform flow, the bed slope and friction slope are equal, and if Manning's equation is substituted for Q, then

$$K = \frac{Q}{S_o^{1/2}} = \frac{1.486}{n} AR^{2/3} \quad .$$

Assuming that the bed slopes for the flood plains and the low-flow channel are equal results in

$$M = \frac{Q_b}{Q} = \frac{K_b S_o^{1/2}}{K S_o^{1/2}} = \frac{K_b}{K} \quad ,$$

where K_b is the conveyance of the opening width, b, and K is the total conveyance for the cross section.

Having a value for the flow opening ratio, M, provides a solution for the backwater equations. Values for K* and C_b may be obtained from Bradley's curves relating K* and C_b to M for the various flow and geometric conditions depicted in Figures 1, 2, and 3. Appendix B contains most of Bradley's experimental curves.

Design Velocities

Energy considerations were successfully used to predict backwater, and this implied that this concept can be used to define the velocity field at a bridge crossing. The energy equation applied between the point of maximum backwater and the downstream point of return to normal depth was utilized in predicting backwater. For this research, the energy equation applied between the point of maximum backwater and the point of minimum depth in Figure 1a yields the relationship

$$\alpha_1 \frac{V_1^2}{2g} + h_1 + S_o L_{1-3} = h_3 + \alpha_3 \frac{V_3^2}{2g} + h_{L\ 1-3} ,$$

where α_1, V_1, h_1, and S_o have been defined, and

L_{1-3} = length along the channel between the points of maximum backwater and minimum jet depth (ft),

h_3 = the minimum depth in the jet (ft),

α_3 = velocity head correction coefficient at the point of minimum depth,

V_3 = the velocity at the point of minimum depth (fps), and

$h_{L\ 1-3}$ = the energy losses between the two sections (ft).

Solving this equation for V_3 produces the equation

$$V_3 = \sqrt{\frac{2g}{\alpha_3} \left[\alpha_1 \frac{V_1^2}{2g} + S_o L_{1-3} + (h_1 - h_3) - h_{L\ 1-3}\right]} .$$

By defining Δh as $h_1 - h_3 + S_o L_{1-3}$, then

$$V_3 = \sqrt{\frac{2g}{\alpha_3} \left[\alpha_1 \frac{V_1^2}{2g} + \Delta h - h_{L\ 1-3}\right]} .$$

A conservative estimate of V_3 is obtained by neglecting the energy losses, so that

$$V_3' = \sqrt{\frac{2g}{\alpha_3}\left(\alpha_1 \frac{V_1^2}{2g} + \Delta h\right)} > V_3 .$$

Because α_3 is greater than or equal to 1.0, assuming a value of unity increases V_3' to

$$V_d = \sqrt{2g\left(\alpha_1 \frac{V_1^2}{2g} + \Delta h\right)} > V_3' > V_3 .$$

This velocity, V_d, represents a conservative estimate of the maximum expected average velocity in the jet. The inclusion of α_3 and $h_{L\ 1\text{-}3}$ serve to reduce V_d to V_3.

Velocity Field

The design velocity derived in the last section theoretically applies near the outlet of the constriction at the vena contracta of the jet. Design velocities for other zones of the crossing may be desired if stable stone sizes determined from the value of V_d are not sufficient for placement at all the critical zones of protection.

Field (24) participated in this study and presents Figure 4 as a solution for the velocities on the upstream side of the approach embankments. The figure is based on ideal flow conditions through a two-dimensional nozzle, and the geometric definition of $M = b/B$ is used. The curves apply to half-embankments placed at various angles to the flow, and may be used as guides in determining stable riprap sizes on the upstream side-slopes of embankments.

Velocities at other regions of the flow are difficult to predict analytically. Two-dimensional approaches similar to Field's are possible

but effects of free water surfaces and separation are difficult to incorporate into these analyses. Callander, Simons, and Lewis are attempting to extend Field's work with two-dimensional solutions for the entire velocity and depth field in the vicinity of bridge crossings. For the present, reliance must be placed on experimental approaches based on data from laboratory and field bridge constrictions.

Design of Riprap

In the absence of waves, the stability of graded gravel and rock riprap is related to (1) the riprap characteristics, (2) the magnitude and direction of the velocity, (3) the depth of flow in the vicinity of the riprap, (4) the angle of the side slope, and (5) the seepage forces. Waves are discussed in the next section.

The interrelation of these factors affecting stability of riprap on the spill-through abutment shown on Figure 5 has been formulated by Stevens and Simons (77). The equations that are derived in the report to describe the stability of the riprap on the abutment are:

$$\eta = \frac{0.4\ u_r^2}{(G-1)gd_m} \quad ,$$

and

$$S = \frac{\cos\theta\ \tan\phi}{(\eta' + \varepsilon)\ \tan\phi + \sin\theta\ \cos\beta} \quad .$$

The second equation may also be written as

$$\eta' = \cos\theta \left[\frac{1}{S} - \cos\beta\ \frac{\tan\theta}{\tan\phi} \right] - \varepsilon \quad .$$

The expression for the stability factor, η, is equivalent to the Shield's beginning of motion parameter for fully turbulent two-dimensional flow over horizontal plane beds. For incipient particle motion conditions $\eta = 1$; if $\eta > 1$ particle movement occurs; if $\eta < 1$ no motion occurs. The variables in the expression for η are: the velocity, u_r, measured one rock diameter above the bed; the specific weight, G, of the rock; the gravitational acceleration, g, taken as 32.2 ft/sec^2; and the volume-weighted effective grain size, d_m, given by the equation

$$d_m = \left[\frac{\sum_{i=1}^{10} d_i^3}{10} \right]^{1/3} ,$$

where $d_i \ (i=1) = \frac{d_0 + d_{10}}{2}$,

$$d_i \ (i=2) = \frac{d_{10} + d_{20}}{2} ,$$

. .

. .

. .

$$d_i \ (i=10) = \frac{d_{90} + d_{100}}{2} .$$

The terms $d_0, d_{10}, \ldots d_{100}$ are the sieve diameters of the riprap for which 0 percent, 10 percent,..., 100 percent of the material (by weight) is finer.

The stability of a particle on a side slope is represented by the safety factor S; if $S = 1$, incipient motion conditions exist; if $S > 1$ the particles are stable; and if $S < 1$ movement of particles occurs. In the equation for S, θ is the side slope angle, ϕ is

the angle of repose of the riprap, η' is the stability factor modified for side slope conditions (equivalent to Shield's parameter for fully turbulent flow along the abutment nose), ε represents seepage forces normal to the riprap face, and β is the angle describing the direction in which the particle will move.

The angle, β, is dependent on the stability factor, η, the side slope angle, θ, the angle of repose, ϕ, and the angle between the horizontal and the velocity vector in the plane of the side slope, λ. The magnitude of β is obtained from the equation

$$\tan \beta = \frac{\cos \lambda}{\frac{2 \sin\theta}{\eta \tan\phi} + \sin\lambda} \quad .$$

The stability factor modified for side-slope conditions is

$$\eta' = \frac{(1+\cos\delta)\ \eta}{2} \quad ,$$

where

$$\delta = 90^{o} - \lambda - \beta \quad .$$

The seepage force factor is

$$\varepsilon = \frac{i(1+e)}{(G-1)} \quad ,$$

where i is the hydraulic gradient through the riprap normal to the side-slope face, and e is the void ratio of the riprap. The hydraulic gradient is defined as positive for seepage through the particles into the flow channel and negative for seepage in the opposite direction.

For the no-flow case with zero seepage the safety factor reduces to

$$S_m = \frac{\tan\phi}{\tan\theta} \quad .$$

For flow over a plane bed that is sloped at an angle, α, to the horizontal, the safety factor is

$$S = \frac{\cos\alpha \tan\phi}{(\eta+\varepsilon) \tan\phi + \sin\alpha} \quad .$$

The above formulations for riprap stability have been compared with those recommended by the Bureau of Public Roads (15), the California Division of Highways (16) and the U. S. Bureau of Reclamation (81). None of the above three agency reports consider cases where λ is not zero. Hence, the comparison must be made for the case where the velocity vector is in the horizontal plane; i.e., $\lambda = 0$ deg.

The method of Stevens and Simons compares closely with that of the Bureau of Public Roads (15) and the California Division of Highways (16) for plane beds and side slopes of 2H:1V or milder. For steeper side slopes and a given rock size, Stevens and Simons predict much lower allowable velocities. For example, the Bureau of Public Roads circular specifies an allowable bottom velocity of 18 fps for 4-foot diameter rock on a 1H:1V side slope whereas Stevens and Simons' method would predict failure on a 1H:1V side slope for any velocity unless the angle of repose for the 4-foot rock is greater than 45 deg. The angles of repose for non-cohesive materials are given on Figure 7.

For the cases where $\lambda = 0$ deg and $G = 2.65$ the set of equations describing the incipient motion criteria (S=1) reduce to

$$\eta = \frac{u_r^2}{133 d_m} \quad .$$

The relationships among the stability factor, η, the side slope angle, θ, and the angle of repose, ϕ, for these cases are shown on Figure 8. The units for u_r and d_m are fps and ft, respectively.

The riprap design curve recommended by the Bureau of Reclamation (81) is based on laboratory and field data, and is shown on Figure 9. According to Stevens and Simons, the safety factor for this curve would be 1.68 if the curve were used to design uniform riprap for flow over a plane horizontal bed. That is, for $\alpha = \theta = \lambda = 0$ deg and $G = 2.65$, the Bureau's curve reduces to

$$\eta = 0.595 = \frac{0.4\ u_r^2}{(G-1)g\ d_m} \quad ,$$

for which

$$S = \frac{1}{\eta} = \frac{1}{0.595} = 1.68 \ .$$

The incipient motion curve (S=1) is also shown on Figure 9. The two field structure failure points between the curves $S = 1$ and $S = 1.68$ (points 1F and 4F) were both on side slopes. Point 5F was a riprap failure on the bottom of a channel. The material in case 5F resisted velocities of 12 fps "for a time but eventually failed." Point 5F is on Stevens and Simons' incipient motion line.

The U.S.B.R. curve can be considered as a design curve ($S = 1.68$) for flow over plane horizontal beds, but does not adequately define stability conditions on side slopes.

The equations developed by Stevens and Simons are employed to design the riprap for sloping spill-through bridge abutments. The safety factor equation permits the use of four possible options:

1. For a given rock size and side slope, the safety factor can be computed and the design accepted or rejected on the basis of the value of the safety factor.

2. For a given rock size, the side slope can be chosen so as to provide a pre-selected safety factor.

3. For a given side slope, the rock size which would give a pre-selected safety factor can be computed.

4. For a given safety factor the proper combinations of rock size and side slope can be computed.

Options 2 and 3 above are not always available in which case option 4 can be used.

Some modifications to the equations describing riprap stability are required for spill-through bridge abutment riprap design. The modifications are:

1. The depth averaged flow velocity at the abutment toe is used to design the riprap. The toe velocity V_t is related to the vena contracta design velocity, V_d, in Chapter IV.

2. The flow velocity, u_r, measured one rock diameter above the bed at the toe is a function of the toe velocity, V_t, the rock diameter d_{50}, and the depth of flow, D. The U. S. Army Corps of Engineers curve given on Figure 10 is recommended for the determination of the velocity adjacent to the bed.

3. For design purposes, it is assumed that the flow at the toe is horizontal and parallel to the side slope; i.e., $\lambda = 0$ deg. With this assumption, the stability factor and the safety factor are related by the equation,

$$\eta = \left(\frac{S_m^2 - S^2}{S\, S_m^2} \right) \cos\theta \quad .$$

To account for discrepancies between assumptions and actual flow conditions it is recommended that the riprap be sized so as to have a safety factor equal to 1.5. That is, for design chose $S = 1.5$. The η, θ, ϕ relationships for $S = 1.5$ are given on Figure 11.

The riprap design procedure for spill-through bridge abutments is outlined in Chapter III. The laboratory verification of the riprap design method is given in Chapter IV, and a design example is given in Chapter V.

Wave Forces

Wind-generated waves can contribute to particle instability on the upstream and downstream sides of an embankment. For the upstream side, wave action and flowing water can contribute individually or collectively to the instability of riprap particles.

The downstream slopes of embankments are not subjected to flowing water, and riprap sizes predicted for wind or turbulence-generated waves are suggested for this region.

Hudson (31) presents an equation for the stone size resistant to wave forces as

$$W_s = \frac{\gamma_s H^3}{3.2\,(S_s - 1)^3 \cot\alpha} \quad ,$$

where γ_s, S_s, and α have been defined, and

W_s = weight of stone required for wave stability (lb), and

H = significant wave height (ft).

Hudson does not specify which stone size is to have the weight, W_s, and the d_m size is used in this report. The factor 3.2 is an empirical value obtained from a study of quarry stone.

The significant wave height in shallow water for fetch widths approximately equal to fetch lengths is obtained (24) from

$$\frac{gH}{V_w^2} = 3.23 \times 10^{-3} \left(g\, F/V_w^2\right)^{0.435} ,$$

in which

V_w = wind velocity (fps), and

F = fetch length (ft), or length of the river subjected to wind.

The fetch widths are usually different from the fetch lengths for rivers, and an effective fetch length, F_e, is suggested (67) as

$$F_e = 1.17\, F^{1/3}\, W_F^{2/3} ,$$

where W_F is the fetch width in feet.

When wave motion and flowing water occur simultaneously, the waves induce an additional bottom velocity given (9) by

$$V_{wm} = \frac{\pi H}{T} \frac{1}{\sinh \frac{2\pi D}{L_w}} ,$$

where

T = wave period (sec),

L_w = wave length (ft), and

D = depth of flow (ft).

When considering stability for these conditions, the velocity vector $\overline{V}_{wm}$ must be added to the flow velocity vector to obtain the resultant velocity.

Freeboard

Embankments that may be overtopped during floods act as broad-crested weirs and require spillway designs on their downstream sides. Due to the high-velocity supercritical flow directly down the slope, very large riprap sizes would be required for this region, and other protection forms should be considered (61).

The usual alternative to flow over the embankments is a provision for sufficient embankment height to prevent overflow. Backwater and possible wave heights should be added to normal stage when determining minimum embankment heights. Wave height considerations may not be necessary in semi-arid regions where flood hydrographs having high peaks and short bases are common. When waves are anticipated, the suggested freeboard above normal stage may be found from

$$F_b = h_1^* + H + h_s \ ,$$

where H and h_1^* have been defined, and h_s is a safety height dependent on the judgment and experience of the design engineer.

Scour at Abutments

Whenever scour of the bed material is anticipated at the abutment toe, protection of the toe must be carried below the expected scour depth to prevent undermining of the abutment. Three types of scour (70) are possible at bridge crossings, and are additive if all three occur at the same time. Local scour is defined as the scour near a pier or

abutment due to the physical presence of the structure in the flow. Bridge piers and approach embankments reduce the net flow area and increase the flow velocity, causing scour of the entire bed in the vicinity of the bridge. Natural scour, or degradation of the entire river channel, may also be occurring, and the measured bed elevation used for design purposes is not dependable. Natural scour is difficult to predict and is omitted in the design procedures. Whenever natural scour data are available at a proposed site, its effect should be included in protection designs.

For vertical wall or wing-wall abutments, protection may be provided by founding the wall below the expected scour depth or by using vertical sheet piles driven at the toe. Spill-through abutments may also be protected by sheet piles, or by creating a horizontal or sloping apron of riprap protection around the toe. The apron must either prevent scour at the abutment or be placed so that the apron armors the scour hole as it develops. If the stream bed is not rigid, riprap protection may be buried along the abutment slope to a depth greater than the predicted scour level, especially at the upstream corner where maximum bed material scour is expected (54, 55).

The flow at abutments may be either clear or sediment-laden, and different scour analyses are required for each case. Clear-water scour occurs at relief bridges or at abutments which are set back from the low-flow channel banks (Figure 3e). For the setback case, the low-velocity flood plain flow carries little sediment, and clear water scour occurs.

Laursen (46) proposes Figures 12 and 13 for the relationship among clear-water contraction scour at piers and abutments, critical tractive shear stress, and the geometry of the contraction.

The values in the figures are defined as

d_{se} = equilibrium scour depth (ft), measured below mean bed elevation,

h_1 = flow depth in the main channel upstream of the pier or contraction (ft), including backwater,

L_e = length of the approach embankment (ft),

τ'_o = shear stress attributed to the grain roughness in the constriction (psf),

τ_c = critical tractive shear stress for incipient motion of the bed material at the contraction (psf),

d_{se}/r = scour in a long contraction, and

r = a coefficient relating the scour in a long contraction to the scour, d_{se}, in a shorter contraction, where the scour in the long contraction is d_{se}/r.

Figure 13 also contains Laursen's curve for sediment-laden flow at the abutments. This curve may be used for sediment-laden flow whenever the bed between the abutments is unprotected, and when the sediment transported as bed load is the same size as the bed material. For riprap-protected beds, the flow is always considered clear because of the large difference between the riprap and bed-load sizes.

The values from Figure 13 are based on the assumption that the scour holes from abutment to abutment, or from pier to abutment, do not overlap. Laursen states that a clear opening between the abutments greater than 5.5 d_{se} should insure non-overlapping scour holes. No

analyses presently exist for overlapping scour holes when piers are present, or when opposite abutments are close to each other.

Laursen's estimates for values of τ_o' and τ_c in Figure 13 are

$$\tau_o' = \frac{V_1^2 D_s^{1/3}}{30 h_1^{1/3}} \text{ (psf)} ,$$

and

$$\tau_c = 4D_s \text{ (psf)}$$

where

D_s = the bed mean particle diameter in the constriction (ft), and

V_1 = velocity of flow in the uncontracted reach upstream of the abutment (fps).

The equation for τ_o' arises from the Manning and Strickler equations, and the equation for τ_c agrees with White's (84) and Shield's critical shear for silica sands and turbulent flow.

Figure 13 is derived from model data only, and predicts unusually large scour depths for prototype structures, especially for clear water scour conditions. Caution and judgment are advised in applying the results of Figure 13 to these cases. The curves should be considered as a guide until future measurements at prototype crossings are available for modifications of the method.

Scour at Piers

Shen (70) proposes the following analyses for local scour at piers, based on the cases of clear-water scour and scour with continuous sediment motion.

For clear water scour

$$d_{se} = 0.00073\ \overline{R}^{0.619} \quad \text{(ft)} ,$$

where

$\overline{R}$ = pier Reynolds number defined as

$$\overline{R} = \frac{2aV_{\infty}}{\nu} ,$$

where

a = half width of the pier, or radius of the pier (ft),

V_{∞} = the average upstream, undisturbed flow velocity (fps), and

ν = the kinematic viscosity of the fluid (ft^2/sec).

This equation was derived from laboratory and field data collected in several investigations (70).

For the case of sediment-laden flow, deposition causes the scour depth to fluctuate about a mean value. Defining d_{se}^* as the maximum equilibrium scour depth measured from mean bed elevation, Shen recommends either

$$d_{se}^* = 1.4b_p ,$$

or

$$d_{se}^* = 1.42\ Kb_p^{0.75} ,$$

in which

b_p = width of pier projected on a plane normal to the undisturbed flow (ft), and

K = a coefficient of pier shape, recommended as 1.0 for cylindrical piers and 1.4 for rectangular piers.

The first equation for d_{se}^* is more conservative, and the second agrees better with the available data.

Whenever dunes are expected to pass through the scour hole, Shen suggests that half the expected dune height be added to d_{se}^* for estimations of scour depths. Dune heights, however, are usually small compared to scour depths, and may usually be neglected unless data are available for the design site.

When piers or pier bents are not aligned with the flow, Laursen and Toch (52) predict a larger scour depth than for piers aligned with the flow. Figure 15 provides a correction coefficient, $K_{\alpha\ell}$, to be multiplied by the equilibrium scour depth for piers aligned with the flow.

Lateral Extent of Scour

Estimates of the lateral extent of possible scour at abutments and piers are required for the design of widths of horizontal aprons or riprap mats around the structures. Laursen (48) suggests a width of $2.75\ d_{se}$ for abutments and piers. This value is measured horizontally from the face or toe of the pier or abutment, and is recommended as a minimum value.

Field (24) participated in the research and recommends the use of Figure 14, obtained from this research, for determining the lateral extent of scour at abutments. The distance, z, along either face of the abutment defines the conical scour hole boundary, and d_{se} is the equilibrium scour depth obtained from Figure 13. Note that the value of z along the upstream face for an angle, θ, of 90 degrees and an

angle of repose of 21^{o} 31' becomes identical to Laursen's value of $z = 2.75\ d_{se}$. The principal advantage of Field's figure is its estimate of lateral extent for skewed abutments.

Chapter III

PROPOSED DESIGN PROCEDURES

This chapter presents an outline of design principles based on the derivations in Chapter II. Laboratory verification of the procedures are presented in Chapter IV, and an example of the design of protection for a prototype bridge is presented in Chapter V.

The design procedure is presented in ten steps. The design uses the backwater and scour predicted from the literature. The results of this research, included in the steps, are the derivation of the vena contracta design velocity, the velocities along the upstream slopes of the approach embankments, the amount of riprap wrap-around for spill-through abutments, the terminal points for riprap placement on the side slopes of approach embankments, the length along the side slopes requiring buried toe protection, and the riprap sizing and gradation designs computed from the design bed velocities.

Stabilization techniques are presented for bridge crossings assuming that the following quantities are given:

(1) the desired crossing with design discharge, Q;

(2) normal flow stage for the design discharge;

(3) the distribution of the design discharge across the unconstricted channel;

(4) the abutment type (Figure 2); and

(5) the geometric properties (Figure 3).

The result of applying the design technique is the required riprap size and gradation. If only one size and gradation is available, the crossing variables must be modified until the computed and actual riprap parameters match for the selected safety factor.

Step 1 - Initial Computations

Several values will be needed in the design, and they should be computed before proceeding.

a) A_{n2} - This is the flow area in the contraction beneath the unconstricted flood stage, and it may be planimetered from a cross-section of the bridge site, or it may be computed as the area of an equivalent trapezoid (Figure 2c) for spill-through abutments, or as an equivalent rectangle for vertical wall or wing-wall abutments. For skewed crossings, the area is computed as the area projected on a plane normal to the flow direction. For designs allowing scour, the expected scour area is included in A_{n2} and is checked in steps 4a through 4c. Steps 1 through 4c are repeated for scoured designs until estimated and computed values of scour agree.

b) $\bar{h}_{n2}$ - This is the average depth in the constriction measured below the unconstricted flood stage (Figure 2c).

c) Q_b - For wing-wall or vertical wall abutments, Q_b is the unconstricted flow confined to the opening width, b, shown in Figure 2d. For spill-through abutments, the value of $b = A_{n2}/\bar{h}_{n2}$ is used in determining Q_b. For skewed crossings, Q_b is determined from the average width of the opening projected on a normal to the flow direction (Figure 3h).

d) M - Compute the bridge opening ratio, M, as Q_b/Q, or as K_b/K if the conveyances of the sections for the unconstricted flow are known.

e) $A_n = A_{n1} = A_{n4}$ - All of these are the cross-sectional flow area in the unconstricted channel flowing at the design discharge, and they may be planimetered from the channel cross-section.

f) $V_n = V_{n1} = V_{n4}$ - All are the average velocity in the unconstricted channel flowing at design discharge. The equation is

$$V_n = Q/A_n \ .$$

g) V_{n2} - This is the average velocity in the constriction, or

$$V_{n2} = Q/A_{n2} \ .$$

h) h_{2c} - This is the average critical depth in the constriction for the design discharge. For an equivalent rectangle

$$h_{2c} = \left(\frac{Q^2}{g\, b_r^2}\right)^{1/3} \ ,$$

where b_r is the width of the rectangle. For an equivalent triangle

$$h_{2c} = \left(\frac{2Q^2}{gm^2}\right)^{1/5} \ ,$$

where m is the triangle side-slope rise for a unit run. For an equivalent trapezoid

$$h_{2c} = \left[\frac{Q^2}{g}\ \frac{\left(\frac{b_r}{h_{2c}} + 2m\right)}{\left(\frac{b_r}{h_{2c}} + m\right)^3}\right]^{1/5} \ ,$$

where b_r is the base width of the trapezoid. This last equation requires a trial and error solution, and a trial value of $b_r/h_{2c} = 2$ usually produces convergence after a few trials. Each trial is made by replacing h_{2c} in the right side of the equation with the value computed from the last trial.

i) V_{2c} - This is the critical velocity in the constriction for design discharge, computed from

$$V_{2c} = Q/A_{2c} \quad ,$$

where A_{2c} is the equivalent rectangular, triangular, or trapezoidal flow area below h_{2c}. Combinations of equivalent shapes may be treated by solving the equation $Q^2 B = g A_c^3$, where A_c is the flow area for critical conditions.

j) $h_{1c} = h_{4c} = h_{nc}$ - All of these are the critical depth in the unconstricted channel flowing at design discharge. The equations in step 2h may be used if equivalent channel shapes exist.

k) α_{1n} = This is the unconstricted velocity head correction coefficient at the section of maximum backwater. If the discharge and average velocity in each of p subsections (flood plains and low flow channel) are known, then

$$\alpha_{1n} = \frac{\sum_{i=1}^{p} Q_i V_i^2}{Q V_{n1}^2} \quad .$$

Step 2 - Backwater

a) Method - Select a suitable method for determining the backwater that will be produced by the crossing. Reference 14 is recommended for this step, and has been summarized in Appendix B.

b) h_1^* and Δh - Compute the backwater, h_1^*, and the total water surface drop through the abutments, Δh, by the chosen method. The determination of backwater should assume a non-scoured condition in the gap unless it is known that the flood gradually rises to its peak with sufficient time for gradual scour, or if the bed material in the gap is to be removed during construction. The flow classification

in accordance with Figure 1 may be determined, after finding Δh, by computing $h_3 = h_n + h_1^* - \Delta h + S_o L_{1-3}$, where L_{1-3} is obtained from Figure B.13 in Appendix B. The value of h_3 is then compared with h_{2c} from step 1h.

c) Waves - If wind waves are anticipated during the design flood, estimate the wind velocity, V_w, fetch length and width, F and W_F, and compute the significant wave height from

$$H = \frac{V_w^2}{g} 3.23 \times 10^{-3} (g F_e / V_w^2)^{0.435} ,$$

where

$$F_e = 1.17 F^{1/3} W_F^{2/3} .$$

d) Freeboard - Verify that the proposed embankment height equals or exceeds the sum of normal stage at design discharge, backwater, h_1^*, and wave height, H. Allow a safety factor between 1 and 3 feet as desired. The Wyoming Highway Commission (86) suggests a height of protection extending three feet above the maximum backwater for spill-through abutments.

Step 3 - Design Velocity

a) α_1 - Compute or estimate a value of the velocity head correction coefficient at the point of maximum backwater. The value obtained for unconstricted flow at design discharge (step 1k) may be used as an estimate. For flow in wide channels the coefficient is close to unity. For the overbank case, the velocity variation significantly increases the coefficient.

If the distribution of flow between the flood plains and the low-flow channel can be determined, an estimate of α_1 may be obtained from

$$\alpha_1 = \frac{\sum_{i=1}^{p} Q_i V_i^2}{Q V_1^2} ,$$

where Q_i and V_i are the discharge and velocity in each subsection, and

$$V_1 = Q/A_1 ,$$

where A_1 is defined as the area, including backwater, at the upstream section of maximum backwater.

b) V_d - Compute the vena contracta depth-averaged design velocity

$$V_d = \sqrt{\alpha_1 V_1^2 + 2 g\Delta h} .$$

c) V_t - Compute the depth-averaged toe velocity using the average ratio from Table 2 in Chapter IV, or $V_t = 0.75 V_d$.

Step 4 - Toe Protection

a) Shear Ratio - If the abutments are constructed on a rigid bed, proceed to step 4h. For alluvial beds, the toe of the abutment will require protection from undermining, and the toe velocity (step 3c) for the non-scour case should be used if the flood rapidly rises to its peak. For designs allowing scour of the bed material, the scour is first estimated prior to step 1. The backwater and upstream depth (including backwater) are then computed for the scoured opening from steps 1a through 2b. Steps 4b, 4c, and Figure 14 provide computed values for the depth and extent of the scour caused by the flow. This procedure

would need to be repeated until the estimated scour and computed scour had the same value at the beginning and end of the trial. A similar process would be required for scour at piers, utilizing steps 1 through 3a and steps 9a and 9c.

Regardless of the form chosen for protection (riprap, sheet piles, etc.) an estimate of the equilibrium depth of scour is required. The bed material mean particle diameter, D_s, and the velocity, V_1, from step 3a provide values for the solution of

$$\frac{\tau_o'}{\tau_c} = \frac{V_1^2}{120\ D_s^{2/3}\ h_1^{2/3}} \quad ,$$

where h_1 is the flow depth including backwater directly upstream of the abutment.

b) Effective Length of Approach Embankment - The effective length, L_e, of the approach embankment is equal to the roadway approach length for vertical wall or wing-wall abutments. For spill-through abutments,

$$L_e = L + \frac{b' - b}{2}$$

where L is the roadway approach length (Figure 16), b' is the top-width between the abutments, and the value of b was found in step 1e.

c) Scour Depth - Compute the ratio, L_e/h_1, and obtain a value of d_{se} from Figure 13. This depth may be increased by half the expected dune height for sediment transporting flow, or by a factor of safety for clear water scour. In either case, a minimum total of five feet is suggested (69).

d) Sheet Piles - If sheet piles or vertical cut-offs are used to protect the abutment toe, they must be placed at least to the depth

determined in step 4c, and must act as retaining walls after scour has removed the bed material. Additional placement depth will be needed to provide this support.

e) Riprap Depth - If riprap is to be buried along a slope for toe protection, it must extend at least to the depth determined in step 4c, and should be placed on the same slope as the abutment spill slope. Wyoming practice employs a depth to competent rock or three feet below the expected scour depth, whichever occurs first (86).

f) Alluvial Bed Riprap - Horizontal aprons dumped at bed level are not recommended in cases where scour may occur, unless the whole bed between the abutments is to be protected.

If bed-level aprons are used, sufficient material should be dumped to allow the apron to armor the scour hole as it develops. The length of protection extending from the toe should equal or exceed $d_{se}/\sin\phi$, where ϕ is the submerged angle of repose of the riprap.

g) Riprap Thickness - Various investigators suggest values for the thickness of riprap protection that are equal to the maximum stone size (69), 1.5 to 2.0 times the maximum diameter (16), or 3.0 times the maximum diameter (31). If the gradation of the riprap can be maintained during placement, thicknesses from 1.5 to 2.0 times the maximum diameter are allowable. A value determined as the maximum of 3 d_m or 2 d_{100} is recommended in this report. For horizontal aprons which are dumped at bed level and are expected to slough into the scour hole as it develops, the thickness determined above should be increased by a factor of 1.5 or more.

g) Rigid-Bed Riprap - If the abutments are constructed on a rigid bed, or if the bed material cannot be excavated, the toe should be

protected with a horizontal apron of riprap extending a minimum distance of 6 feet (69) from the abutment toe. The thickness of the layer should be determined as 1.5 times the value obtained from step 4g.

i) Riprap d_m - If riprap is to be used for toe protection, the d_m size can be determined from step 5. The design velocity, V_d, was determined in step 3b, and the value of D for any option in step 5 may be taken as the depth at the toe of the abutment below normal stage.

Step 5 - Riprap Sizing

a) General - This step is used to compute the d_m size mentioned in step 4i. The procedures in this section are also recalled in later steps to find d_m sizes for other zones requiring protection.

The following steps are based on the assumption that riprap is to be used for protection. If wire-enclosed riprap is to be used, the size and gradation computed in these steps will not be required. The requirements for wire-enclosed riprap are that the baskets are thick enough and contain riprap particles of sufficient size to prevent pumping of the embankment material through the riprap voids. These considerations are only mentioned herein, and other reports (16, 80) are suggested for more thorough discussions.

Wire-enclosed rock protection is not recommended in designs where corrosion from alkali or abrasion from coarse-gravel bed loads may occur. Costs of hand placing the baskets should also be considered when end-dumping of riprap may prove more economical, especially for submerged zones requiring protection. A combination of dumped riprap at low points of abutments and smaller, wire-enclosed riprap at higher points may prove to be economical for these troublesome areas.

b) Options available to the designer. - Generally the designer will want to determine the rock size needed to protect the chosen bridge geometry. If this rock size is not readily available, the designer can either use a different rock size and accept the safety factor associated with that different rock size, or the designer can change the abutment geometry so that he can obtain the chosen safety factor for another rock size. The list of options available to the designer are:

Option 1: Find the rock size required for a recommended safety factor of 1.5 on the given side slope.

1. Estimate u_r; since d_{50} is not yet known, an approximate value for u_r can be taken as

$$u_r = 0.45\ V_t \quad ,$$

using V_t from step 3c.

2. Estimate ϕ; since d_{50} is not yet known, assume a value for ϕ consistent with the anticipated d_{50} size and angularity (Figure 7).

3. Compute the maximum possible safety factor, S_m, given by

$$S_m = \frac{\tan \phi}{\tan \theta} \quad .$$

If S_m is less than 1.5, instability at no flow is indicated and another option should be selected. If S_m is greater than 1.5 continue with this option.

4. Compute the stability factor, η, given by

$$\eta = \left(\frac{S_m^2 - S^2}{S\ S_m^{\ 2}} \right) \cos \theta \quad ,$$

where θ is the side slope angle and S is the selected safety factor (1.5 recommended).

5. Compute the required rock size for the estimated value of u_r from the equation

$$d_m = \frac{0.4\, u_r^2}{(G-1)g\eta} ,$$

where G is the specific weight of the rock.

6. Select the gradation of any riprap which has a d_m equal to the computed value and obtain a value of d_{50}. Riprap placement by dumping may produce segregation of the particles and a maximum ratio of $d_m/d_{50} = 1.4$ is recommended for controlled dumping which will assure a homogeneous riprap mixture. Smaller values of d_m/d_{50} should be used if little control is maintained during placement of the riprap.

7. Compute d_{50}/D and obtain the corrected value for u_r/V_t from Figure 10. The value of D was determined in step 4i. Recompute u_r and compare with the original estimate. Repeat the above steps 1 through 7 if the values are not in agreement.

8. Obtain the correct value of ϕ for the final d_{50} size from Figure 7. This value should agree with the former estimate.

9. Recompute η and d_m using the new values of u_r and ϕ. A homogeneous mixture of rock with a d_m given by the above equation will provide the required riprap for stability.

Option 2: For a given rock size find the side slope which will give a safety factor of 1.5.

1. Compute d_{50}/D and obtain u_r/V_t from Figure 10. Compute u_r using the value of V_t from step 3c.

2. Obtain ϕ from Figure 7.

3. Compute the stability factor, η, from

$$\eta = \frac{0.4\ u_r^2}{(G-1)g\ d_m} \quad .$$

4. Obtain the side slope angle, θ, by solving the equation

$$\eta = \left(\frac{S_m^2 - S^2}{S\ S_m^2} \right) \cos \theta \quad ,$$

where

$$S_m = \frac{\tan \phi}{\tan \theta} \quad .$$

The solution of these equations for $S = 1.5$ is given on Figure 11. Enter Figure 11 with the appropriate values of η and ϕ and obtain the required side slope angle θ. Note that if $\eta > 0.667$, a safety factor of 1.5 cannot be obtained on a "horizontal" side slope (a side slope with zero slope, or $\theta = 0$ deg).

Option 3: For a given rock size, d_m, and side slope, θ, find the safety factor.

1. Compute d_{50}/D and obtain u_r/V_t from Figure 10. Compute u_r using the value of V_t from step 3c.
2. Obtain ϕ from Figure 7 and compute $\tan \phi$.
3. Compute the stability factor, η, from

$$\eta = \frac{0.4\ u_r^2}{(G-1)g\ d_m} \quad .$$

4. Compute the maximum safety factor, S_m, from

$$S_m = \frac{\tan \phi}{\tan \theta} \quad .$$

5. Compute the safety factor, S, from

$$S = \frac{S_m}{2} \left[(S_m^2 \eta^2 \sec^2\theta + 4)^{1/2} - S_m \eta \sec\theta \right] ,$$

which is the positive root of the equation

$$\eta = \left(\frac{S_m^2 - S^2}{S S_m^2} \right) \cos\theta \quad .$$

The design can be accepted or rejected on the basis of the computed safety factor value.

Option 4: Find the combinations of rock sizes and side slopes that will give a safety factor of 1.5.

The easiest method is to chose a rock size and to use the method outlined in Option 2 to calculate the required side slope angle. This procedure may be repeated for several rock sizes in order to determine the most economical combination of rock size and side slope.

c) Recommended Procedure.

Check if the chosen bridge geometry can be riprapped with a rock size that will give S = 1.5. Figure 11 shows that for the no-flow case ($\eta = 0$), a 1.5 safety factor is obtained for the conditions listed below:

ϕ deg	θ deg
25	17.3
30	21.0
35	25.0
40	29.2
45	33.7

The largest angle of repose, ϕ, that can be anticipated for dumped angular riprap is about 42.5 deg (Figure 7). The table above

indicates that the maximum side slope that could be riprapped for a safety factor of 1.5 is only 31.4 deg, which corresponds to a slope of 1.6H:1V. Therefore, all abutment toe slopes, below the water line, must be milder than 1.6H:1V if a safety factor of 1.5 is to be achieved.

If the given side slope is milder than 1.6H:1V, use Option 1 to determine the required rock size, d_m.

If the rock size, d_m, computed in the preceding step is not available, select a value of d_m which is available and adjust the geometry of the opening to accommodate the value of d_m. One way to do this is to adjust the slope of the spill-slope using Option 2 to obtain a safety factor of 1.5. For a first estimate use V_t and D computed for the previous side slope geometry. If this computed side slope is acceptable for design, return to Step 1 so that the correct V_d and D can be determined for the new side slope. With the correct V_d and D, either (1) determine with Option 3 the safety factor for the available riprap d_m and the new side slope θ, or (2) compute the required d_m for the new side slope using S = 1.5 in Option 1.

Option 4 can be used to study the overall problem of riprapping spill-through bridge abutments. That is, for a given toe velocity, all combinations of riprap size and abutment spill slopes which will give a 1.5 safety factor can be determined and examined considering economic and environmental factors.

Step 6 - Abutment Spill-Slope Protection

a) Riprap d_m - The spill-slopes of spill-through abutments can be protected with riprap by using the toe velocity from step 3c and

any of the options for slopes of spill-through abutments in steps 5a through 5c. The value for D in step 5 should be the same as computed in step 4i.

b) Riprap Thickness - The thickness of the nose protection on spill-through abutments is determined from step 4g. If desired, the thickness can be increased at the points of greatest scour potential.

c) Riprap Extent - The riprap size obtained in step 6a can be placed on all the slopes of the spill-through abutment or limited to the nose if a sufficient quantity of the riprap is not available for the sides. Steps 7 and 8 provide values for the smaller riprap sizes required on the upstream and downstream side slopes.

Turbulent eddies from the wake of separation require placement of the large riprap around the downstream shoulder at least to the tangent with the embankment side slope (point G in Figure 5). Extreme velocities and plunging flow produce the same requirement for the upstream shoulder (Point E in Figure 5).

One estimate of the distance requiring protection along the upstream side slope of spill-through embankments is obtained (86) from the rational equation

$$L = [1 - (V_n/V_2)]\, L^* ,$$

where

L = the length (ft) requiring the protection, measured from the beginning of curvature on the upstream side slope of the spill-through abutment,

V_n = the average flood velocity (fps) in the unconstricted channel (step 1f),

V_2 = the constricted flood velocity (fps), and

L* = the distance to the point of maximum backwater (ft) obtained in step 2b.

Another estimate for L, obtained from the research, is presented in step 8.

d) Filter Layer - Filter layers may not be required when the riprap is well-graded with a minimum size equal to the size of the embankment material, or when the riprap is dumped, causing the smaller material to settle against the slope. When filters are required, filter cloth, graded gravel, or some other suitable material may be used. The recommended Terzaghi-Vicksburg (T-V) specifications (61) for graded-gravel riprap are

$$\frac{d_{15}(\text{Filter})}{d_{85}(\text{Base})} < 5 ,$$

and

$$4 < \frac{d_{15}(\text{Filter})}{d_{15}(\text{Base})} < 20 ,$$

and

$$\frac{d_{50}(\text{Filter})}{d_{50}(\text{Base})} < 25 .$$

The words "Riprap" and "Filter" should be substituted for "Filter" and "Base" in these inequalities to check the filtering properties of the riprap. The thickness of the filter layer may be determined from step 4g, using the d_m and d_{100} sizes of the filter or riprap material.

Step 7 - Downstream Side Slope Protection

a) d_m - If the riprap size determined in step 6a is not plentiful, a smaller size may be used on the downstream side slopes of the embank-

ments. The riprap must be of sufficient size to withstand expected wave forces, and the weight of the d_m size is estimated from

$$W_s = \frac{\gamma_s H^3}{3.2(S_s - 1)^3 \cot\theta},$$

where

W_s = weight of stone (lb) required for stability,

H = wave height (ft) from step 2c,

S_s = specific gravity of the riprap, and

θ = side slope angle with the horizontal.

b) Turbulent Waves - If wind-generated waves are not anticipated, the riprap on the downstream side slopes must withstand the waves from the turbulent mixing downstream of the crossing.

c) Extent - The riprap on the downstream slope should be placed to a height equal to the anticipated downstream depth plus the wave height. Downstream depths are generally less than normal stage, and the use of h_n would provide a conservative estimate. Figure 14, and the value of d_{se} from step 4e, will produce an estimate of the length along the abutment toe requiring buried protection.

d) Filter Layer - The filter layer requirements for the downstream embankment slope may be determined from step 6d.

Step 8 - Upstream Side Slope Protection

a) General - Upstream side slopes of embankments may be protected with riprap designed for wave and drag forces. The size computed in step 7a should be considered a minimum size, and its stability for lift and drag forces should be checked in step 5.

b) Velocities - For skewed crossings, expected velocities are obtained from Figure 4 and should be increased by 50 percent for design. For normal crossings, the experimental curves (solid lines) of Figure 35 are suggested for values of x/L greater than the value at the intersection of the experimental and theoretical curves. The experimental curves indicate that the parameter VM'/V_n becomes zero at a value of x/L close to 0.3. Stagnation (defined by V = 0.0) did occur at this point for the model embankments, but other investigators (10, 37) report that stagnation in prototype crossings occurs at a value of x = 0.0. For this reason, the theoretical values should be used for values of x/L less than the intersection value. These curves produce stagnation at a value of x/L = 0.0.

c) Riprap d_m - After obtaining design velocities along the upstream slope, the required riprap size and gradation at any point are found from the options in steps 5a through 5c. The riprap size determined for waves in step 7a must be used if the size required for flow stability is smaller.

A riprap size that is stable at any point along the upstream slope could be placed along the slope to the point where x = 0 (Figure 35). One required size may be determined at a single point (e.g., x/L = 0.8), and this size may be placed from that point to the point defined by x = 0.0. If desired, a third riprap size could be placed from some other point (e.g., x/L = 0.4) to the point defined by x = 0.0. This procedure would result in a small riprap size from x = 0.0 to x/L = 0.4, a larger size from x/L = 0.4 to x/L = 0.8, and the largest size (step 6a) from x/L = 0.8 around to the downstream slope of the embankment.

If different sizes of riprap are to be used along the upstream slope, each must be larger than the size required for anticipated wave action, and the large riprap from step 6a should always extend at least to the beginning of curvature (point E in Figure 5), or to the distance L from step 6c.

If wave action is not anticipated on the upstream embankment side slope, the riprap placement can be terminated at a point where the actual velocity equals the critical erosive velocity for the embankment core material. This point is defined by the distance, x, from Figure 35 at which the velocity, V, is equal to the velocity which causes movement of the embankment material. To obtain this value of x, the critical depth-averaged velocity for movement of the embankment core material is found and substituted for V in Figure 35. The critical velocity can be found by entering Figure 11 with the angle of repose of the embankment core material to obtain a value of η. Using the known d_{50} value and a value of D equals to the depth along the upstream side slope provides a value of d_{50}/D for use in Figure 10. The magnitude of u_r is computed from the equation

$$u_r^2 = \frac{(G-1)g\,\eta\,d_m}{0.4} \quad ,$$

and V_t may be obtained from Figure 10 and substituted for V in Figure 35. Riprap placement can be terminated at the resulting value of x because the embankment core material will safely withstand the smaller velocities between this point and the point at which x = 0.0.

This result of the research indicates a considerable saving in the initial cost of protection for a structure which would otherwise be protected with the large riprap along the length, L (step 6c).

d) Toe Protection - The toe along the upstream slopes of embankments is vulnerable to scour, especially with embankments which are skewed downstream (Figure 14).

During the construction of an embankment, the flood plain along the upstream slope is sometimes cleared to facilitate construction. This practice leaves a low-resistance channel along the embankment toe, creating greater scour hazards from increased velocities. If this condition cannot be avoided, the toe of the embankment should be protected with buried riprap.

e) Riprap Size and Extent - The riprap size determined in step 8c should be placed to the height determined in step 2d. Buried riprap is to begin at a point determined from Figure 14, using the value of d_{se} determined in step 5c. The depth of buried riprap should vary from the bed level at this point to the depth, d_{se}, at the point of maximum scour.

f) Filter Layer - The particle size and thickness of the filter layer for the upstream slopes are determined from step 6d.

g) Spur Dikes - If spur dikes are used to reduce scour at the abutment, the dikes should be protected as if they were abutments. References 14, 28, and 38 present discussions of the need for spur dikes and the optimum size and shape required. Reference 2 provides an estimate of the anticipated scour at spur dikes, and the extent of riprap protection is discussed in reference 39.

Step 9 - Pier Protection

a) Scour Depth - For piers at relief bridges or on the flood plains, compute the clear-water scour depth from the relationship

$$d_{se} = 0.00073\ \bar{R}^{0.619} ,$$

where

$$\bar{R} = \frac{2aV_1}{\nu} .$$

The mean velocity of the undisturbed flow, V_1, was found in step 3a, and the radius or half-width of the pier is known from structural requirements.

For piers at locations which are exposed to sediment transporting flow, compute the scour depth from the equation

$$d_{se}^* = 1.42\ K\ b_p^{0.75} .$$

Values of 1.0 for cylindrical piers and 1.4 for rectangular piers may be substituted for K. Half the expected dune height should be added to d_{se}^* for design.

b) Pier Alignment - Minimum scour occurs for piers which are aligned with the flow direction. Cylindrical piers eliminate alignment problems, but structural requirements frequently call for "Hammer Head" piers or pier bents composed of multiple columns or piles. If the piers are not aligned with the flow direction, the depth of scour obtained in step 9a should be multiplied by the value of $K_{\alpha\ell}$ obtained from Figure 15.

c) Extent of Protection - If piers are not founded on competent rock or below the possible scour depth, the footings may be lost during

a flood. Footings or piles which are designed from soil strength and structural considerations should be placed at or below the expected scour depth. Buried riprap protection could be placed around the piers, and an estimate of the extent of the riprap may be obtained from step 4f.

Step 10 - Protection of Special Cases

a) Flood Plains - If the flood plains between the abutments at a setback crossing (Figure 3e) are to be maintained for livestock passage beneath the superstructure, protection may be placed at bed level on the flood plains and on the low-flow channel side slopes. Livestock are reluctant to cross loose riprap, and a soil cover or concrete or grouted riprap path may be required. It may be more economical to bury the horizontal layer of riprap beneath a foot or more of earth, and replace the soil cover after each flood. The size of the riprap is determined from step 4i using θ = 0 deg for flood plains and from steps 5a through 5c for the low-flow channel sides. The thickness of the riprap layer is determined from step 4g.

The horizontal extent of flood plain protection will be determined by the degree of setback and other factors. Figure B.13 in Appendix B could be used as an estimate of the upstream distance requiring protection. The dashed line encloses the region of flow acceleration, and velocities are small at other upstream points.

Downstream protection is difficult to evaluate. If the protection is placed for a short distance downstream and then terminated, the extreme roughness difference between the protected zone and the unprotected zone may produce vertical scour at the terminus of the protection. Undermining could eventually cause the loss of the riprap

protection. Smooth transitions between the riprap and the flood plain material, or buried riprap or sheet piles might be used to alleviate this problem.

b) Eccentric Crossings - Backwater and protection for eccentric bridge crossings (Figure 3d) may be determined by treating each abutment as half of an equivalent non-eccentric crossing. The equivalent crossing would consist of each abutment and its mirror image reflected from the center of the flow distribution.

An estimate of the backwater for eccentric crossings may also be obtained by applying an empirically determined correction coefficient to the backwater for non-eccentric crossings. This procedure is presented in Appendix B.

Chapter IV

LABORATORY VERIFICATION OF DESIGN PROCEDURE

Laboratory investigations of the validity of the design procedures developed in Chapter II and presented in Chapter III were conducted in the engineering research facility at Colorado State University. The research included studies of spill-through bridge abutments protected with riprapped spill-slopes and side-slopes. The design of the riprap was tested for all the model abutments, and velocity and depth data were collected for several of the abutments.

The facilities, test program, data reduction, data analysis and the verification of design are presented in this chapter. A description of the experimental program and tabulations of all the recorded data are presented in a separate data report (76).

Facilities

Two laboratory flumes shown in Figures 36 and 37 were used for the tests of spill-through abutment models with riprap-protected slopes. Smaller models were tested in the 6-foot wide by 64-foot long horizontal recirculating flume, and larger models were constructed in the 20-foot wide by 180-foot long outdoor flume. The flumes were capable of discharges of 10 and 100 cfs, respectively, and the outdoor flume was equipped with a 30-foot long recessed section which was filled with 5 feet of river sand having a median fall diameter of 0.47 mm. Models constructed on the sand bed in the outdoor flume were used to investigate the bed scour characteristics and abutment riprap stability of bridge crossings constructed on alluvial beds.

Models

Table 1, with reference to Figure 16, describes the models tested in the two flumes. The models were constructed with a core of river sand protected by rock riprap having a thickness, t, equal to twice the maximum stone size. The first three models were constructed on a sand bed, and all the rest were built on plywood or broken-concrete riprapped beds.

Wide channel (W.C.) models were constructed in both flumes, with skewed and normal spill-through abutments constructed on sand and plywood beds.

By assuming that the flow through a normal bridge crossing is symmetrical about the flow centerline, only half the channel and one abutment would need to be studied. This assumption is not valid for skewed or eccentric crossings which are not symmetrical with respect to the flow centerline. Symmetry was assumed for all the tests in the 6-foot wide flume, and the model abutments were constructed from one flume wall only. This assumption places the flow centerline along one wall and produces an effective width of 12 feet for the 6-foot wide flume. Three of the tests in the outdoor flume assumed flow symmetry, and the other four tests employed abutments from both walls of the flume, reducing the widths in Table 1 to 20 feet.

All the overbank (O.B.) models were constructed perpendicular to the flow direction. The small values of width-to-depth ratios that would be produced by two abutments prevented the construction of skewed abutment models from both walls of the 6-foot wide flume.

The low-flow channel and flood plain shown in Figures 16 and 36 were constructed of plywood, and the flood plain was raised 0.25 feet above

Table 1. Summary of Model Geometry Values for Spill-through Abutments (see Figure 16)

Model No.	Channel Type	B (ft)	h (ft)	W (ft)	L (ft)	r (ft)	α	θ deg	d_m (in)	d_{50} (in)	t (in)
1	W.C.	20	1.5	1.0	4.25	3.0	2:1	90	2.42	2.43	2.50
2	W.C.	20	1.5	1.0	4.25	3.0	2:1	90	1.24	1.20	3.00
3	W.C.	40[a]	3.2	2.0	8.68	6.4	2:1	90	1.24	1.20	3.00
4	W.C.	40[a]	3.2	2.0	8.68	6.4	2:1	90	1.24	1.20	3.00
5	W.C.	40[a]	3.0	2.0	10.1	6.0	2:1	120	1.24	1.20	3.00
6	W.C.	20	2.0	1.0	6.40	4.0	2:1	60	.405	.311	2.00
6A	W.C.	20	2.0	1.0	6.40	4.0	2:1	120	.405	.311	2.00
1[b]	O.B.	12[a]	1.0	1.0	1.50	2.0	2:1	90	.238	.230	1.00
2[b]	O.B.	12[a]	1.0	1.0	1.50	2.0	2:1	90	.238	.230	1.00
3[b]	O.B.	12[a]	1.0	1.0	2.25	2.0	2:1	90	.238	.230	1.00
4[b]	O.B.	12[a]	1.0	1.0	2.25	2.0	2:1	90	.238	.230	1.00
5[d]	O.B.	12[a]	1.0	1.0	2.25	2.0	2:1	90	.238	.230	1.00
6	O.B.	12[a]	1.0	1.0	2.25	2.0	2:1	90	.238	.230	1.00
7	O.B.	12[a]	0.5	0.5	3.25	1.0	2:1	90	.238	.230	0.75
7A	O.B.	12[a]	0.5	0.5	3.25	1.0	2:1	90	.238	.230	0.75
8	O.B.	12[a]	0.5	0.5	3.25	1.0	2:1	90	.238	.230	0.75
9	O.B.	12[a]	0.5	0.5	3.25	1.0	2:1	90	.238	.230	0.75
10	O.B.	12[a]	1.0	1.5	2.50	2.0	2:1	90	.519	.517	1.25
11	O.B.	12[a]	1.0	1.5	2.50	2.0	2:1	90	.519	.517	1.25
12	O.B.	12[a]	1.0	1.5	2.50	2.0	2:1	90	.519	.517	1.25
13	O.B.	12[a]	1.0	1.5	2.75	2.0	2:1	90	.519	.517	1.25
14	O.B.	12[a]	1.0	1.5	2.75	2.0	2:1	90	.519	.517	1.25
15	O.B.	12[a]	1.0	1.5	2.75	2.0	2:1	90	.238	.230	1.25
16	O.B.	12[a]	1.0	1.5	2.75	2.0	2:1	90	.238	.230	1.25
17	O.B.	12[a]	1.0	1.5	3.00	2.0	2:1	90	.519	.517	1.25
18	O.B.	12[a]	1.0	1.5	3.00	2.0	2:1	90	.519	.517	1.25
19	O.B.	12[a]	1.0	1.5	3.00	2.0	2:1	90	.553[r]	.548	1.25
19A	O.B.	12[a]	1.0	1.5	3.00	2.0	2:1	90	.553[r]	.548	1.25
20	O.B.	12[a]	1.0	1.5	3.00	2.0	2:1	90	.553[r]	.548	1.25
21	O.B.	12[a]	1.0	1.5	3.00	2.0	2:1	90	.705	.698	2.00

Table 1. Summary of Model Geometry Values for Spill-through Abutments (see Figure 16) (Continued)

Model No.	Channel Type	B (ft)	h (ft)	W (ft)	L (ft)	r (ft)	α	θ deg	d_m (in)	d_{50} (in)	t (in)
22	O.B.	12[a]	1.0	1.5	3.00	2.0	2:1	90	.705	.698	2.00
23	O.B.	12[a]	1.0	1.5	2.00	2.0	2:1	90	.519	.517	1.25
24	O.B.	12[a]	1.0	1.5	2.00	2.0	2:1	90	.519	.517	1.25
24A	O.B.	12[a]	1.0	1.5	2.00	2.0	2:1	90	.519	.517	1.25
25	O.B.	12[a]	1.0	1.5	0.00	2.0	2:1	90	.519	.517	1.25
26	O.B.	12[a]	1.0	1.5	0.00	2.0	2:1	90	.238	.230	0.75
26A	O.B.	12[a]	1.0	1.5	0.00	2.0	2:1	90	.238	.230	0.75
27	O.B.	12[a]	1.0	1.5	0.00	2.0	2:1	90	.238	.230	0.75
28	O.B.	12[a]	1.0	1.5	0.00	2.0	2:1	90	.238	.230	0.75
29[d]	O.B.	12[a]	1.0	1.5	0.00	2.0	2:1	90	.238	.230	0.75
1	W.C.	12[a]	1.0	1.0	1.5	2.0	2:1	90	2.42	2.43	c
2	W.C.	12[a]	1.0	1.0	1.5	2.0	2:1	90	.761	.705	c
3	W.C.	12[a]	1.0	1.0	1.5	2.0	2:1	90	.171	.180	c
3A	W.C.	12[a]	1.0	1.0	1.5	2.0	2:1	90	.171	.180	c
4[b]	W.C.	12[a]	1.0	1.0	1.5	2.0	2:1	90	.171	.180	0.75
4A[b]	W.C.	12[a]	1.0	1.0	1.5	2.0	2:1	90	.171	.180	0.75
4B[b]	W.C.	12[a]	1.0	1.0	1.5	2.0	2:1	90	.171	.180	0.75
4C[b]	W.C	12[a]	1.0	1.0	1.5	2.0	2:1	90	.171	.180	0.75
5[b]	W.C.	12[a]	1.0	1.0	1.5	2.0	2:1	90	.761	.180	0.75

[a]These models were constructed from one wall only, doubling the effective flume width by assuming symmetry.

[b]These models were constructed with a roughened plate beneath the models.

[c]The riprap extended to the flume floor with no sand core.

[d]The flood plain and low flow channel sides for models 5 through 29 were coated with the d_{50} = 0.230 inch riprap.

[r]The riprap was extremely rounded.

the bed of the low-flow channel. The assumed symmetry of flow produces a low-flow channel 2.0 feet wide from bank to bank.

Side slopes in the low-flow channel and on the abutments were 2H:1V, producing an angle, α, of 26^{o} 34'.

Lengths of the overbank models were varied to investigate the effects of setback shown in Figure 3e. The case in Figure 3f was produced in Models 17 through 22.

Widths of embankments in the direction of flow were also varied to investigate the effect of this variable on the flow field and stability of the embankment material.

Mean riprap sizes for the model spill-through abutments ranged from 0.19 to 2.50 inches in diameter. Sieve analyses of samples of each class were taken to obtain the d_m values listed in Table 1.

Testing Procedure

In order to evaluate the validity of the design procedures in Chapter III, all the model embankments in Table 1 were tested to failure.

Incremental increases in the discharge were applied until the beginning of visual losses of embankment riprap. After determining if the losses were continuous or intermittent, the discharge was again increased by small increments until continual failure of the riprap occurred.

Testing to failure was accomplished in the outdoor flume with repeated increases of the discharge. The upstream water surface and velocity distribution were smoothed with a series of floating baffles and hardware-cloth screens, and the discharge was measured with a rectangular 24 by 36 inch orifice in the supply line (Figure 37).

Testing to failure in the 6-foot wide flume (Figure 36) was accomplished with control of the depth downstream of the model. The discharge was increased to a point close to failure conditions, and the tailwater was adjusted to a pre-determined value by the addition or release of water in the recirculating flume. This process allowed measurements of velocity and depth data for different values of tailwater with all other variables being held constant. Additional increments of discharge were then applied until failure occurred. The depths upstream and downstream of the model were recorded for each increment of discharge, providing a record of the depth field during failure conditions. An 11 by 14 inch orifice in the supply line for this flume was used for discharge measurements.

Depths in the 6-foot wide flume for the overbank tests were controlled in order to approximate prototype design floods with a return period between 50 and 100 years. Flood plain depths of flow equal to approximately twice the depth above the low-flow channel bed were observed from available prototype crossings, and this ratio was applied in the tests.

Velocity Data

In order to describe and evaluate the flow properties in the vicinity of spill-through bridge abutments, velocity and depth data were taken at constant discharge for several of the models listed in Table 1. The discharge used for data collection was slightly less than the failure discharge for each model.

Vertical distributions of velocity were recorded at various points in the flow field with a Prandtl pitot tube. The pressure differences from the static and stagnation holes in the pitot tube were converted to velocity values using a pitot calibration obtained earlier in the

investigation. A differential pressure transducer and strip-chart recorder provided time-averaged values of the velocity at each depth of the vertical profile. Depth-integrated averages at each vertical provided a mean velocity through the depth.

Average velocities through the depth were obtained for points upstream and downstream of the constrictions, and for points directly in the flow area between the abutments. Figures 17 and 18 are typical drawings of the velocity measurements taken, and similar data plots for the other models are available on request.

Depth Data

Depth data were taken in both flumes at various points of a square grid superimposed on the flow field. For the outdoor flume, a two by two foot grid was used with smaller subdivisions in the region of rapidly changing depth. A one by one foot grid was used for the 6-foot wide flume with the overbank models.

Traversing point gauges with a measuring accuracy of 0.001 ft were referenced to the mean flume bed at each point in the grid and were used for flow depth and bed scour measurements.

Water surface contour maps were drawn from the depth measurements to provide a visual interpretation of the flow. Figures 19 and 20 are typical drawings of the patterns noted.

Characteristics common to all the model embankments included the steep water surface gradients at the nose, the standing surface waves in the contraction, the flow separation at the abutment, the contracting jet downstream, and the turbulent wake and stagnation zones bordering the expanding jet.

Photographic Data

To provide a visual record of the model abutment failures, still photographs of the flow and scoured abutments were taken at different discharge values during the failure of each abutment. These photographs were later used for qualitative interpretation of critical scour zones and extent of scour at various discharge values.

Figures 21 through 28 depict a typical sequence of photographs taken during the failure of one of the wide-channel models listed in Table 1. The first photograph is a view looking downstream in the 20-foot wide flume showing the headbox, instrument carriage, and the series of floating baffles. Figures 22 and 23 illustrate the water surface characteristics at a discharge of 11.1 cfs. Some scour and deposition of the left abutment material due to the discharge of 11.1 cfs can be seen in Figure 24. Figure 25 reveals the failed form after passing a discharge of 12.7 cfs. The scoured material was for the most part deposited on the abutment slope in the separation wake.

Scour on the right abutment in Figure 24 was minor at the discharge of 12.7 cfs. In order to facilitate failure of this abutment, the downstream abutment was protected with a larger riprap size. Figures 26 through 28 reveal the scour stages for the upstream abutment after the downstream abutment had been armored.

Figures 29 through 34 illustrate a typical series of photographs taken during the testing of an overbank model. In this case the abutment was set back from the bank of the low-flow channel shown on the right in Figure 30. Scour of the riprap material was occurring when both photographs for Figures 31 and 32 were taken.

Data Analysis

The objective of the experimental program was the verification of the proposed design procedures for model embankments. Due to the limited number of tests for which velocity and depth data were collected, experimental relationships among the many possible variables could not be derived. Future research and additional analyses of the data from this research are necessary to provide these relationships.

Sufficient velocity and depth data at discharges less than the failure discharge were collected for comparison with the theoretical design velocity, V_d, given in the last chapter, and with the theoretical backwater, h_1^*, and water surface drop, Δh, computed from reference 14. Verification of the riprap design was based on the assumption that the theoretical design velocities and backwater were accurate at failure conditions.

Backwater and Design Velocities

The backwater, h_1^*, and the total water surface drop, Δh, through the constriction were computed using the methods in Chapter III for each of the models for which velocity and depth data were taken. Comparisons of measured values with theoretical values are shown in Table 2. Verification of the methods in reference 14 are presented therein, and Table 2 is intended only as a comparison of measured and theoretical values. Verification of the stable design of riprap is presented in the next section.

The velocity, V_d, listed in Table 2 was computed from the theoretical value of Δh and the equation

$$V_d = \sqrt{2g\Delta h + \alpha_1 V_1^2} \quad .$$

Table 2. Comparison of Measured and Theoretical Velocities and Backwater for Spill-through Abutments

Model No.	Chnl Type	Maximum[a] Recorded Velocity (fps)	Theory V_d (fps)	Δh_m[c]	Δh_t[e]	$\frac{\Delta h_m - \Delta h_t}{\Delta h_m}$ (%)	$\frac{V_t}{V_d}$[d] (%)	$\frac{Q_b}{Q}$
1	W.C.	2.05[b]	3.01	.128	.133	-3.9	65.7	.359
2	W.C.	2.57[b]	3.10	.145	.141	2.8	82.9	.361
3	W.C.	3.80[b]	4.75	.228	.335	-46.9	80.0	.339
4	W.C.	4.73[b]	6.57	.430	.656	-52.6	69.7	.331
5	W.C.	5.08	4.98	.468	.366	21.8	60.8	.396
6	W.C.	3.44[b]	4.20	.201	.271	-34.8	81.9	.211
1	O.B.	2.44	2.74	.099	.102	-3.0	89.0	.559
2	O.B.	2.80[b]	3.42	.143	.167	-16.8	79.5	.574
3	O.B.	2.51[b]	3.14	.120	.146	-21.7	74.5	.455
4	O.B.	3.11	3.74	.188	.209	-11.2	71.9	.480
5	O.B.	2.45[b]	3.47	.131	.176	-34.4	65.7	.525
6	O.B.	3.13	3.80	.207	.212	-2.4	65.8	.547
7	O.B.	2.53[b]	3.18	.129	.146	-13.2	79.6	.574
11	O.B.	4.06	4.16	.296	.258	12.8	62.2	.475
14	O.B.	4.58	4.41	.347	.293	15.6	69.8	.427
19	O.B.	4.04	4.50	.303	.308	-1.7	72.2	.406
24	O.B.	4.37	4.34	.317	.274	14.6	72.1	.537
29	O.B.	3.50	3.73	.192	.138	28.1	86.9	.813

[a] Averaged through the depth.

[b] These velocities are the values at the model centerline or in the expanding jet -- vena contracta velocities were not recorded.

[c] Maximum measured water surface drop, excluding the stagnation depth.

[d] The average velocity through the depth at the toe along the abutment centerline.

[e] Theoretical water surface drop from Appendix B.

Most of the velocity data were measured in the vicinity of the embankment side slopes and abutment nose near the riprap surfaces. As a result, the maximum velocities in the vena contracta were not recorded for all the models. However, the agreement between the measured and theoretical design velocities for the cases where vena contracta velocities were measured suggests that the theoretical values of V_d closely approximate the maximum values in the flow field.

Ratios of the toe velocity at the abutment centerline to the design velocity are tabulated in Table 2. Based on these data, the average ratio of V_t/V_d is 0.75, or $V_t = 0.75\ V_d$. The suggested use of V_t for design of the toe and abutment protection was based on this laboratory observation.

Values of velocity greater than the values at the centerline toe were recorded upstream of the model centerline at the point of maximum curvature of the toe. Studies by other investigators (54, 55) revealed the greatest scour at this point in the flow, and these observations indicate that the greatest amount of toe protection is required for this region.

Computed and measured values of Δh deviate significantly for some of the models listed in Table 2. Depth measurements for the wide channel flow models 3, 4, and 6 were not taken far enough upstream to include the point of maximum backwater. The water surface contours for these models indicated an increasing water surface elevation at the farthest upstream point for which data were taken. The measured values of Δh for the models are therefore less than the actual drop.

Model 5 was skewed from one wall of the flume only, thereby violating the assumption of symmetry for one-sided models. The

theoretical water surface drop was derived using the assumption of symmetry, and this may account for the difference indicated in Table 2.

Maximum backwater was measured for the overbank flow cases listed in Table 2, and comparisons with theoretical values of Δh are tabulated. Deviations greater than 20 percent were found for three of the models, and the discrepancies may be attributed to the use of theoretical values derived from sloping flumes and river channels for horizontal flumes. Normal stage does not exist in horizontal flumes, and recommendations found in the literature suggest that the average depth in the upstream portion of the constriction may be used for h_n in backwater computations. The average depth above the low-flow channel across the channel from point A in Figure 5 was substituted for h_n in computing the theoretical backwater and water surface drop for the models listed in Table 2.

Upstream Velocities

Values of depth-averaged velocities were recorded at several points along the upstream slopes of the embankments for all the models listed in Table 2. Figure 35 illustrates a comparison of the measured and theoretical upstream velocities. The solid lines are based on data from the models listed in Table 2, and the dashed lines are reproductions of Fields' curves from Figure 4. Insufficient data were taken for the skewed models, and the curves in Figure 35 apply only to normal crossings. Eccentric crossings (Figure 3d) may be treated as two non-eccentric abutments by assuming symmetry for each side with respect to the flow centerline.

For values of M' greater than 0.20, the solid experimental curves in Figure 35 predict larger values of upstream velocities than do the

theoretical curves. Stagnation, or zero velocity, occurred for all the model embankments at a value of x/L approximately equal to 0.3. Stagnation for prototype crossings occurs at $x/L = 0$, and the solid curves are not extended to the abscissa for this reason. Any design based on Figure 35 should utilize the empirical curve for large values of x/L and the theoretical curve for smaller values.

Riprap Stability

Stability of riprap on the spill-slopes of spill-through abutments was investigated for both overbank and wide channel flow conditions. Table 3 lists the measured failure discharge and computed parameters for all the model abutments that were tested to failure. The listed failure discharges represent the values at which riprap particles were being lifted from the slope and washed downstream. These values all fell between the points of initial loose-gravel movement and continual losses.

Abutment riprap for models 1, 2, and 3 in the 20-foot outdoor flume (Table 1), and for model 1 in the 6-foot wide flume with wide channel flow could not be failed due to oversized riprap or from riprap sloughing into the scour hole downstream of the models. Abutment spill-slope riprap failure from drag and lift forces occurred for all the models listed in Table 3.

Initial riprap losses for the model abutments usually occurred on the upstream abutment shoulder whenever the flow depth was great enough to approach the roadway elevation and produce a small radius of curvature of the flow around the shoulder. However, when the radius became larger due to shallow upstream and downstream depths relative to the embankment height, initial riprap losses occurred slightly downstream of the embankment centerline near the toe of the spill-slope.

Table 3. Computed Values at Failure Conditions for Model Spill-through Abutment Riprap

Model No.	Chnl Type	Flume Width ft	Failure[a] Q_f cfs	$\frac{Q_b}{Q}$	Δh ft	V_d fps	V_t fps	d_m ft	D ft	$\frac{d_{50}}{D}$	$\frac{u_r}{V_t}$	u_r fps	n	S
4	W.C.	20	85.6	.341	.618	6.39	4.79	.103	1.573	.064	.47	2.25	.370	1.11
5	W.C.	20	96.8	.408	.392	5.17	3.88	.103	1.697	.059	.46	1.78	.231	1.24
6	W.C.	20	15.2	.221	.407	5.14	3.86	.0338	1.076	.024	.40	1.54	.527	.89
6A	W.C.	20	10.3	.207	.271	4.20	3.15	.0338	.956	.027	.40	1.26	.353	1.00
1	O.B.	6	7.40	.561	.128	3.06	2.30	.0198	.483	.040	.43	.989	.372	.99
2	O.B.	6	4.30	.564	.147	3.23	2.42	.0198	.264	.073	.48	1.16	.512	.90
3	O.B.	6	3.50	.453	.182	3.50	2.62	.0198	.270	.071	.48	1.26	.604	.85
4	O.B.	6	2.64	.500	.199	3.65	2.74	.0198	.177	.108	.52	1.42	.767	.76
5	O.B.	6	3.14	.526	.184	3.55	2.66	.0198	.268	.072	.48	1.28	.623	.84
6	O.B.	6	3.32	.542	.274	4.29	3.22	.0198	.212	.090	.50	1.61	.986	.67
7	O.B.	6	1.88	.593	.151	3.23	2.42	.0198	.145	.132	.55	1.33	.673	.81
7A	O.B.	6	2.20	.568	.162	3.33	2.50	.0198	.172	.112	.52	1.30	.643	.82
8	O.B.	6	2.08	.607	.236	3.99	2.99	.0198	.132	.145	.56	1.67	1.060	.64
9	O.B.	6	2.64	.526	.128	2.98	2.24	.0198	.248	.077	.49	1.10	.460	.93
10	O.B.	6	4.50	.467	.263	4.20	3.15	.0432	.346	.124	.54	1.70	.503	.95
11	O.B.	6	5.06	.468	.351	4.83	3.62	.0432	.337	.128	.54	1.95	.661	.85
12	O.B.	6	4.90	.471	.358	4.88	3.66	.0432	.323	.133	.55	2.01	.703	.83
13	O.B.	6	4.60	.423	.292	4.40	3.30	.0432	.383	.112	.52	1.72	.514	.94
14	O.B.	6	4.66	.429	.372	4.95	3.71	.0432	.343	.126	.54	2.00	.696	.83
15	O.B.	6	2.66	.478	.273	4.25	3.19	.0198	.212	.091	.50	1.60	.973	.67
16	O.B.	6	2.82	.483	.326	4.64	3.48	.0198	.205	.094	.50	1.74	1.151	.61
17	O.B.	6	3.60	.397	.364	4.89	3.67	.0432	.306	.141	.55	2.02	.710	.82
18	O.B.	6	3.42	.405	.378	4.97	3.73	.0432	.281	.153	.57	2.13	.789	.78
19	O.B.	6	3.40	.401	.350	4.79	3.59	.0461	.292	.156	.57	2.05	.684	.80
19A	O.B.	6	3.54	.396	.343	4.74	3.56	.0461	.310	.147	.56	1.99	.645	.82
20	O.B.	6	3.72	.398	.400	5.11	3.83	.0461	.301	.152	.56	2.14	.746	.77
21	O.B.	6	4.48	.377	.336	4.70	3.53	.0588	.404	.144	.56	1.98	.501	.97
22	O.B.	6	6.16	.371	.464	5.52	4.14	.0588	.472	.123	.54	2.24	.642	.88
23	O.B.	6	5.88	.539	.309	4.59	3.44	.0432	.333	.129	.54	1.86	.602	.89
24	O.B.	6	6.42	.534	.279	4.38	3.28	.0432	.382	.123	.54	1.77	.545	.92
24A	O.B.	6	5.80	.539	.297	4.51	3.38	.0432	.335	.129	.54	1.82	.576	.90
25	O.B.	6	5.80	.540	.312	4.62	3.46	.0432	.327	.132	.55	1.90	.628	.87
26	O.B.	6	5.52	.806	.147	3.63	2.72	.0198	.226	.085	.49	1.33	.672	.81
26A	O.B.	6	6.54	.804	.144	3.65	2.74	.0198	.265	.072	.48	1.32	.662	.81
27	O.B.	6	7.44	.804	.141	3.64	2.73	.0198	.299	.064	.46	1.26	.604	.86
28	O.B.	6	7.78	.806	.106	3.27	2.45	.0198	.339	.057	.45	1.10	.461	.93
29	O.B.	6	10.40	.808	.174	4.05	3.04	.0198	.372	.052	.44	1.34	.683	.80
2	W.C.	6	12.00	.587	.124	3.06	2.30	.0634	.777	.076	.48	1.10	.143	1.29
3	W.C.	6	6.80	.536	.104	2.74	2.06	.0142	.547	.027	.40	.824	.359	.97
3A	W.C.	6	5.00	.531	.062	2.14	1.60	.0142	.523	.029	.41	.656	.228	1.06
4	W.C.	6	5.80	.533	.081	2.43	1.82	.0142	.531	.028	.40	.728	.280	1.03
4A	W.C.	6	6.20	.534	.090	2.56	1.92	.0142	.537	.028	.40	.768	.312	1.00
4B	W.C.	6	6.00	.533	.085	2.49	1.87	.0142	.534	.028	.40	.748	.296	1.01
4C	W.C.	6	6.20	.534	.090	2.56	1.92	.0142	.537	.028	.40	.768	.312	1.00
5	W.C.	6	13.00	.601	.115	2.98	2.24	.0634	.840	.070	.48	1.08	.138	1.29
													average =	.90

[a]Measured failure discharge values have been doubled for models constructed from one wall of the flume. This value was then used in the computation of Δh.

Insufficient data were obtained to accurately define the parameters that determine which mode of failure will occur. The radius of curvature, the water surface drop through the abutments, the length of the embankment in the flow direction, and other variables require further research to accurately define this phenomenon.

The total water surface drop through the constriction, Δh, was computed for each model in Table 3 using the methods presented in reference 14 and Appendix B. Normal depth, h_A, was defined as the average stage across the channel at point A in Figure 5, and the failure discharges in Table 3 were substituted for design discharges in the computations of Δh for each model.

The discharge for which initiation of motion occurred in each model has been recorded in Table 3. Theoretically, initiation of motion should occur when the safety factor, S, is unity. The model data given in Table 3 was analyzed according to the equations recommended for design in Chapters II and III. The safety factor, S, was computed for each model test in the following manner:

1. In model test 4 W.C., for example, the failure discharge was 85.6 cfs.

2. According to the model geometry and the backwater calculations outlined in Appendix B,

$$\Delta h = 0.618 \text{ ft},$$

and

$$V_d = \sqrt{2g\Delta h + \alpha_1 V_1^2}$$

$$= 6.39 \text{ fps}.$$

3. The toe velocity, V_t, is

$$V_t = 0.75\ V_d$$

$$= 0.75 \times 6.39 = 4.79 \text{ fps.}$$

4. The riprap used in model 4 W.C. was slightly angular with

$$d_{50} = 0.100 \text{ ft,}$$

and

$$d_m = 0.103 \text{ ft,}$$

indicating that the riprap was uniformly graded. According to Figure 7, the angle of repose is

$$\phi = 37 \text{ deg}$$

for this rock.

5. The depth of flow at the toe, D, is approximated by the normal depth, h_n, or

$$D = 1.573 \text{ ft.}$$

6. The ratio of the rock size to depth of flow at the toe is

$$\frac{d_{50}}{D} = \frac{0.100}{1.573} = 0.064.$$

7. From Figure 10, the ratio of the bed velocity u_r to the average toe velocity is

$$\frac{u_r}{V_t} = 0.47 \quad .$$

Therefore, $u_r = 0.47 \times 4.79 = 2.25$ fps.

8. The stability factor, η, for the model flow condition is

$$\eta = \frac{0.4\ u_r^2}{(G-1)g\ d_m}$$

$$= \frac{0.4 \times 2.25^2}{(2.65-1)32.2 \times 0.103} = 0.370 \quad .$$

9. The stability factor, η', for the 2H:1V side slope is determined from

$$\tan \beta = \frac{\eta \tan \phi}{2 \sin \theta}$$

$$= \frac{0.370 \times .754}{2 \times .448} = 0.311 \quad ,$$

$$\beta = 17.3 \text{ deg},$$

$$\lambda = 0 \text{ deg (assumed)},$$

$$\delta = 90 - \lambda - \beta$$

$$= 90 - 17.3 = 72.7 \text{ deg.}$$

$$\cos\delta = .297 \quad ,$$

$$\eta' = \frac{1 + \cos\delta}{2}\ \eta$$

$$= \frac{1.297}{2} \times .370 = 0.240.$$

10. The computed safety factor for model 4 W.C. is

$$S = \frac{\cos\theta \ \tan\phi}{\eta' \tan\phi + \sin\theta \cos\beta}$$

$$= \frac{0.894 \times 0.754}{0.240 \times 0.754 + 0.448 \times 0.955}$$

$$= 1.11 \quad .$$

Theoretically, S should be unity for initiation of motion conditions.

The average of the 45 computed safety factors is 0.90 for the observed initiation of motion in the models. The anticipated safety factor was unity. The conclusion is that if each model riprap size had been designed by the recommended design procedure, using S = 1.5 and the given model discharge and geometry, then no model would have failed at the design discharge.

Summary

Verification of the design of riprap for the sloping tips of spill-through abutments was accomplished by a "reverse" design consisting of measured failure conditions and theoretical indications of instability. The validity of this method is based on the theoretical indication of instability when instability did in fact occur. Another way to verify the design method would be to compute theoretically stable riprap sizes for the given flow and geometric conditions using a safety factor of 1.0. Tests could then be conducted to determine if the designed riprap was in fact stable at the design discharge and unstable at larger discharges.

As stated earlier, effects of each possible variable for bridge crossings were not evaluated. The design procedure includes most of the variables in some form, and the parameters which were varied in the experimental program appeared to incorporate satisfactorily into the design procedure. Various values of set back, riprap angularity, flow depth, channel type, riprap size, abutment width, skewness, and bed scour conditions all entered the computations for stability.

Prototype construction based on the design methods will provide the final verification of the theory presented herein. Data from prototype crossings enter in the computations of the water surface drop, Δh, through the constriction, but no data were available for prototype verification of the proposed riprap designs.

Chapter V

DESIGN EXAMPLE

An example of the design of stable riprap protection for a prototype bridge crossing is presented in this chapter. The example was obtained from reference 14, which included the backwater computations for the crossing. Stabilization techniques based on all the steps in Chapter III are presented and summarized in Figure 39 to illustrate the intended design procedures.

Design Example (Normal Crossing with Spill-through Abutments Set Back from the Low-Water Channel)

Given:

Design discharge = 19,500 cfs

h_n = 28.0 ft above datum

S_o = 2.6 ft/mi = 0.00049 ft/ft

Spill-through abutments with 2H:1V side slopes

Cross section and plan shown in Figure 38

Step 1. Computed Parameters

a) By planimetering, A_{n2} is found to be 2,534 sq ft, assuming no time for scour to occur.

b) From the equivalent trapezoid (Figure 38), $\bar{h}_{n2}$ is 12.35 ft.

c) For the spill-through abutment, the value of b is found from $b = A_{n2}/\bar{h}_{n2}$ = 2,534/12.35 = 205 ft, and Q_b is computed by Mannings' equation as 12,040 cfs. This is the unconstricted design discharge flowing in the width, b (Figure 38).

d) The opening ratio is found from $M = Q_b/Q$ = 12,040/19,500 = 0.62.

e) The cross-sectional flow area, A_n, in the unconstricted channel is planimetered from Figure 38 and found to be 5,664 sq ft.

f) The average velocity in the unconstricted channel is

$V_n = Q/A_n = 19,500/5,664 = 3.44$ fps.

g) The average velocity in the constriction is

$V_{n2} = Q/A_{n2} = 19,500/2,534 = 7.70$ fps.

h) The critical depth in the constriction at design discharge for the equivalent trapezoid is $h_{2c} = 6.76$ ft. This value required seven iterations of the method presented in Chapter III, using $b_r = 190$ ft, and $m = 2.0$.

i) The critical average velocity in the constriction is

$V_{2c} = Q/A_{2c} = 19,500/1,376 = 14.17$ fps.

j) The critical depth in the unconstricted channel flowing at design discharge is not required for this design because the flow is assumed subcritical. Critical depth for the whole channel would be less than critical depth for the constricted channel.

k) The velocity correction coefficient for the seven subsections in Figure 38 is

$$\alpha_{1n} = \frac{\sum_{i=1}^{7} Q_i V_i^2}{Q V_n^2} = \frac{374,895}{19,500(3.44)^2} = 1.62 \quad .$$

Step 2. Backwater

a) The methods of reference 14 are selected for backwater computation (Appendix B).

b) Using the computed values from step 1 and assuming a non-scoured condition, the backwater, h_1^*, is found to be 1.13 ft, and the total

drop through the constriction, Δh, is 1.89 ft. Checking the flow classification, the minimum depth above datum is $h_3 = h_n + h_1^* - \Delta h + S_o L_{1-3}$. From Figure B.13, using $\Delta h/\bar{h}_{n2} = 1.89/12.35 = 0.153$ one obtains a value of 0.78 for L^*/b, and $L^* = 0.78 \times 205 = 160$ ft. The embankments are 70 ft wide, and the minimum depth is $h_3 = 28.0 + 1.13 - 1.89 + 0.00049 \times (160 + 70)$ or 27.3 ft above datum. Critical depth in the constriction was found to be 6.76 ft (step 1h) so that critical depth is 6.76 + 15.65 (Figure 38), or 22.41 ft above datum (Figure 38). The flow classification is therefore subcritical.

c) Assume that waves are expected at the upstream and downstream embankments during the flood. Assume also that the river is straight for a distance of 1500 ft in each direction, and that channel bends occur at both extreme points. The fetch length, F, is therefore 1500 ft, and the fetch width may be taken as the river width, or 745 ft. This analysis assumes that a 40 mph, or 58.7 fps, wind will come from the upstream direction.

The effective fetch length is computed as $F_e = 1.17\ F^{1/3} W_F^{2/3} = 1.17 \times (1500)^{1/3} \times (745)^{2/3} = 1096$ ft, and the significant wave height is

$$H = \frac{V_w^2}{g}\ 3.23 \times 10^{-3} (gF_e/V_w^2)^{0.435} = \frac{(58.7)^2}{32.2}\ 3.23 \times 10^{-3}\ \left[\frac{32.2(1096)}{58.7^2}\right]^{0.435},$$

or $H = 0.95$ ft.

d) The minimum embankment height above datum is the sum $h_n + h_1^* + H$, or 28.0 + 1.13 + 0.97, or 30.1 ft. The proposed roadway is at an elevation of 30.0 ft.

Step 3. Design Velocity

a) Using the value from step 1k of $\alpha_{1n} = 1.62$, and computing A_1 as $A_n + h_1{}^*B$, or 5,664 + 1.13 x 745, or 6506 sq ft, then $V_1 = Q/A_1 = 19{,}500/6506$, or $V_1 = 3.00$ fps.

b) The vena contracta design velocity is

$$V_d = \left(2g\Delta h + \alpha_1 V_1^2\right)^{\frac{1}{2}} = \left(2(32.2)(1.89) + 1.62(3.00)^2\right)^{\frac{1}{2}} = 11.68 \text{ fps.}$$

c) The toe velocity is $V_t = 0.75 \times V_d = 0.75 \times 11.68 = 8.76$ fps.

Step 4. Toe Protection

a) Assuming that the bed material in the constriction has a mean diameter of 0.8 ft, and obtaining $h_1 = 8.6$ ft by adding $h_1{}^*$ (1.13 ft) to the depth below normal stage at the abutment (7.5 ft), then

$$\frac{\tau_o'}{\tau_c} = \frac{V_1^2}{120 D_s^{2/3} h_1^{2/3}} = \frac{(3.00)^2}{120(0.8)^{2/3}(8.6)^{2/3}} ,$$

or

$$\frac{\tau_o'}{\tau_c} = 0.0212.$$

b) The average roadway approach length is 265 ft, and the effective length is

$$L_e = L + \frac{b'-b}{2} = 265 + \frac{229 - 205}{2} = 277 \text{ ft.}$$

An eccentric crossing would require a value of L_e for each approach.

c) The ratio, L_e/h_1, is 277/8.6, or 32.2. From Figure 13, the ratio of d_{se}/h_1 is 1.5. Solving for d_{se} produced a value of

1.5 x 8.6, or 12.9 ft. A value of 15 ft would include some allowance for safety.

d) Sheet piles are not used for this crossing.

e) Riprap toe protection for this example is to be placed (on a slope of 2H:1V) to a depth of 15.0 ft below the bed.

f) Horizontal riprap layers at the abutment toe are not recommended for this design.

g) A riprap layer thickness equal to either 2.0 times the maximum diameter or 3.0 times d_m, whichever is greater, is suggested.

h) The bed material should be excavated and the riprap placed and backfilled with the excavated material.

i) For this example, the protection for the abutment toe is to be the same size and placed on the same slope as the riprap for the spill-slope above the bed level. The size will be determined in step 5 for the spill-slope and should extend from the roadway at the abutment top because of the results of step 2. The riprap should also be placed to the scour depth determined in step 4e. If field evidence indicates that the low-flow channel is migrating, precautions must be taken to prevent the channel from migrating over against one of the abutments. If migration is possible, training works will be required to either prevent migration or allow for abutment protection after migration. If migration is allowed, steps 1 through 5 will need to be repeated using a cross-section which places the low-flow channel against one of the abutments. The end result will be greater expected scour depths at the abutment, and greater depths requiring protection. Economic considerations will determine if training works upstream or additional riprap protection at the abutment is better.

Step 5. Riprap Sizing

a) The riprap size, d_m, is determined here for the spill-slope of the abutment, and any riprap having this parameter is to be placed both above and below the bed level on the spill-slope.

b) The geometry of the bridge crossing is known and the riprap size is desired for this example.

c) The recommended procedure given in Chapter II, step 5c, follows:

Check if it is possible to obtain a safety factor of 1.5. On the 2H:1V side slope. From Figure 11, with θ = 26.6 deg (2H:1V), n is found to be greater than zero if the angle of repose, ϕ, is greater than 37 deg. Hence, it will be possible to obtain a safety factor of 1.5 only if $\phi > 37^o$. Because the side slope angle and safety factor are given, Option 1 is chosen to determine the required rock size. The steps in this option follow:

1. Estimate u_r; since d_{50} is unknown, choose

$$u_r = 0.45\ V_t$$

$$= 0.45 \times 8.76 = 3.94 \text{ fps.}$$

2. Estimate a value for ϕ. The anticipated d_{50} for the riprap should be between 6 inches and 15 inches. From Figure 7 the angle of repose should be approximately 40 deg so that

$$\tan\phi = 0.839 \quad .$$

3. Compute S_m from

$$S_m = \frac{\tan\phi}{\tan\theta}$$

$$= \frac{.839}{.500} = 1.68 \quad .$$

$S_m > S = 1.5$, therefore continue.

4. Compute the stability factor, η, from

$$\eta = \left(\frac{S_m^2 - S^2}{SS_m^2} \right) \cos\theta$$

$$= \left(\frac{1.68^2 - 1.5^2}{1.5 \times 168^2} \right) \times 0.894$$

$$= \frac{0.57}{4.23} \times .894 = 0.120 \quad .$$

5. Compute the required rock size, d_m, from

$$d_m = \frac{0.4\ u_r^2}{(G-1)g\eta}$$

Assume $G = 2.65$

$$d_m = \frac{0.4 \times 3.94^2}{1.65 \times 32.2 \times 0.120}$$

$$= 0.97 \text{ ft.}$$

6. For dumped riprap, the recommended upper limit for d_m/d_{50} is 1.4. The minimum value for d_{50} is therefore

$$d_{50}(\text{min}) = \frac{0.97}{1.4} = 0.69 \text{ ft}$$

7. Compute d_{50}/D; from Figure 38, the depth at the toe is

$$D = 10 \text{ ft},$$

and

$$\frac{d_{50}}{D} = \frac{0.69}{10.0} = 0.07 \quad .$$

The estimated value of u_r may be checked from this ratio and Figure 10 using the value of V_t from step 3c. From Figure 10,

$$\frac{u_r}{V_t} = 0.47 \quad ,$$

and

$$u_r = 0.47\ V_t$$

$$= 0.47 \times 8.76 = 4.12 \text{ fps}$$

Repeated trials of steps 1 through 7 produce the final values of:

$u_r = 4.3$ fps,

$\phi = 40$ deg,

$S_m = 1.68$,

$n = 0.12$,

$d_m = 1.16$ ft

and $d_{50} = 0.83$ ft.

8. Obtain the correct value for ϕ. From Figure 7, for d_{50} = 0.83 ft or 10.0 inches,

$$\phi = 40 \text{ deg, approximately.}$$

9. Recompute S_m from

$$S_m = \frac{\tan\phi}{\tan\theta}$$

$$= \frac{0.839}{0.500} = 1.68 \quad .$$

Recompute η from

$$\eta = \left(\frac{S_m^2 - S^2}{S\, S_m^2} \right) \cos\theta$$

$$= \left(\frac{1.68^2 - 1.5^2}{1.5 \times 1.68^2} \right) 0.894$$

$$= 0.120 \quad .$$

Recompute d_m from

$$d_m = \frac{0.4\, u_r^2}{(G-1) g\, \eta}$$

$$= \frac{0.4 \times (4.3)^2}{(2.65-1) 32.2 \times 0.120}$$

$$= 1.16 \text{ ft.}$$

The required rock riprap should therefore have:

Minimum d_m = 1.2 ft (14.4 in)

Minimum d_{50} = 0.8 ft (9.6 in).

That is, if a d_m of 14.4 in. is used, then the d_{50} size should not be less than 9.6 in. The selected gradation should also act as a filter for the embankment filter material.

Step 6. Abutment Spill-slope Protection

a) Riprap having the d_m and d_{50} sizes determined in step 5 is to be placed as toe protection and as spill-slope protection. The extent of wrap-around for this riprap is determined for the upstream and downstream sides in step 7 and 8.

b) The thickness of the riprap layer determined from step 4g is $3\ d_m$, or 3 x 14.4, or 43.2 inches. If d_{100} is greater than 21.6 in., then the thickness should become $2\ d_{100}$.

c) Due to the large size of the spill-slope riprap, it is desired to use a smaller size of riprap on the sides of the approach embankments. The large riprap should begin at point G in Figure 5 and should terminate somewhere between points E and H. Using the value from step 2b of 160 ft for L^*, and substituting the value of V_{n2} for V_2 results in a length, L, of

$$L = \left[1 - \frac{V_n}{V_2}\right] L^* = \left[1 - \frac{3.44}{7.70}\right] 160 ,$$

or L = 88.6 ft. The 14-inch riprap is to extend from point G, around the abutment, to point E or point H in Figure 5. Point H is chosen for this example even though point E or some point between E and H could be chosen. Step 8c illustrates a better method for determining the distance L when wave forces are not anticipated. Steps 7 and 8 provide the required riprap size for the remaining unprotected side slopes.

d) Either gravel or filter-cloth filter layers could be used beneath the riprap layer depending on economic considerations. Assume, for illustrative purposes, that a gravel layer is desired and that the embankments are constructed from a material having values of 0.2, 1.0, and 4.0 inches for the d_{15}, d_{50}, and d_{85} sizes. The riprap filter layer determined from the T-V specifications would require values of

d_{15} (Filter) < 20 in ,

0.8 in < d_{15} (Filter)< 4 in, and

d_{50} (Filter) < 25 in .

Any filter satisfying the three inequalities should prevent losses of the embankment material.

The thickness of the gravel filter layer should be computed as the larger of 2.0 times the maximum filter sone diameter or 3 times the d_m size of the filter material.

Step 7. Downstream Side Slope Protection

a) The riprap size required for wave force stability for the downstream embankment side slopes is obtained from

$$W_s = \frac{\gamma_s H^3}{3.2(S_s-1)^3 \cot\theta} = \frac{165(0.95)^3}{3.2(2.65 - 1)^3(2)}$$

or W_s = 4.92 lb per sone. The equivalent spherical diameter assumed equal to the d_m size for a 4.92-lb stone is

$$d_m = \left[\frac{8}{4\pi/3}\left(\frac{W_s}{\gamma_s}\right)\right]^{1/3} = \left[\frac{8}{4\pi/3}\left(\frac{4.92}{165}\right)\right]^{1/3}$$

or 0.385 ft (4.62 in.). The downstream protection should be a well-graded riprap with d_m = 4.6 in.

b) Wind-generated waves produced the required riprap size for the downstream slopes in the last step.

c) The 4.6-inch riprap for the downstream slopes should extend to the top of the embankment (elev. 30.0) because the sum of wave height and normal stage is found to be 29.0 ft.

Figure 14 produces a value of $z \tan\phi/d_{se} = 0.69$ for the downstream face. Using the values of ϕ = 38 deg for the bed material and d_{se} = 12.9 ft (step 4c) results in a value of z = 11.4 ft for the length requiring buried toe protection on the downstream side. The depth

of buried riprap is to vary linearly from bed level at a value of $z = 12$ ft to a depth of 15 ft at a value of $z = 0.0$ (Point G in Figure 5).

d) The same filter material determined from step 6d should be placed beneath the 6.5-inch riprap unless the core material for the downstream side slope is different from the material for the spill-slope.

Step 8. Upstream Side Slope Protection

a) The 14-inch riprap is to extend to point H (step 6c) in Figure 5, and the size required at point H by the velocities of Figure 35 will be placed along the remaining upstream slope to a point where the velocities are smaller than the critical velocity for movement of the embankment material. A minimum value of $d_m = 4.6$ in. was determined from the wave analysis in step 7a.

b) For the normal crossing, point H in Figure 35 occurs at a value of $x = 270 - 89 = 181$ ft (steps 4b and 6c). From Figure 35 and steps 1a and 1b, $M' = 2{,}534/(745 \times 12.35) = 0.275$, and $L = 270$ ft. The value of x/L is 0.67, and $VM'/V_n = 0.325$ is found from the solid lines in Figure 35. Solving for V produces a depth averaged value of $V_t = 4.05$ fps at point H.

c) Repeating step 5, Option 1, with values of $V_t = 4.05$ fps, $\theta = 26^{o}34'$, $S = 1.5$, and D = half the depth below the normal water surface averaged at distances of 89 ft from the ends of each roadway in Figure 36, or $D = (5 \text{ ft} + 11 \text{ ft})/2 = 8$ ft., produces the final values:

u_r = 1.48 fps,

d_m = 0.137 ft = 1.6 inches,

min d_{50} = 0.098 ft = 1.2 inches,

ϕ = 40 deg,

S_m = 1.68,

and η = 0.120.

Because the minimum d_m of 4.6 in. was established by the wave analysis in step 7a, the d_m value of 1.6 in. cannot be used, and the 4.6-inch riprap is to be placed from point H in Figure 5 back to the beginning of the approach embankment.

For illustrative purposes, assume that wind waves are not expected, and it is desired to determine the point along the upstream slope of the approach embankment at which the velocity reduces to the critical value for movement of the embankment material. This point coincides with the point of all riprap termination because the embankment material is no longer subjected to erosive velocities at this point. The method outlined in step 8c of Chapter III would proceed as follows:

Using the embankment core material d_{50} value of 1.0 inch and d_m value of 1.04 inch (step 6d) produces an angle of repose of 40 deg (Figure 7) and a stability factor, η of 0.120 (Figure 11). Using the value of D = 8 ft produces a value of $d_{50}/D = 0.01$ and u_r/V_t is found to be 0.36 from Figure 10. The magnitude of u_r is found from

$$u_r^2 = \frac{(G-1)g\,\eta\,d_m}{0.4} = \frac{1.65 \times 32.2 \times 0.12 \times 0.087}{0.4} = 1.39 \quad ,$$

and

$$u_r = 1.18 \text{ fps.}$$

Because $u_r/V_t = 0.36$, then $V_t = 1.18/0.36 = 3.28$ fps which may be substituted for V in Figure 35 to obtain the value of x at which the riprap may be terminated.

The final step for solution of x involves computing the parameter VM'/V_n or 3.3 (0.275)/3.44, or 0.26. From Figure 35, a value of x/L of 0.61 and a value of L equal to 270 ft produces a value of x equal to 165 ft. Point E in Figure 5 occurs at a value of x equal to 270 ft, and the riprap for the case of no wind waves can be terminated at a point H where L is computed as 270 - 165, or 105 ft. The embankment core material is theoretically stable on the remaining side slope of the approach embankment.

The above value of L = 105 ft (Figure 5) indicates that the value of L = 89 ft obtained from the rational equation in step 6c is not valid for the case with no wind waves. Both values are estimates of the point at which the embankment core material no longer requires riprap protection, and the largest value should be accepted. Riprap sizes smaller than the d_m size for the spill-slope (step 5c) could be placed between points E and H in Figure 5, and the design procedure for these sizes is listed in step 8 of Chapter III.

For the example problem being presented, wind waves are expected, and the 4.6-inch riprap is to be placed along the upstream side slope in Figure 37.

d) If the flood plain along the upstream toe of the approach embankment is to be cleared during construction, the toe will require either buried riprap protection or some other desired form such as finger dikes or flow retards. Assume for this example that buried protection is to be used.

e) For the upstream face, Figure 14 produces a value of 1.0 for $z \tan\phi/d_{se}$. Using the values for ϕ and d_{se} from step 7c produces a value of 16.5 ft for z. This value, rounded to 17 ft, is suggested as an estimate for the length along the upstream face requiring buried riprap protection. The depth of buried riprap is to vary linearly from bed level at a value of z equal to 17 ft (Figure 39a) to a depth of 15 ft at a value of $z = 0.0$ (Point E in Figure 5). The riprap should also extend to the top of the embankment (step 2d).

f) The filter layer determined in step 6d can also be used along the upstream embankment, because the same embankment material is being protected.

Step 9. Pier Protection

a) The piers for the crossing are shown in Figure 38. Three of the piers are placed on the flood plain, and the other two are founded in the low-flow channel.

For the flood-plain piers 1, 2, and 5, the clear water scour depth is

$$d_{se} = 0.00073 \left(\frac{2aV_1}{\nu}\right)^{0.619} = 0.00073 \left[\frac{2(1.25)(3.00)}{1.2 \times 10^{-5}}\right]^{0.619},$$

or $d_{se} = 2.81$ ft. For the other two piers, the scour is $d_{se}^* = 1.42K b_p^{0.75} = 1.42\ (1.3)(3.0)^{0.75}$, or $d_{se}^* = 4.21$ ft.

b) Assume that piers 1 and 5 are positioned close enough to the abutments so that the issuing flow from the spill-slopes strikes the piers at an angle, α, equal to 20 deg as shown in Figure 15, a value of 3.7 is obtained for $K_{\alpha\ell}$, and the expected scour depth at these piers becomes $K_{\alpha\ell}\, d_{se} = 3.7 \times 2.8 = 10.4$ ft. Better estimates of the angle

of flow at these piers are anticipated from continued analytical and experimental work being conducted at CSU.

c) Due to the proximity of piers 1 and 5 with the abutment toes, the abutment protection and pier footings should be founded 15 feet below the bed (steps 5c and 9b). Pier 2 could be founded at any depth greater than 2.8 ft, although overlapping scour holes may cause greater depths than anticipated. Piers 3 and 4 should have footings located at depths greater than 4.2 ft below the low-flow channel bed. If the low-flow channel is allowed to migrate between the abutments (see step 4i) then the scour depths in steps 9a, b, and c, must be re-computed using a cross-section which places the low-flow channel at all possible positions. As in step 4i, training works may be more economical than pier footings founded at greater depths.

Figure 39 summarizes all the recommended stabilization requirements for this example

Step 10. Protection for Special Cases

a) For illustrative purposes, assume that the left flood plain between the abutment tip and the low-flow channel bank is to be maintained for livestock (Figure 38). Assume also that the riprap is to be placed as a horizontal apron and buried under 1 ft of soil as discussed in step 10a of Chapter III. The riprap size determined from step 5c may be used for the horizontal apron, even though a smaller size would be allowed. The size from step 5c was derived for a sloping apron, and step 5 could be repeated using the relationships for horizontal aprons (θ = 0 deg).

The side slope of the low-flow channel should also be protected to a depth of 15 ft below the channel bed (step 4c), preventing migration of the channel.

A value of L* was obtained in step 2b, and the flood plain and channel wall could be protected for this distance upstream and possibly downstream of the crossing. This proposal entails a considerable amount of rock, and it may be more economical to allow the flood plains to scour instead. Occasional replacement of the flood plains could be accomplished during periods of low flow.

b) The bridge crossing shown in Figure 38 was treated as a non-eccentric crossing when the backwater and water surface drop were computed. The abutment lengths of 230 and 300 ft actually produce an eccentric crossing.

The first method of treating eccentric crossings (step 10b of Chapter III) would proceed by concealing half the crossing in Figure 38 and proceeding with steps 1 through 10 as if an identically symmetrical half were being concealed. This procedure would result in backwater values, design velocities, and riprap sizes for the unconcealed half. The process would be repeated for the opposite abutment, resulting in different backwater values, velocities, and riprap sizes. The basic assumption for validity of this procedure is that the flow conditions at the vertical "folding line" for each design are identical. A trial procedure would be required to locate the position of the folding line which provides the same backwater and velocity on each side of the line.

Reference 14 (Appendix B) provides a different method of computing backwater for eccentric crossings without using the trial folding technique. This backwater value can then be used with the folding line placed at the center of the flow distribution to design riprap protection for each side of the line. For this method, the eccentricity of a bridge crossing is defined as $e = 1 - Q_c/Q_a$, where $Q_c < Q_a$ (the

values of Q_c and Q_a are defined in Figure 38). For this example, e = 1 - 1479/5980, or 0.753. Experimental results (14) indicate that backwater at an eccentric crossing is no different from backwater at a symmetrical crossing for values of e less than 0.8, and this explains the assumption of symmetry in the example.

Bridge crossings which are fully eccentric are defined as having a value of e equal to 1.0. This condition occurs at bends in natural channels or when a meandering low-flow channel migrates to one side of the flood plain. Under these conditions, only one approach embankment constricts the flow. Reference 14 provides allowances for this possibility, and the backwater and other computed parameters can be used to design the protection for the single abutment in the same manner described for both abutments of symmetrical crossings. The channel wall and bridge footing across the channel from the single abutment can be protected as a channel side slope using step 5.

BIBLIOGRAPHY

1. Ahmad, M., "Effect of scale distortion, size of model bed material, and time scale on geometrical similarity of localized scour," Proc. IAHR, The Hague, Netherlands, 1955.

2. Ahmad, M., "Experiments on design and behavior of spur dikes," 5th Congress, IAHR, Minneapolis, Minnesota, 1953, pp. 145-159.

3. Ahmad, M., "Spacing and projections of spurs for bank protection," Civil Engineering, London, March 1951.

4. Andre, P., "Study of scour at obstructions in non-cohesive bed," M.S. thesis, University of Alberta, Edmonton, Alberta, Canada, 1956.

5. Appel, D. W., "Flexible mats may reduce scour at piers of small bridges," Engineering News Record, May 25, 1950.

6. ASCE Subcommittee on Slope Protection of the Committee on Earth Dams of the Soil Mechanics and Foundations Division, "Review of slope protection methods," Proc. ASCE, Vol. 74:8, June 1948, p. 845.

7. ASCE Task Committee on Preparation of Sedimentation Manual, "Sediment transportation mechanics: Initiation of motion," Proc. ASCE, Vol. 92, HY2, 1966, pp. 291-314.

8. Bhowmik, N. G., "The mechanics of flow and stability of alluvial channels formed in coarse materials," Ph.D. dissertation, Colorado State University, Ft. Collins, Colorado, 1968.

9. Bhowmik, N. G. and D. B. Simons, "Stabilization of alluvial channels," preprint of paper presented at the Institute of River Mechanics, Colorado State University, Ft. Collins, Colorado, June 15-26, 1970, 28 pp.

10. Biery, P. F. and J. W. Delleur, "Hydraulics of single span arch bridge constrictions," Proc. ASCE, Journal of Hydraulics Division, HY2, Paper 3076, March 1962, pp. 75-108.

11. Bradley, J. N., "Hydraulics of bridge waterways," Bureau of Public Roads, U.S. Department of Commerce, Washington, D.C., August 1960.

12. Bradley, J. N., "Use of backwater in designing bridge waterways," Highway Research Board Bulletin 242, Washington, D.C., 1960, pp. 57-68.

13. Bureau of Public Roads, "Computation of backwater caused by bridges," preliminary draft by Division of Hydraulic Research, Washington, D.C., October 1958.

14. Bureau of Public Roads, "Hydraulics of bridge waterways," Hydraulics Branch, Bridge Division, Office of Engineering and Operations, reported by J. N. Bradley, consultant, 2nd edition, Hydraulic Design Series No. 1, U.S. Government Printing Office, Washington, D.C., 1970.

15. Bureau of Public Roads, "Use of riprap for bank protection," Hydraulic Engineering Circular No. 11, U. S. Government Printing Office, Washington, D. C., June 1967.

16. California Division of Highways, "Bank and shore protection in California highway practice," State of California, Department of Public Works, November 1960.

17. Campbell, F. B., "Hydraulic design of rock riprap," U.S. Army Engineer Waterways Experiment Station, Miscellaneous Paper No. 2-777, Vicksburg, Mississippi.

18. Carlson, E. J. and W. W. Sayre, "Canal bank erosion due to wind-generated water waves," U.S. Bureau of Reclamation, Progress Report 1, Hydraulic Laboratory, Report No. Hyd-465, 1961.

19. Carstens, M. R., "Similarity laws for localized scour," Proc. ASCE, Journal of Hydraulics Division, Vol. 92, HY3, Paper 4818, May 1966, pp. 13-36.

20. Davidian, J., P. H. Carrigan, Jr., and J. Shen, "Flow through openings in width constrictions," U.S. Geological Survey, Water Supply Paper 1369-D, U.S. Government Printing Office, Washington, D.C., 1962, 32 pp.

21. de Abreu-Lima, J. O. and W. B. Morgan, "Protection of earth embankments by riprap of uniform size," M.S. thesis, State University of Iowa City, Iowa, 1951.

22. de Souss, P. and L. Nelson, "Riprap protection against scour around bridge piers," M.S. thesis, State University of Iowa, Iowa City, Iowa, 1959.

23. Engels, H., "Experiments pertaining to the protection of bridge piers against undermining," ASME, Hydraulic Laboratory Practice, Chapter V, New York, 1929.

24. Field, W. G., "Flood protection at artificial river constrictions," Preprint 906, ASCE National Meeting on Transportation Engineering, Washington, D.C., July 21, 1969, 46 pp.

25. Gales, R., "Principles of river training for railway bridges and their application to the case of the Hardinge Bridge over the lower Ganges at Sara," Journal of the Institution of Civil Engineers, Paper No. 5167, December 1938.

26. Hallmark, D. E. and G. L. Smith, "Stability of channels by armor-plating," Proc. ASCE, Journal of Waterways and Harbors Division, Vol. 91, No. WW3, August 1965, pp. 117-135.

27. Hedman, E. R., "Effect of spur dikes on flow through contractions," ASCE, Journal of Hydraulics Division, Vol. 91, HY4, Paper 4412, July 1965, pp. 155-165.

28. Herbich, J. B., "Spur dikes prevent scour at bridge abutments," Lehigh University Institute of Research, Fritz Engineering Laboratory Report 280.20, Bethlehem, Pennsylvania, December 1966.

29. Herbich, J. B., R. J. Carle, and J. E. Kable, "The effects of spur dikes on flood flows through highway bridge constrictions," Lehigh University Institute of Research, Fritz Engineering Laboratory, Bethlehem, Pennsylvania, June 1959.

30. Herr, L. A., discussion of "Effect of spur dikes on flow through contractions," by E. R. Hedman, ASCE, Journal of Hydraulics Division, Vol. 92, HY2, March 1966, p. 430.

31. Hudson, R. Y., "Laboratory investigations of rubble mound breakwaters," Proc. ASCE, Journal of Waterways and Harbors Division, Paper 2171, September 1959.

32. Inglis, C. C. and D. V. Joglekar, "Investigations carried out by means of models at the Khodakwasla Hydrodynamics Research Station near Poona in connection with the protection of the Hardinge Bridge which spans the river Ganges near Paksey," East Bengal Railway, Public Works Department, Bombay, India, Technical Paper No. 55, 1936.

33. Isbash, S. V. and I. V. Lebeder, "Change of natural streams during construction of hydraulic structures," Proc. 9th Congress, IAHR, Dubrovnik, 1961, p. 1114.

34. Izzard, C. F., discussion of "Backwater effects of open-channel constrictions," by H. J. Tracy and R. W. Carter, Trans. ASCE, Vol. 120, 1955, pp. 1008-1013.

35. Izzard, C. F., discussion of "Tranquil flow through open-channel constrictions," by C. E. Kindsvater and R. W. Carter, Trans. ASCE, Vol. 120, 1955, pp. 985-989.

36. Izzard, C. F. and J. N. Bradley, discussion of "Flood erosion protection for highway fills," by C. J. Posey, Trans. ASCE, Vol. 122, 1957, p. 544.

37. Izzard, C. F. and J. N. Bradley, "Field verification of model tests of flow through highway bridges and culverts," Proc. 7th Hydraulics Conference, Studies in Engineering, Bulletin 39, State University of Iowa, Iowa City, Iowa, June 1958, p. 225.

38. Karaki, S. S., "Hydraulic model study of spur dikes for highway bridge openings," Colorado State University, Civil Engineering Section, Report CER59SSK36, Ft. Collins, Colorado, September 1959, 47 pp.

39. Karaki, S. S., "Laboratory study of spur dikes for highway bridge protection," Highway Research Board Bulletin 286, Washingont, D.C., 1961, pp. 1-12.

40. Kindsvater, C. E., discussion of "Flood erosion protection for highway fills," by C. J. Posey, Trans. ASCE, Vol. 122, 1957, p. 548.

41. Kindsvater, C. E. and R. W. Carter, "Tranquil flow through open channel constrictions," Trans. ASCE, Vol. 120, 1955, pp. 955-980.

42. Kindsvater, C. E., R. W. Carter, and H. J. Tracy, "Computation of peak discharge at contractions," U.S. Geological Survey Circular 284, Washington, D.C., 1953, 35 pp.

43. Lane, E. W., "Design of stable channels," Trans. ASCE, Vol. 120, 1955, pp. 1234-1260.

44. Lane, E. W., "Experiments on the flow of water through contractions in an open channel," Trans. ASCE, Vol. 83, 1910-20, pp. 1149-1219.

45. Lane, E. W. and E. J. Carlson, "Some observations on the effects of particle shape on the movement of coarse sediments," Trans. AGU, Vol. 35, No. 3, 1954, pp. 453-462.

46. Laursen, E. M., "An analysis of relief bridge scour," Proc. ASCE, Journal of Hydraulics division, Vol. 89, No. HY3, Paper 3516, May 1963, pp. 93-118.

47. Laursen, E. M., "Progress report of model studies of scour around bridge piers and abutments," Highway Research Board, Research Report 13-B, 1951.

48. Laursen, E. M., "Scour at bridge crossings," Proc. ASCE, Journal of Hydraulics Division, No. 2369, February 1960.

49. Laursen, E. M., "Scour at bridge crossings," Trans. ASCE, Vol. 127, Part 1, 1962, pp. 166-179.

50. Laursen, E. M., "Scour at bridge crossings," Iowa Highway Research Board, Bulletin 8, August 1958, 53 pp.

51. Laursen, E. M. and A. Toch, "A generalized model study of scour around bridge piers and abutments," 5th Congress, IAHR, Minneapolis, Minnesota, 1953, pp. 123-131.

52. Laursen, E. M. and A. Toch, "Scour around bridge piers and abutments," Iowa Highway Research Board, Bulletin 4, May 1956, 60 pp.

53. Liu, H. K., J. N. Bradley, and E. J. Plate, "Backwater effects of piers and abutments," Colorado State University, Civil Engineering Section, Report CER57HKL10, Ft. Collins, Colorado, October 1957, 364 pp.

54. Liu, H. K., F. M. Chang, and M. M. Skinner, "Effect of bridge constriction on scour and backwater," Colorado State University, Civil Engineering Section, Report CER60HKL22, Ft. Collins, Colorado, 1961.

55. Liu, H. K. and M. M. Skinner, "Laboratory observations of scour at bridge abutments," National Research Council, Highway Research Board, Bulletin 242, January 1959, pp. 69-77.

56 Matthai, H. F., "Measurement of peak discharge at width constrictions by indirect methods," U.S. Geological Survey, Techniques of Water Resources Investigations, Book 3, Chapter A4, U.S. Government Printing Office, Washington, D.C., 1967, 44 pp.

57. Moore, W. L. and F. D. Masch, "The influence of secondary flows on local scour at obstructions in a channel," Proc. Federal Inter-agency Sedimentation Conference, Miscellaneous Publication No. 970, 1963.

58. Nagler, F. A., "Obstruction of bridge piers to the flow of water," Trans. ASCE, Vol. 82, 1918, p. 334.

59. Owen, H. J. and A. Sooky, discussion of "Hydraulics of single span arch bridge constrictions," by P. F. Biery and J. W. Delleur, Proc. ASCE, Vol. 88, HY5, Part 1, Paper 3076, September 1962, pp. 327-333.

60. Parkin, A. K., D. H. Trollope, and J. D. Lawson, "Rockfill structures subject to water flow," Proc. ASCE, Journal of Soil Mechanics and Foundations Division, Vol. 92, No. SM6, 1966, pp. 135-151.

61. Posey, C. J., "Flood erosion protection for highway fills," Trans. ASCE, Vol. 122, Paper 2871, 1957, pp. 531-542.

62. Posey, C. J., "Flood erosion protection for highway fills," Iowa Highway Research Board, Bulletin 13, December 1960, 27 pp.

63. Posey, C. J., "Rock 'sausages' provide economical protection against erosion," Engineering News Record, May 13, 1954, p. 45.

64. Posey, C. J., "Some basic requirements for protection against erosion," Proc. 5th Congress, IAHR, Minneapolis, Minnesota September 1-4, 1953, pp. 85-87.

65. Posey, C. J., "Why bridges fall in floods, model tests of erosion around bridge piers indicate depth of scour in erodible materials," Civil Engineering, February 1949, p. 42.

66. Sanden, E. J., "Scour at bridge piers and erosion of river banks," Department of Highways, Province of Alberta, Canada, October 3, 1960.

67. Saville, T., Jr., "The effect of fetch width on wave generation," Beach Erosion Board, Corps of Engineers, Tech. Memo No. 70, 9 pp.

68. Schneible, D. E., "Field observations on performance of spur dikes at bridges," paper presented at ASCE Transportation Engineering Conference, Philadelphia, Pennsylvania, October 17-21, 1966.

69. Searcy, J. K., "Use of riprap for bank protection," Bureau of Public Roads, Hydraulic Engineering Circular No. 11, U.S. Government Printing Office, Washington, D.C., June 1967, 43 pp.

70. Shen, H. W., "Scour near piers," preprint of paper presented at the Institute of River Mechanics, Colorado State University, Ft. Collins, Colorado, June 15-26, 1970, 23 pp.

71. Shen, H. W., V. R. Schneider, and S. Karaki, "Mechanics of local scour," Colorado State University, Civil Engineering Section, Report CER66HWS-VRS-SK-22, Ft. Collins, Colorado, 1966.

72. Shen, H. W., V. R. Schneider, and S. Karaki, "Mechanics of local scour and supplement methods of reducing scour," Colorado State University, Civil Engineering Section, Report CER66HWS-VRS-SK36, Ft. Collins, Colorado, 1966.

73. Simons, D. B., "Theory and design of stable channels in alluvial materials," Ph.D. dissertation, Colorado State University, Ft. Collins, Colorado, 1957, 394 pp.

74. Simons, D. B., G. L. Lewis, and W. G. Field, "Embankment protection at river constrictions," Proc. 11th Annual Bridge Engineering Conference, Colorado State University, Ft. Collins, Colorado, 1970, pp. 160-206.

75. Simons, D. B., M. A. Stevens, and F. J. Watts, "Flood protection at culvert outlets," Report prepared for Wyoming State Highway Department, Planning and Research Division, in cooperation with the U.S. Department of Transportation, Federal Highway Administration, Bureau of Public Roads, 1970

76. Simons, D. B., and G. L. Lewis, "Basic data report - flood protection at bridge crossings," Report prepared for Wyoming State Highway Department, Planning and Research Division, in cooperation with the U. S. Department of Transportation, Federal Highway Administration, Bureau of Public Roads, 1971.

77. Stevens, M. A. and D. B. Simons, "Stability analysis for coarse granular material on slopes," Paper presented at the Institute on River Mechanics, Colorado State University, Fort Collins, Colorado, June 15-26, 1970.

78. Tracy, H. J. and R. W. Carter, "Backwater effects of open-channel constriction," Trans. ASCE, Vol. 120, 1955, pp. 993-1006.

79. U.S. Army Engineer Waterways Experiment Station, "Velocity forces on submerged rocks," Corps of Engineers, Waterways Experiment Station Miscellaneous Paper No. 2-265, Plate 1, Vicksburg, Mississippi, 1958.

80. U.S. Army Engineer Waterways Experiment Station, "Waterways Experiment Station hydraulic design criteria," Corps of Engineers, Vicksburg, Mississippi, 1960.

81. U.S. Bureau of Reclamation, "Hydraulic design of stilling basins and energy dissipators," by A. J. Peterka, Engineering Monograph No. 25, Technical Information Branch, Denver Federal Center, Denver, Colorado, 1958.

82. Vallentine, H. R., "Flow in rectangular channels with lateral constriction plates," La Houille Blanche, No. 1, January - February 1958, pp. 75-84.

83. Welty, K. H., M. L. Corry, and J. L. Morris, "Hydraulics of bridge waterways," Bureau of Public Roads, Electronic Computer Program HY-4-69, Washington, D.C., 1969.

84. Wend, J. H., "Stabilization of channels with gravel," M.S. thesis, Colorado State University, Ft. Collins, Colorado, 1967.

85. White, C. M., "The equilibrium of grains on the bed of a stream," Proc. Royal Society of London, Series A, Vol. 174, p. 331.

86. Wyoming Highway Department, Hydraulic Design Practice, Chapter 3, January 1966.

87. Yarnell, D. L., "Bridge piers as channel obstructions," U.S. Department of Agriculture, Technical Bulletin No. 442, U.S. Government Printing Office, Washington, D.C., November 1934, 52 pp.

88. Yarnell, D. L., "Pile trestles as channel obstructions," U.S. Department of Agriculture, Technical Bulletin No. 429, U.S. Government Printing Office, Washington, D.C., July 1934.

89. Yarnell, D. L. and F. A. Nagler, "Flow of flood waters over railroad and highway embankments," Public Roads, Vol. II, No. 2, April 1930.

90. Young, J. C., "Economics of self-protection of highways against flood damage," ASCE, Journal of Highway Division, HW3, Paper 1075, October 1956.

APPENDIX A

FIGURES

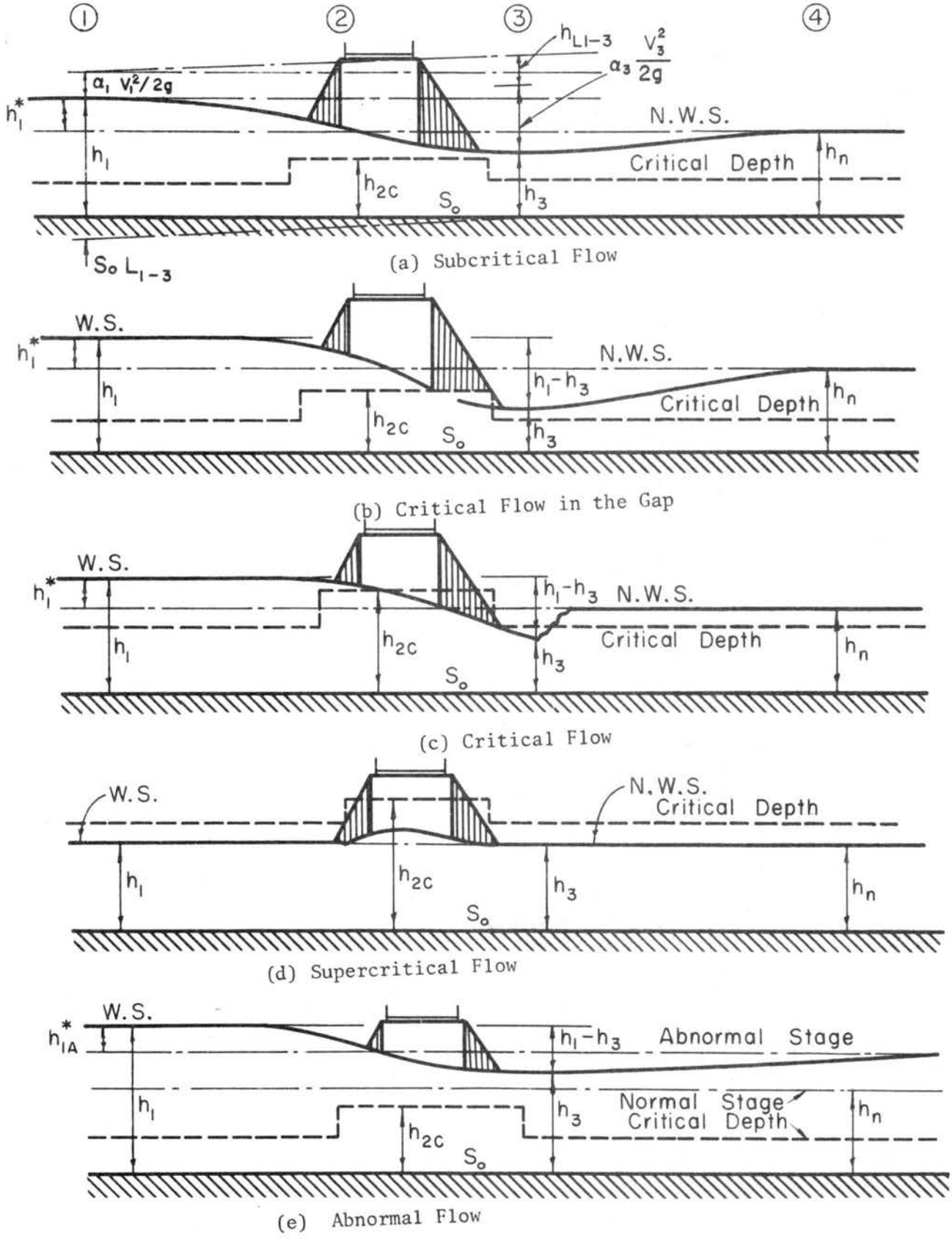

Fig. 1 Classification of Flow Conditions, from Bradley (14)

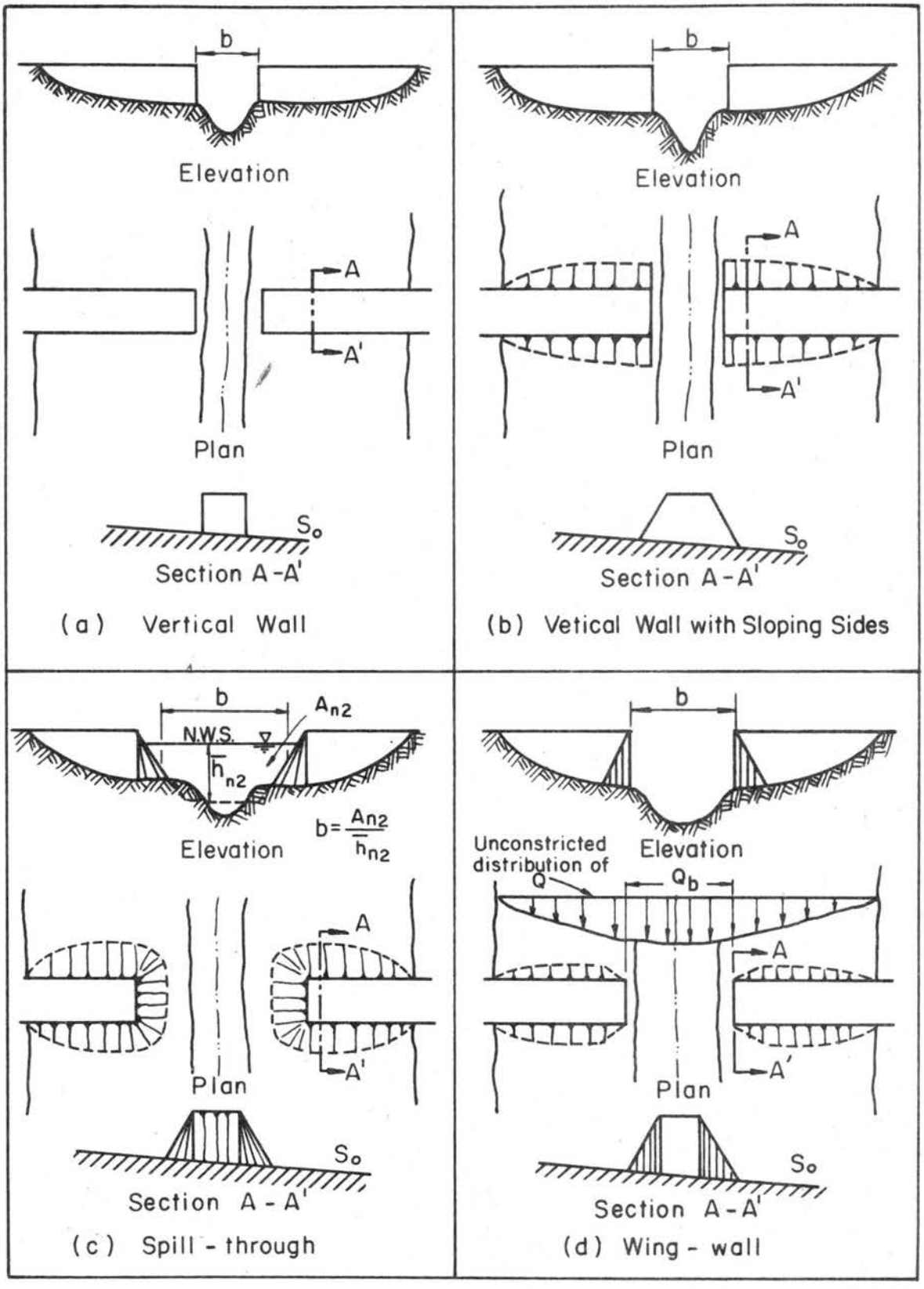

Fig. 2 Classification of Abutment Types

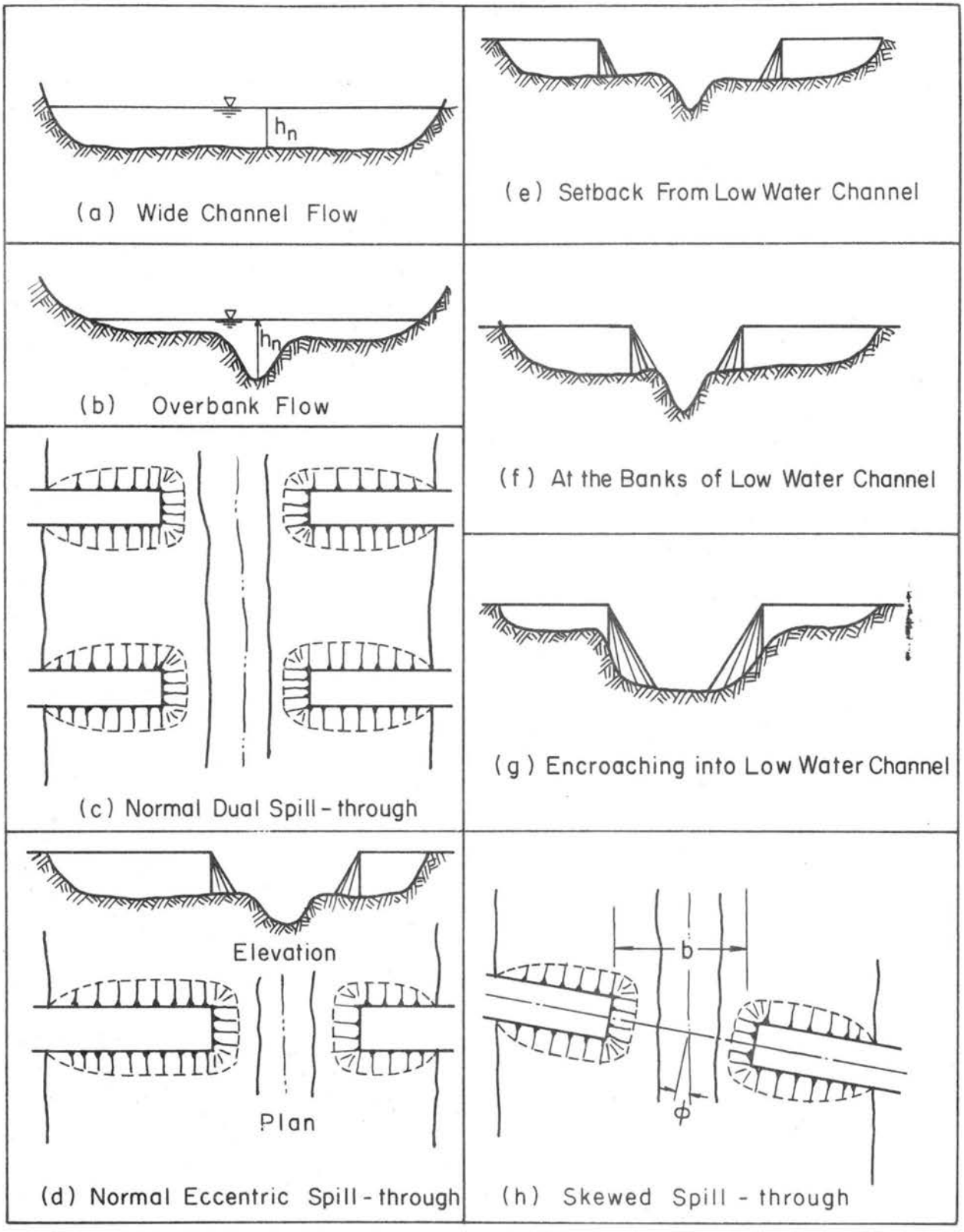

Fig. 3 Classification of Geometry

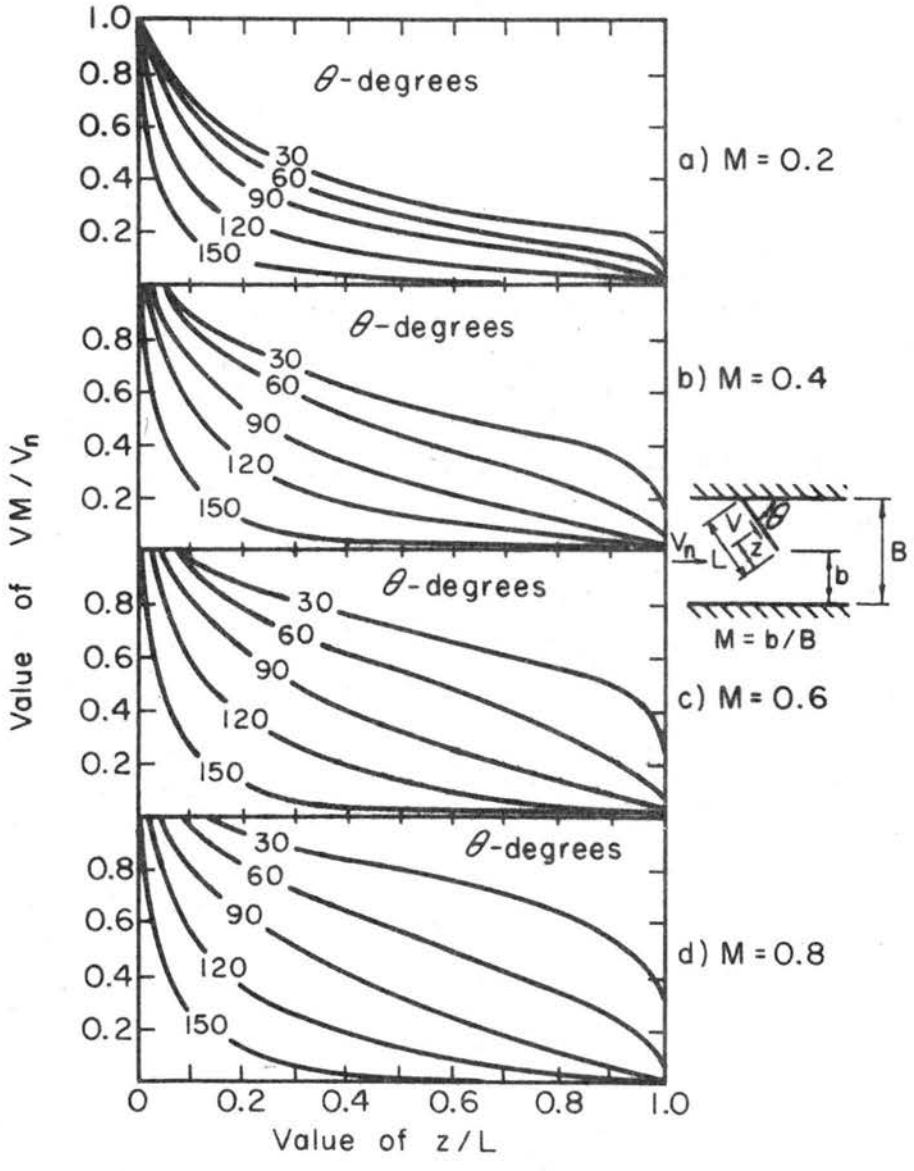

Fig. 4 Variation of Velocity with distance along Embankment, from Field (24)

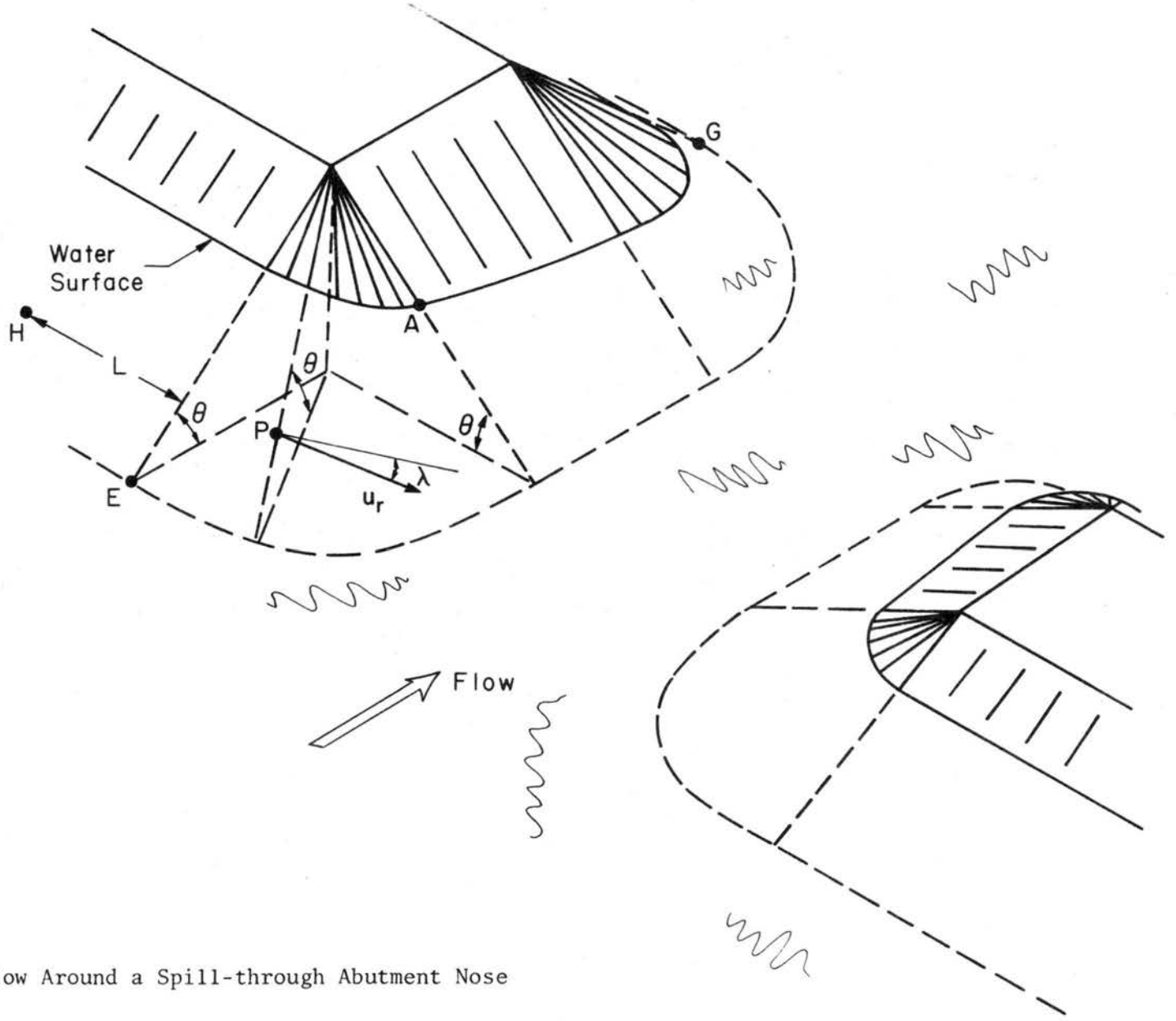

Fig. 5 Flow Around a Spill-through Abutment Nose

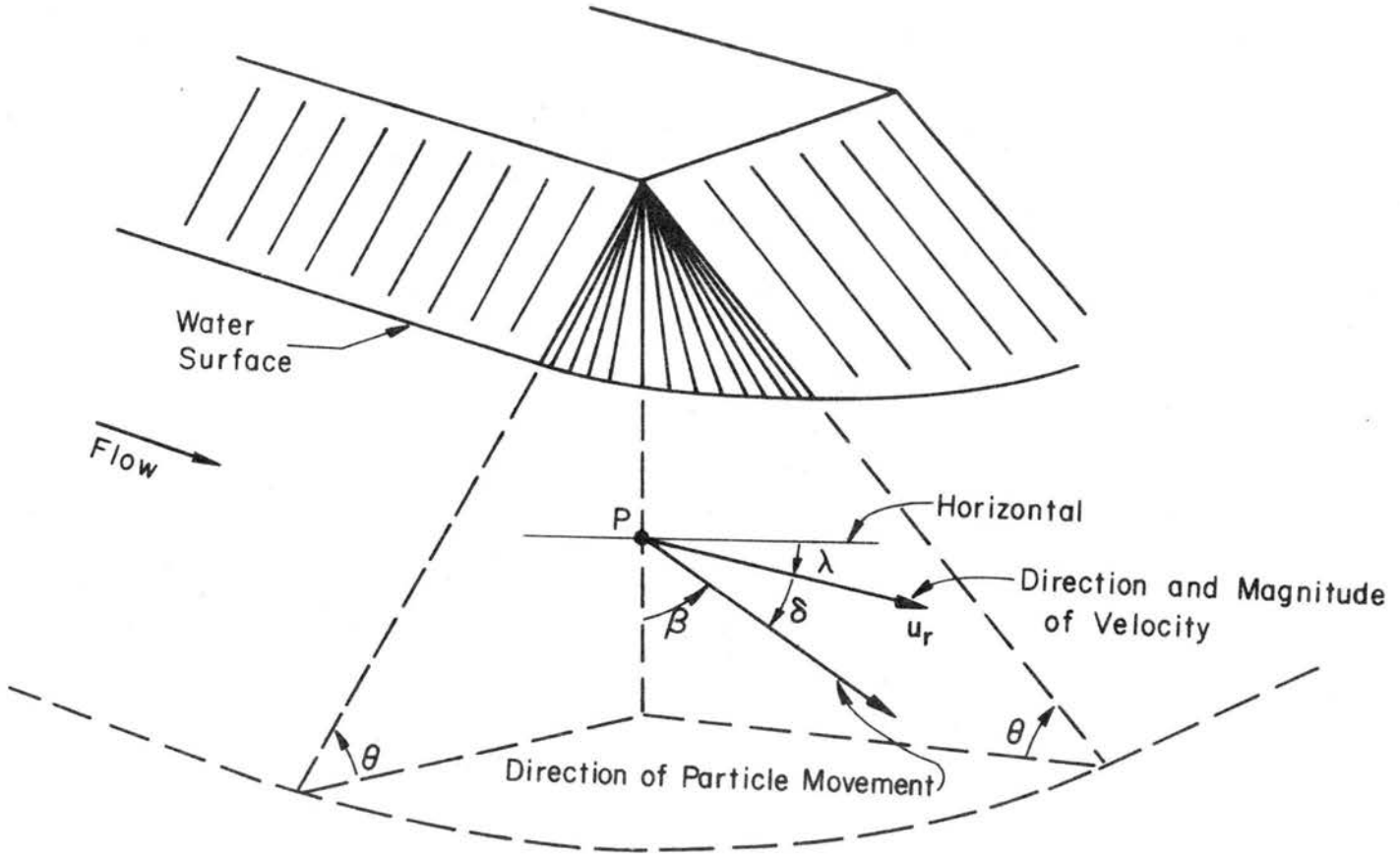

Fig. 6 View Normal to the Side-slope Face at P

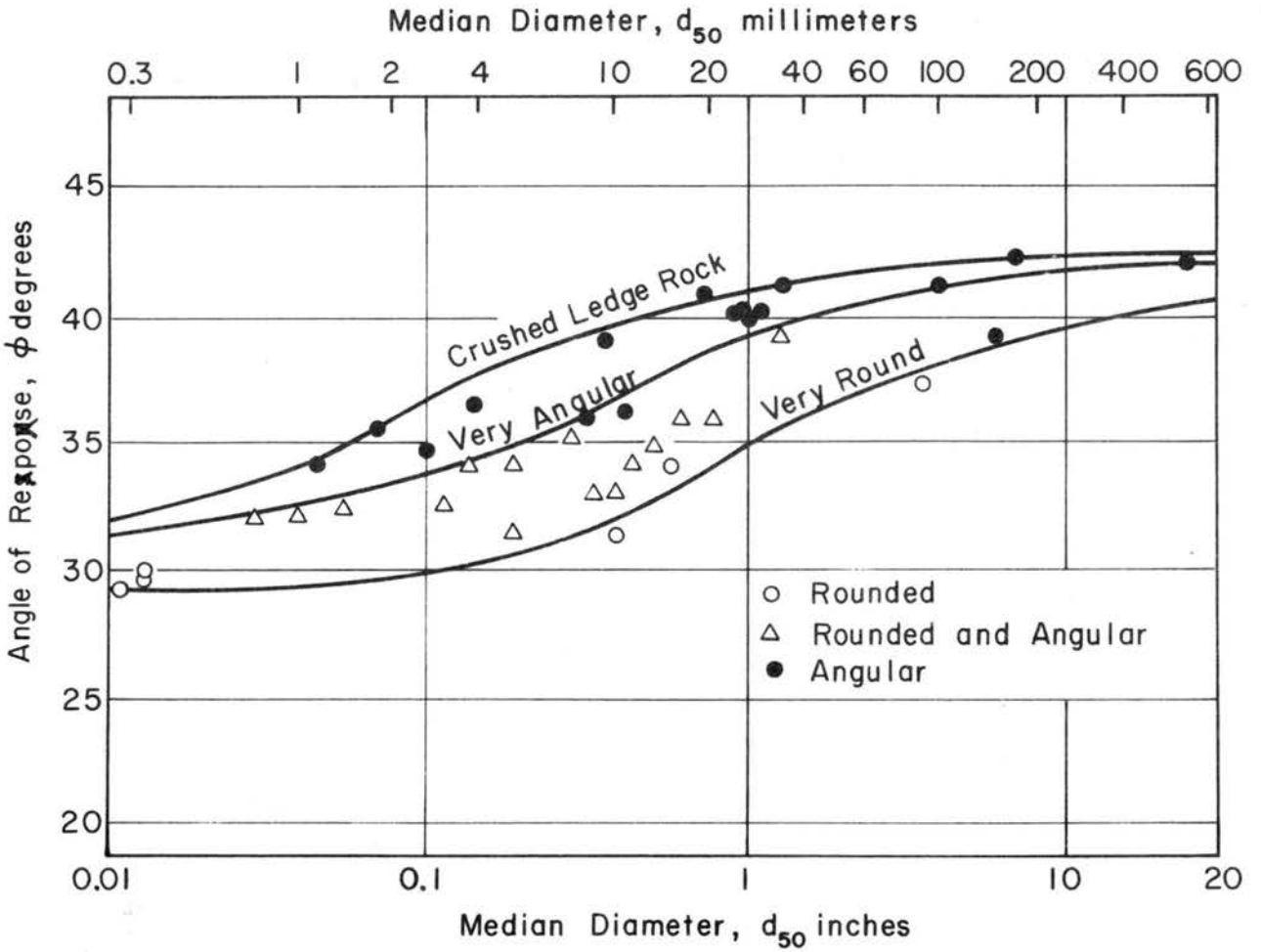

Fig. 7. Angle of Repose of Non-cohesive Material, from Simons (73)

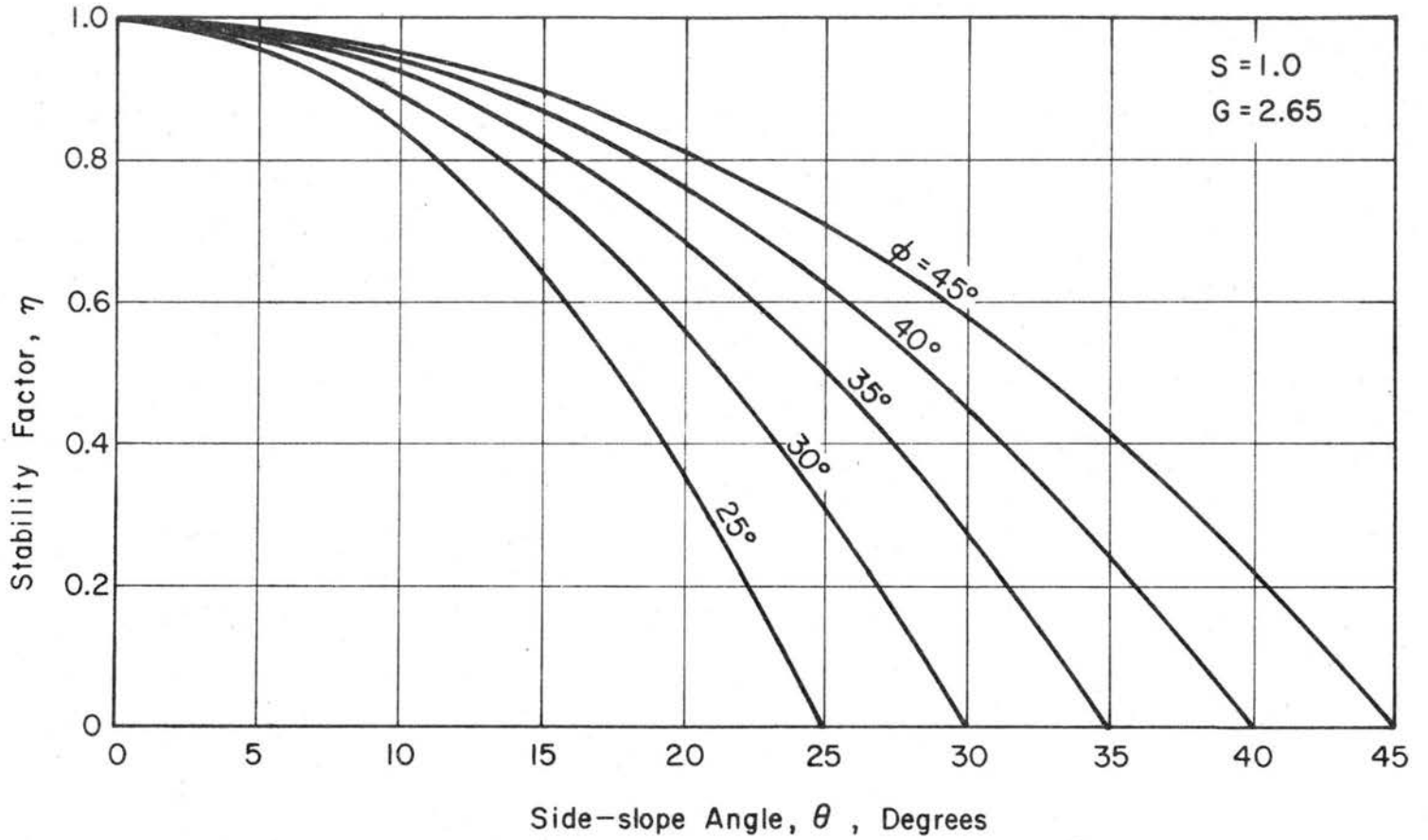

Fig. 8 Stability Factors for a Unity Safety Factor for Horizontal Flow Along a Side Slope

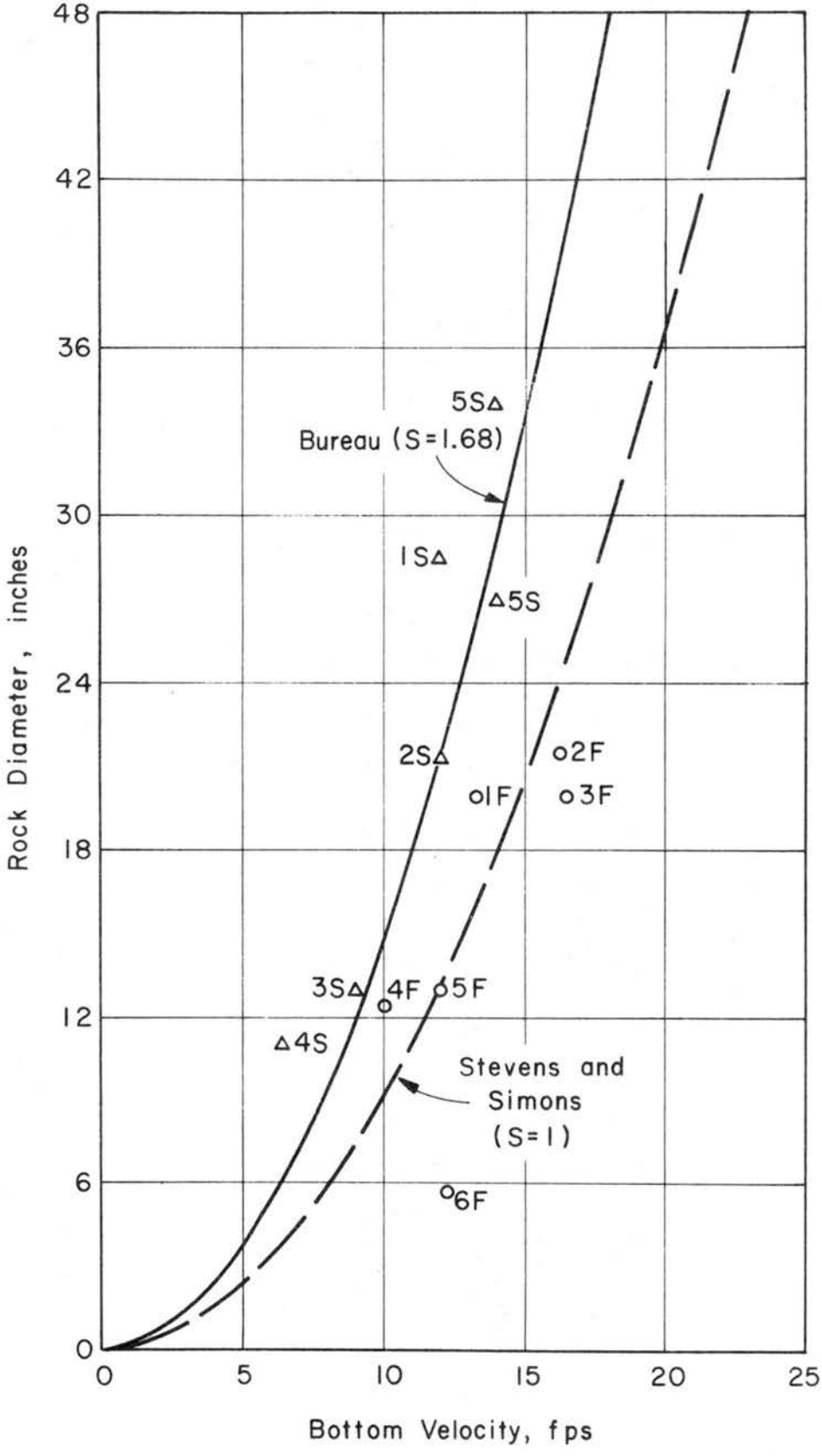

Fig. 9 Rock Size - Bottom Velocity Relationship (after U.S.B.R., 1963)

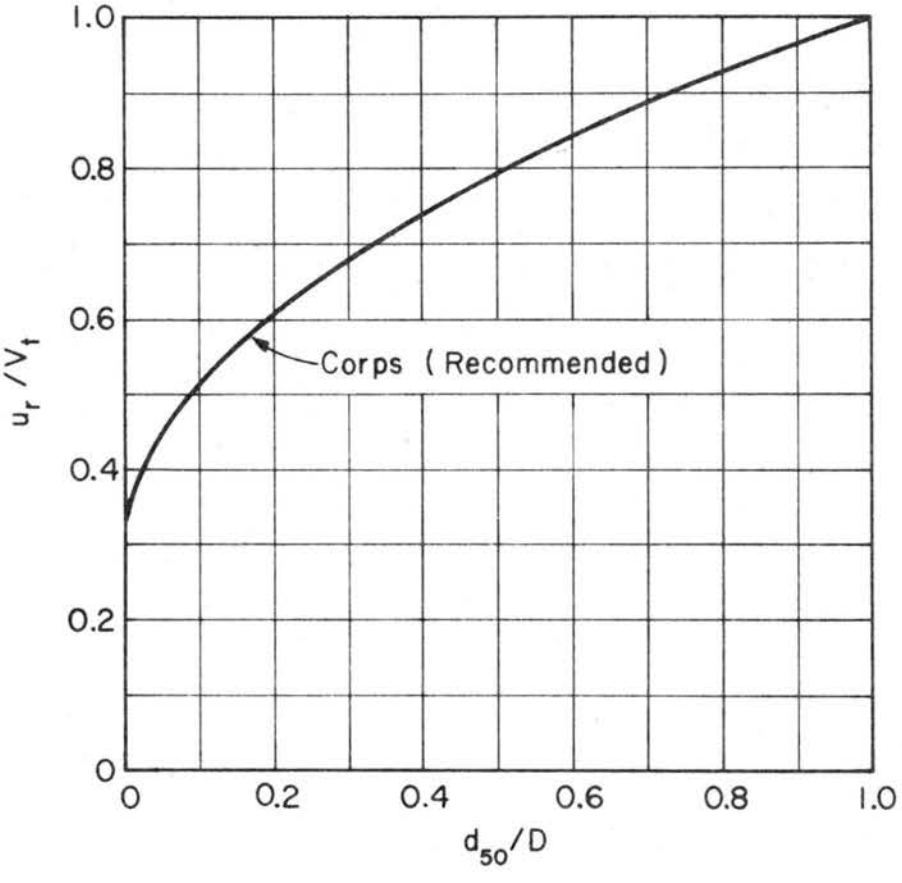

Fig. 10 Relation Between Velocity and Depth for Sizing Riprap

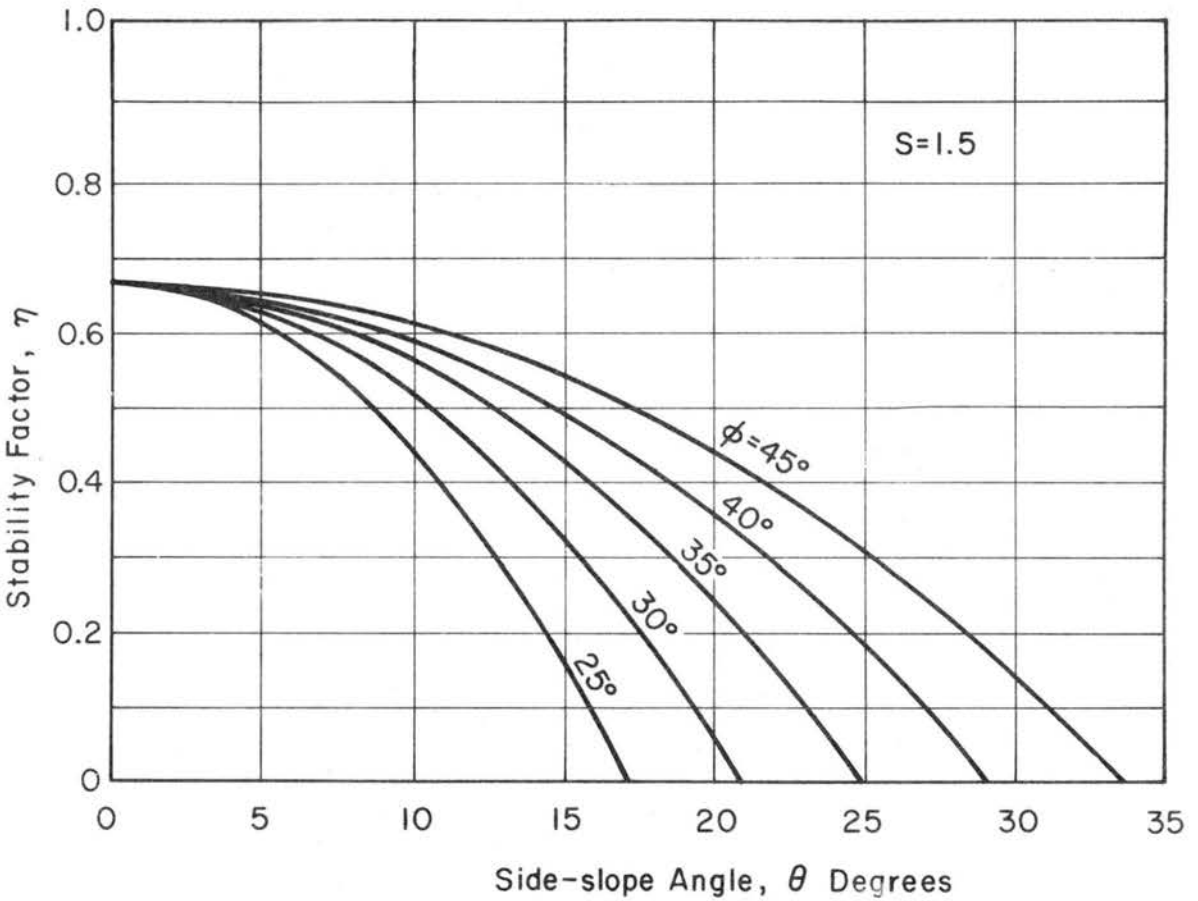

Fig. 11 Stability Factors for a 1.5 Safety Factor for Horizontal Flow Along a Side Slope

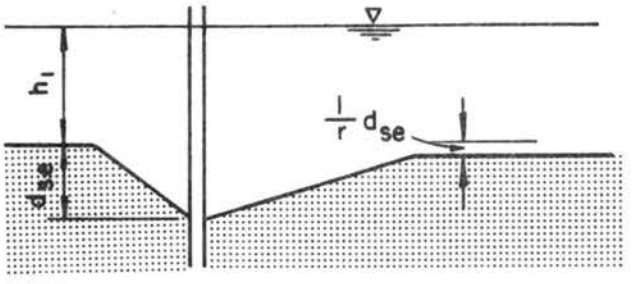

Fig. 12 Definition Sketch for Pier and Abutment, from Laursen (46).

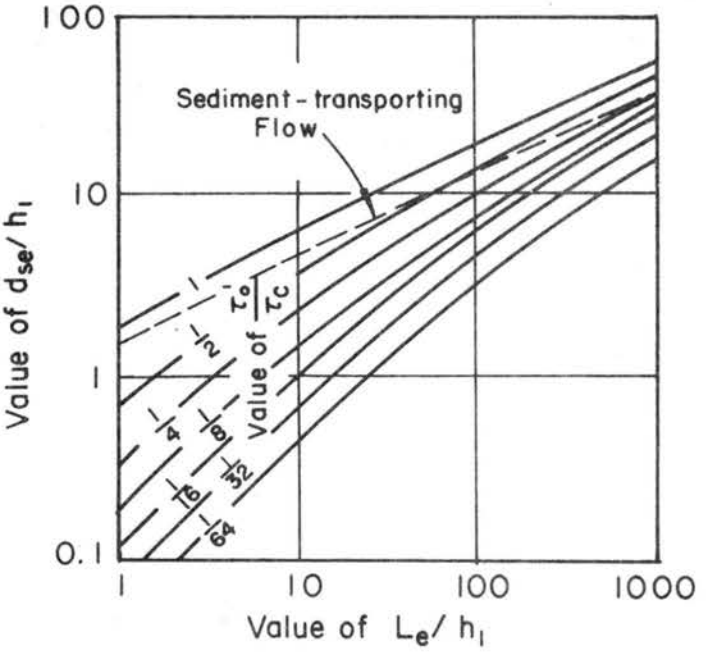

Fig. 13 Clear-water Scour at an Abutment, from Laursen (46)

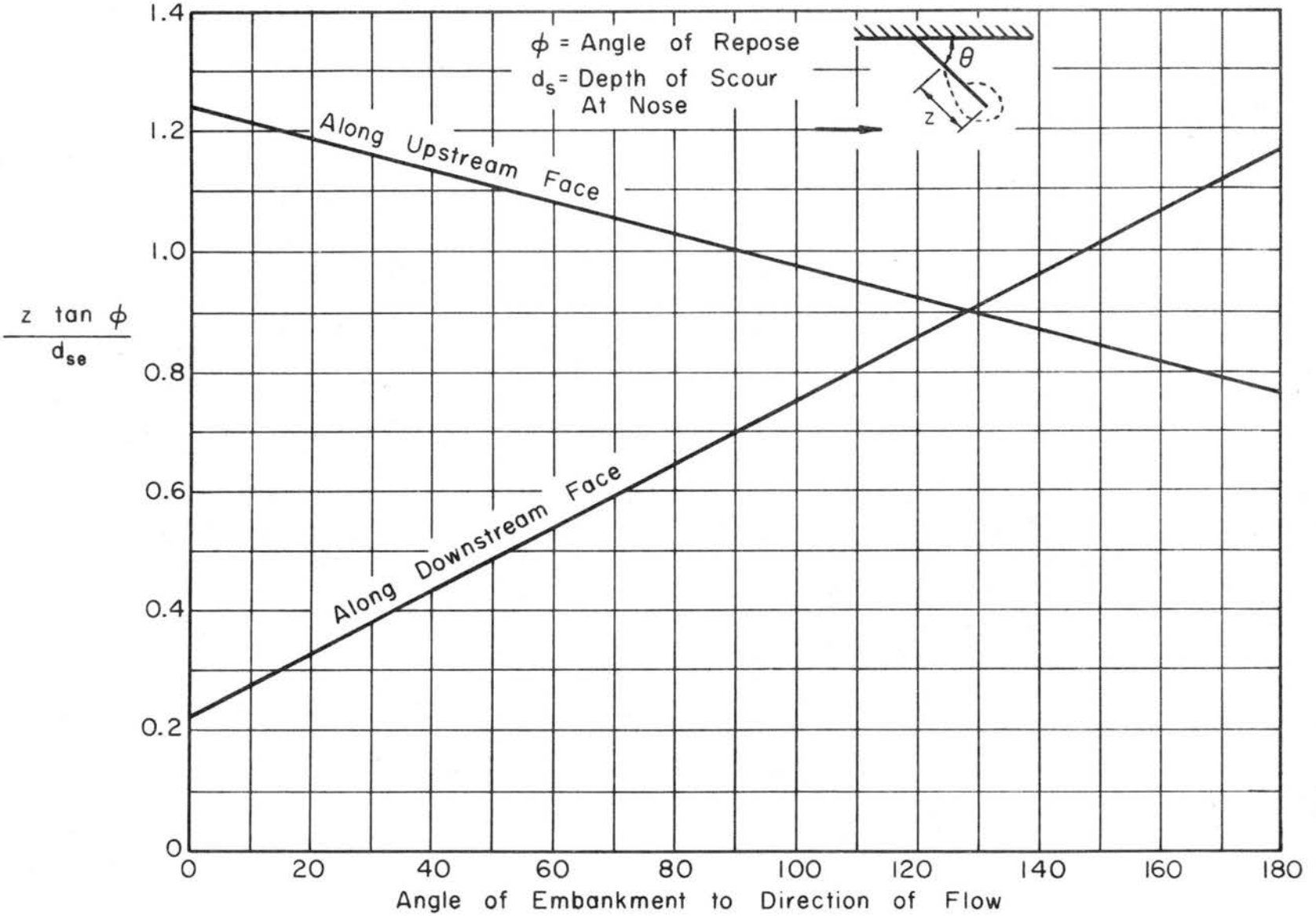

Fig. 14 Length Requiring Protection Against Scour as a Function of Embankment Skew, from Field (24)

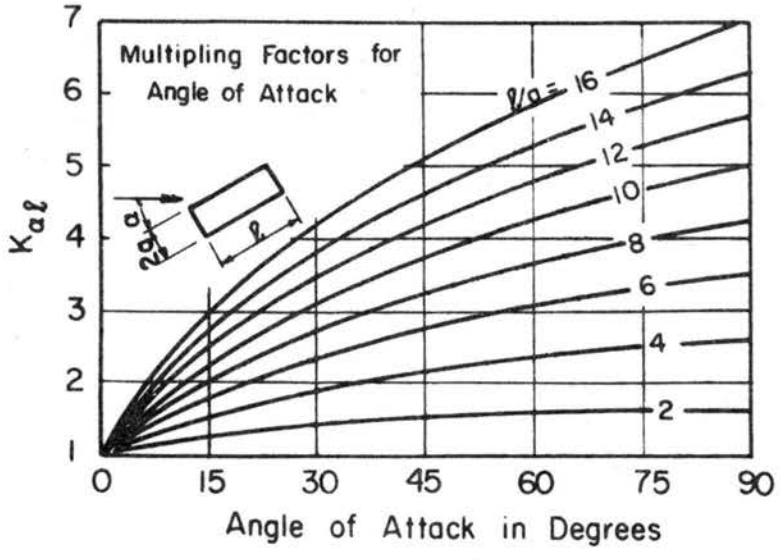

Fig. 15 Design Factors for Piers Not Aligned with Flow, from Laursen and Toch (52)

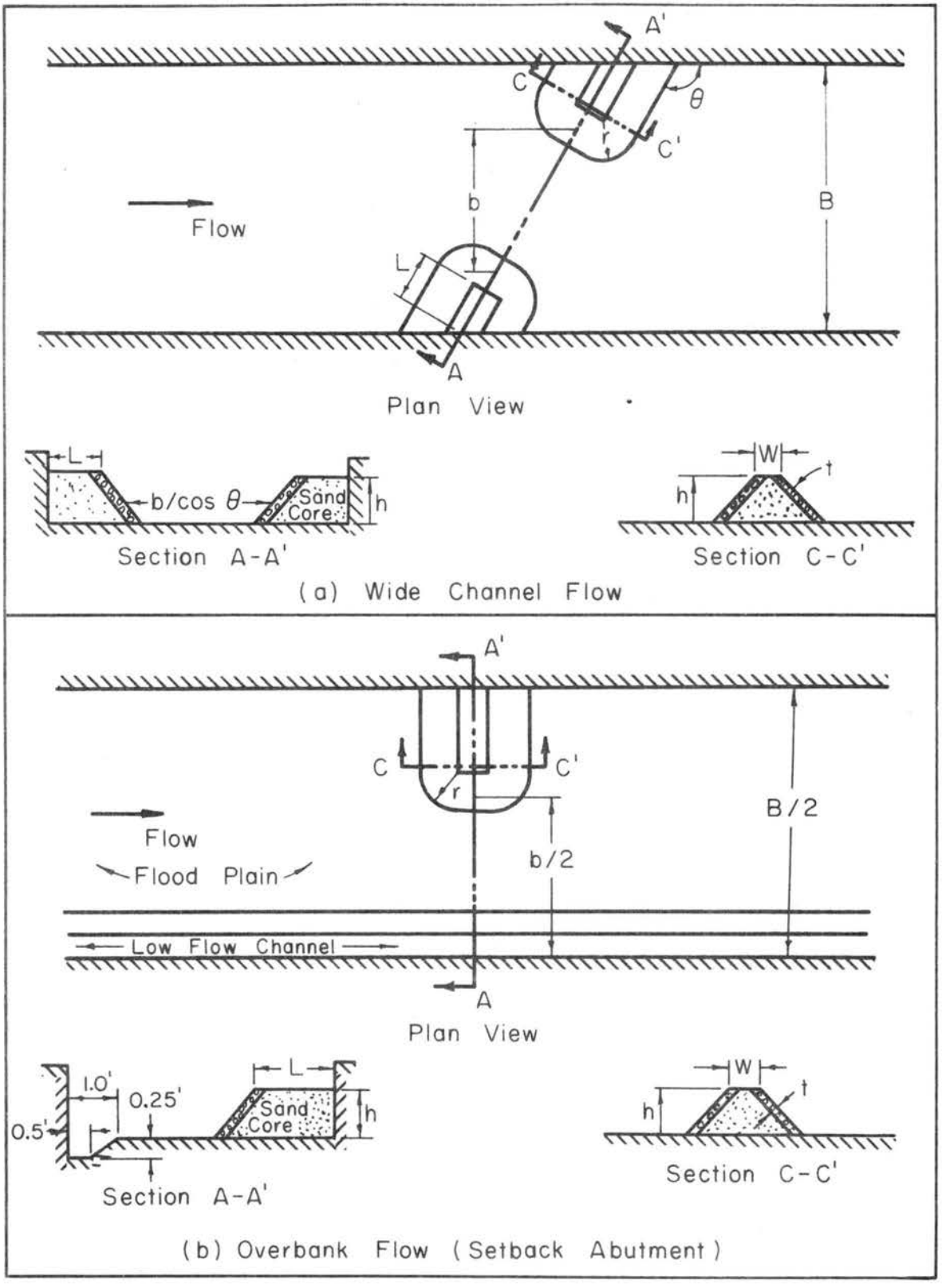

Fig. 16 Model Geometry Variables for the Spill-through Abutments in Table 1

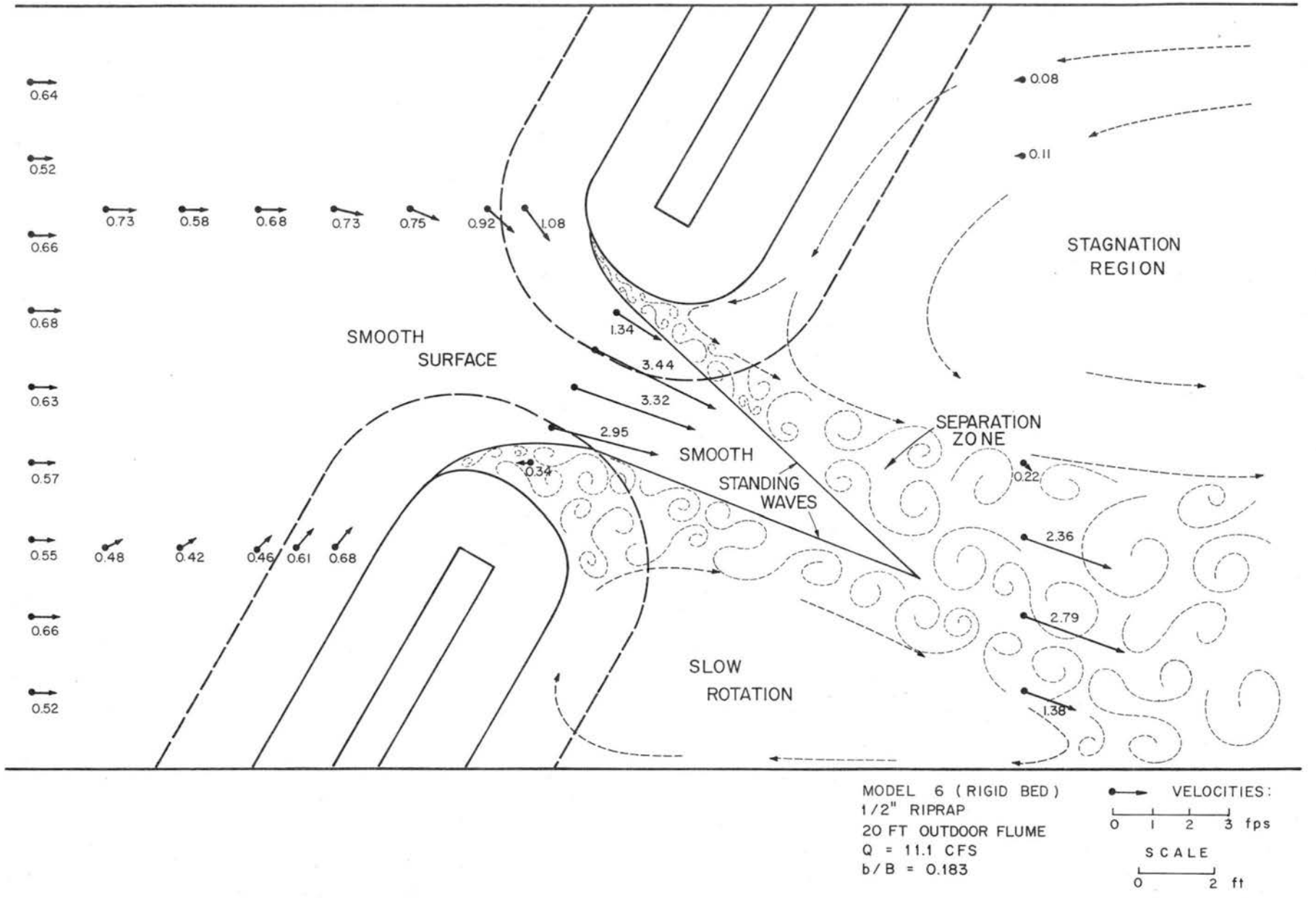

Fig. 17 Measured Velocities and Water Surface Patterns for Wide Channel Flow

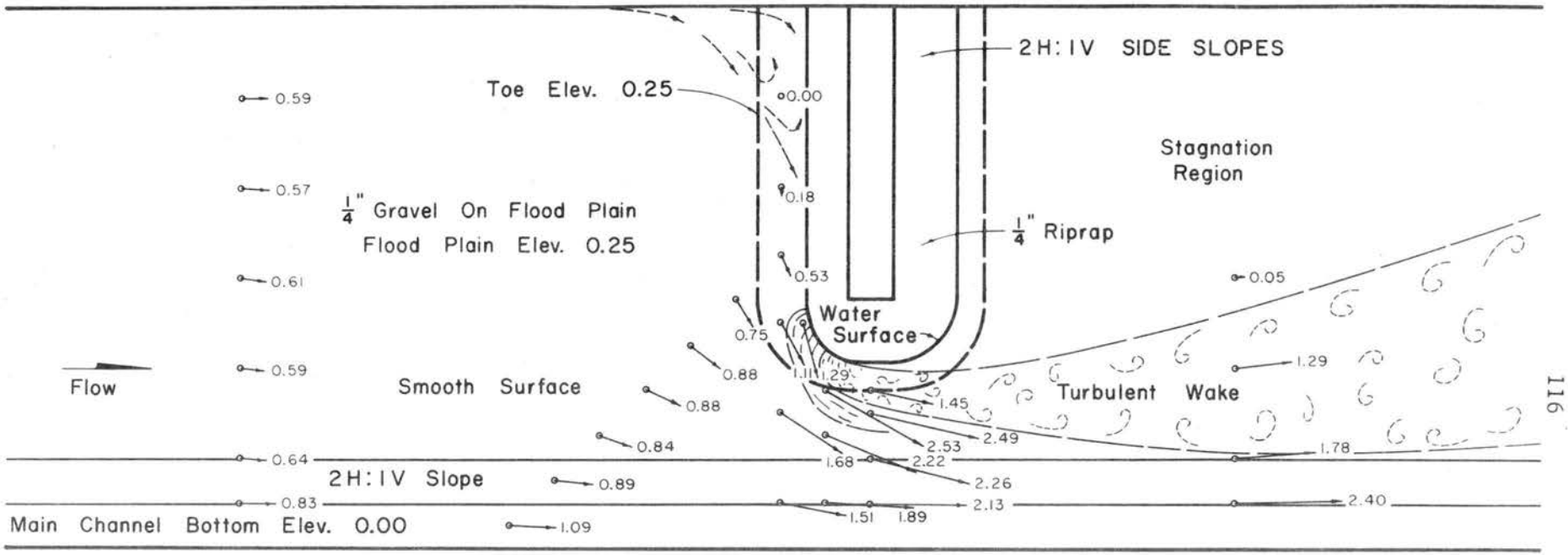

MEASURED VELOCITIES AND WATER SURFACE PATTERNS

PLAN

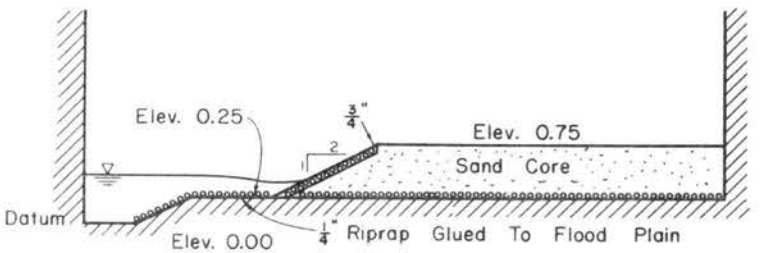

CENTERLINE CROSS SECTION

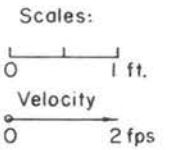

Overbank Flow
Model 7 Six-foot Wide Flume
Riprap d_{50} = 0.230" & d_m = 0.238"
1/4" Riprap On Floodplain & Main Channel Wall
Plywood Main Channel Bottom
Q = 1.02 cfs
Flow Depth 16' Upstream Of ℄ = 0.529'
Flow Depth 16' Downstream Of ℄ = 0.403'
Velocities Are Averages Through The Depth
Velocity Directions From Dye Streaklines

Fig. 18 Measured Velocities and Water Surface Patterns for Overbank Flow

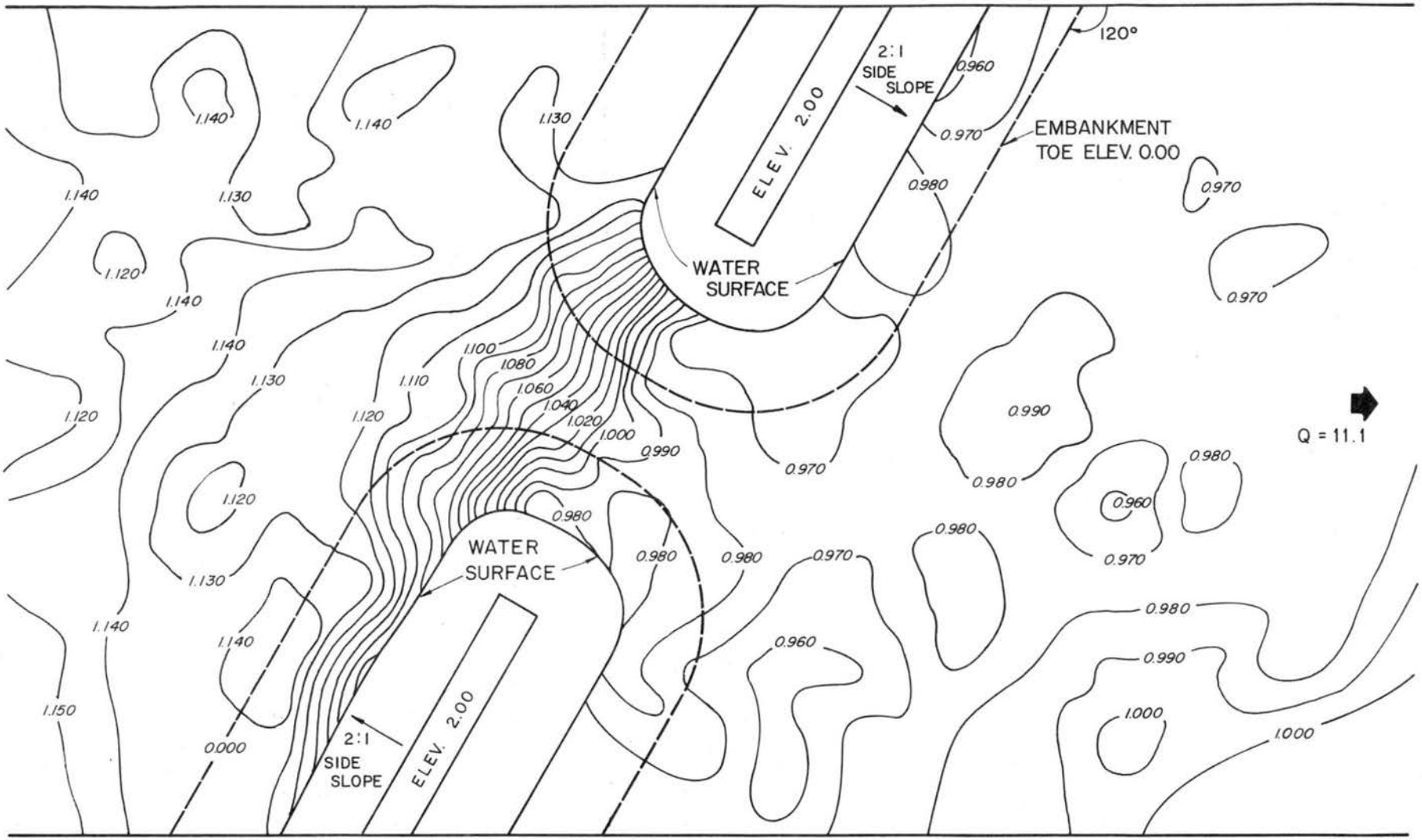

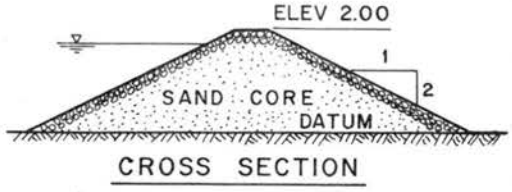

CROSS SECTION

MODEL 6 (RIGID BED)
1/2" RIPRAP
20 FT OUTDOOR FLUME
Q = 11.1 CFS
b/B = 0.183

DATUM: FLUME BED
SCALE
0 2 ft
INTERVAL = 0.010 FT
FROM 2' x 2' GRID

Fig. 19 Water Surface Contours for Wide Channel Flow

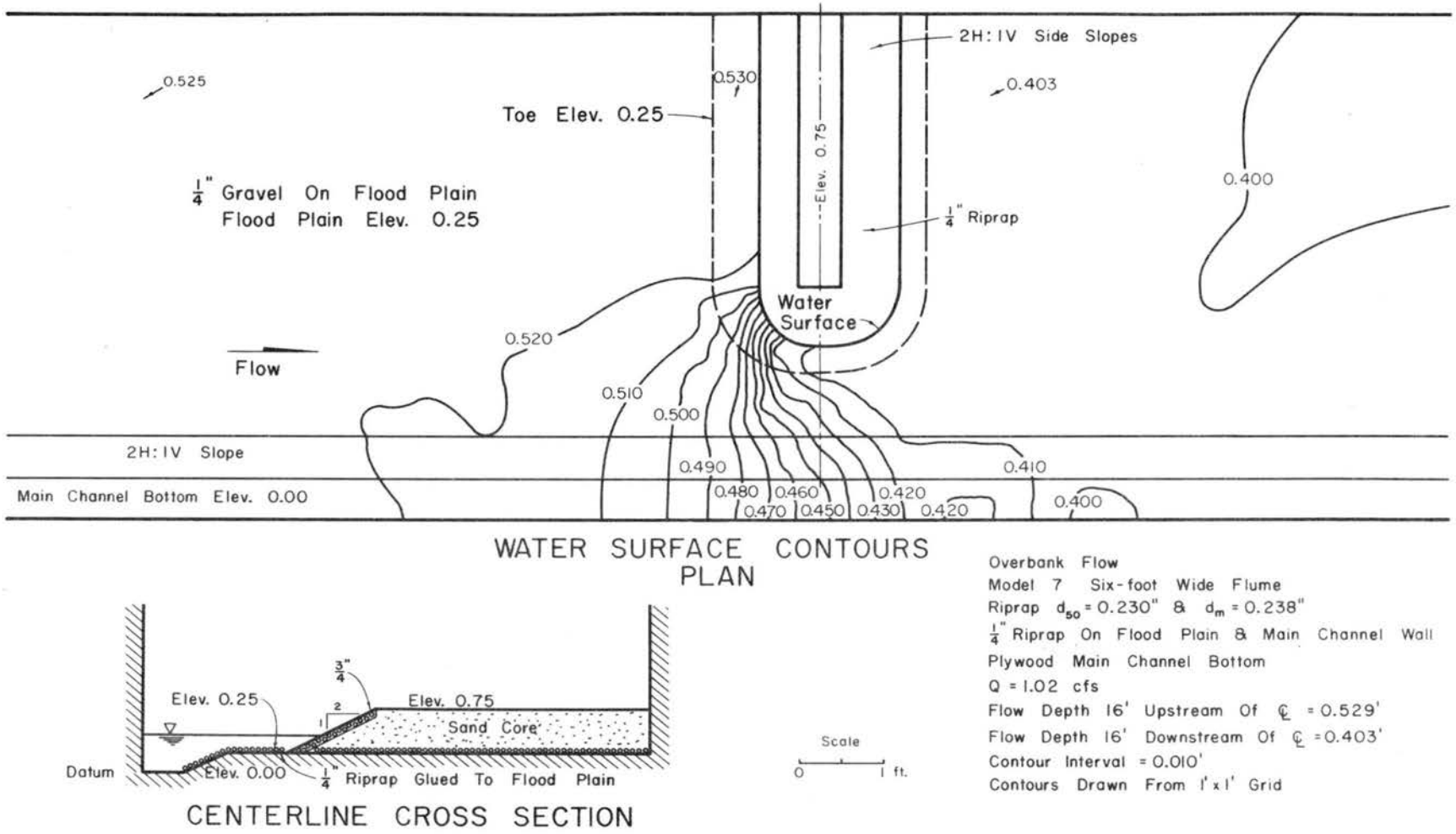

Fig. 20 Water Surface Contours for Overbank Flow

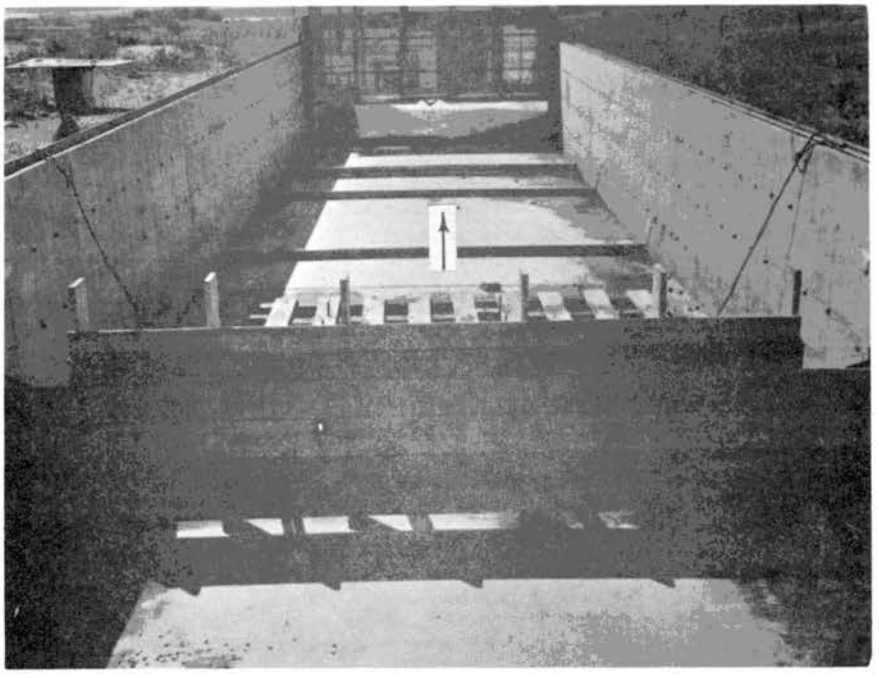

Fig. 21 - Photograph of the 20-foot wide flume showing the headbox, floating baffles, and rail-mounted instrument carriage

Fig. 22 - Photograph of the water surface characteristics for a skewed model at Q = 11.1 cfs

Fig. 23 - Photograph of the separation at the upstream embankment for the skewed model at Q = 11.1 cfs

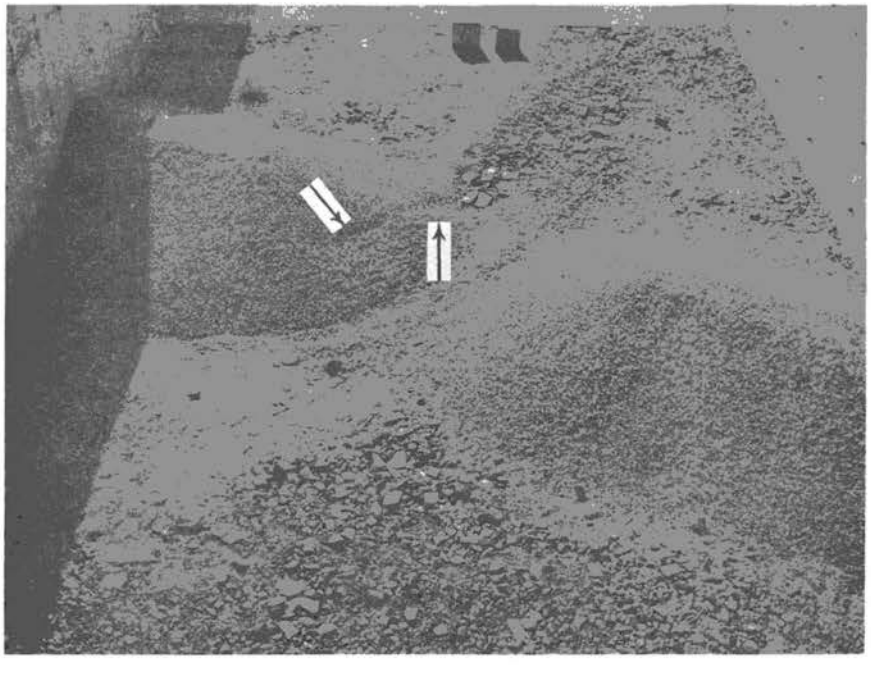

Fig. 24 - Photograph of the scour on the downstream abutment and the jet boundary for the skewed model at 11.1 cfs

Fig. 25 - Photograph of the scour on the downstream abutment after increasing the discharge to 12.7 cfs

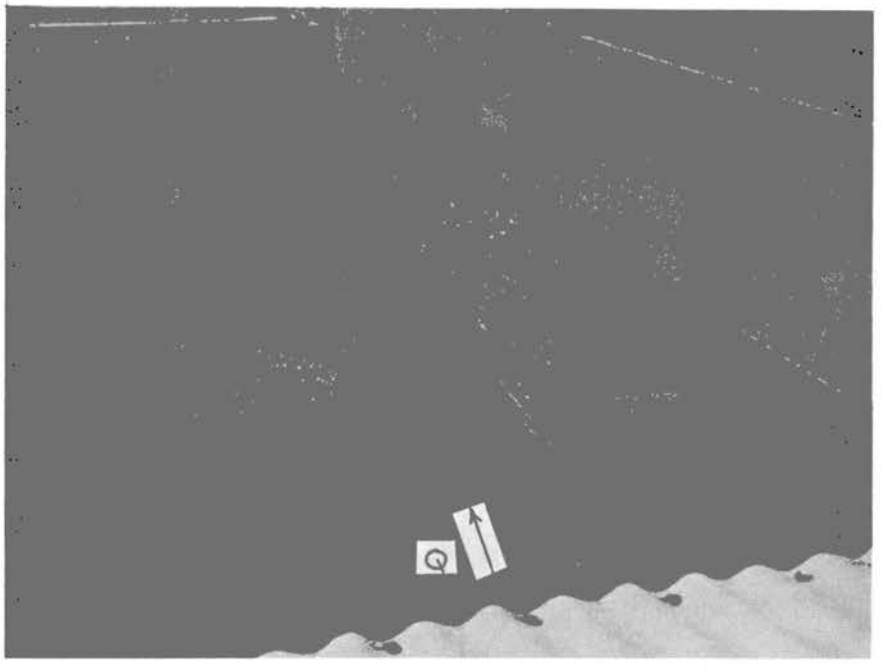

Fig. 26 - Photograph of the protected nose of the downstream embankment and the jet properties at Q = 13.9 cfs

Fig. 27 - Photograph of the scour on the upstream abutment of Figure 26 for a discharge of 16.0 cfs

Fig. 28 - Photograph of the same abutment in still water after scour had reached the sand core

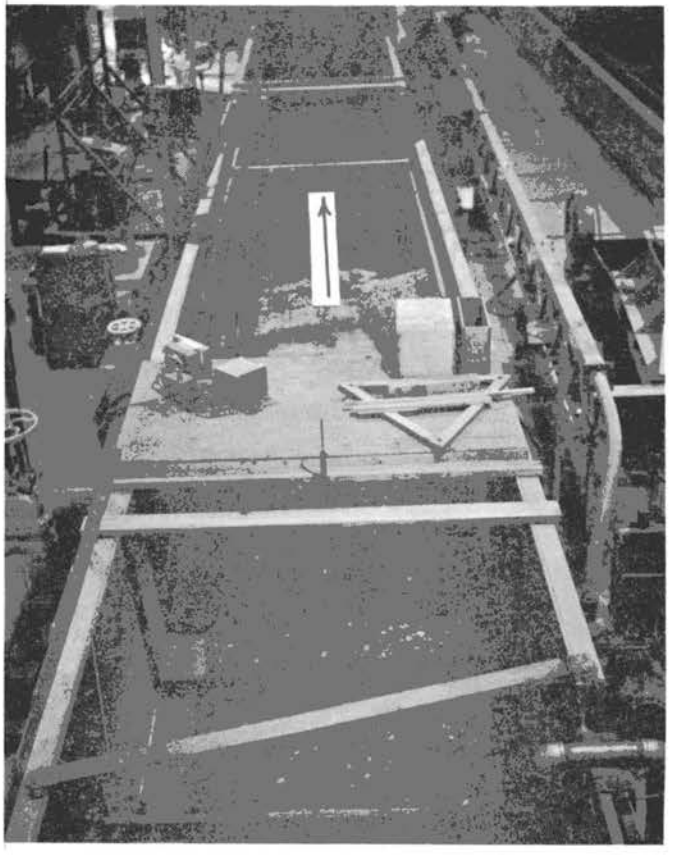

Fig. 29 - Photograph of the 6-foot wide flume showing the overbank-flow flood plain and the low-flow channel

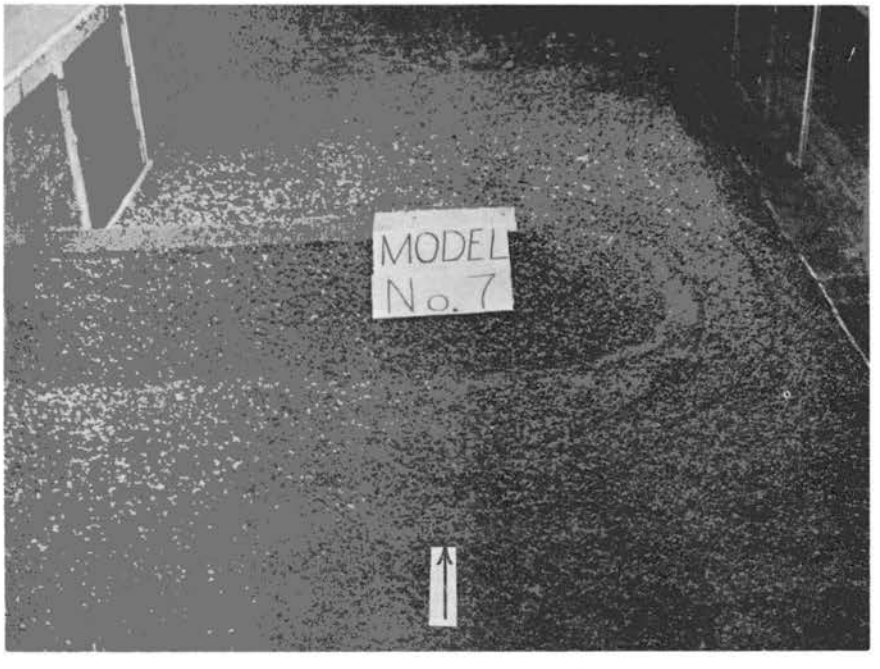

Fig. 30 - Photograph of an overbank flow model which is set back from the low-flow channel

Fig. 31 - Photograph of the abutment for a discharge of 0.94 cfs showing the separation on the upstream (left) shoulder

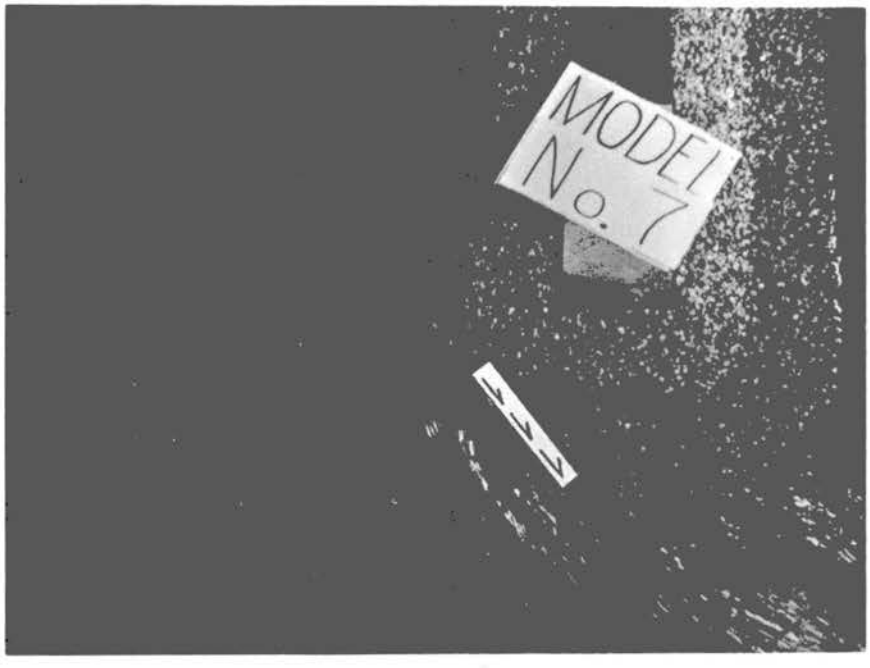

Fig. 32 - Photograph of the same abutment showing the scour at Q = 1.10 cfs

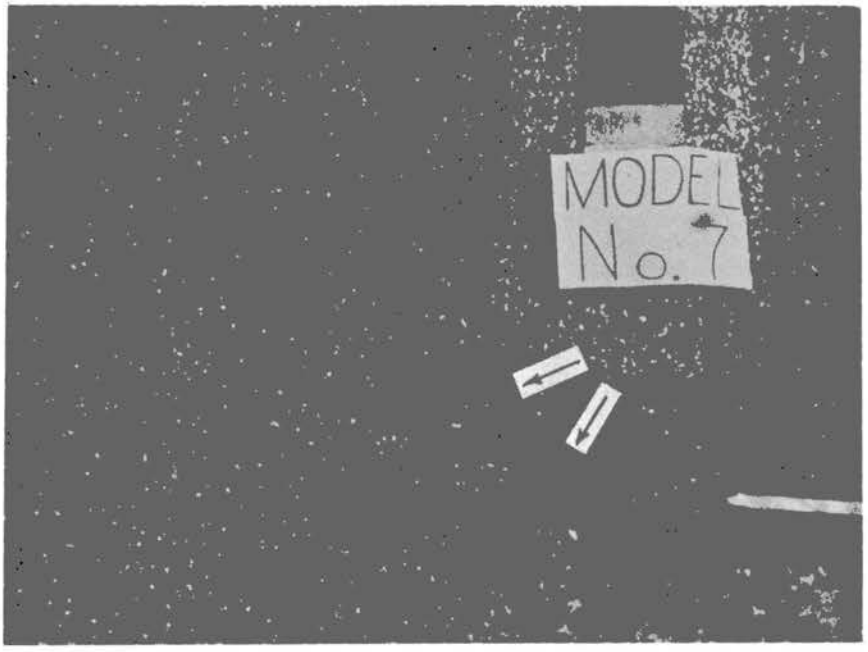

Fig. 33 - Photograph of the abutment after draining the flume

Fig. 34 - Photograph looking downstream showing the scoured abutment and the deposition downstream

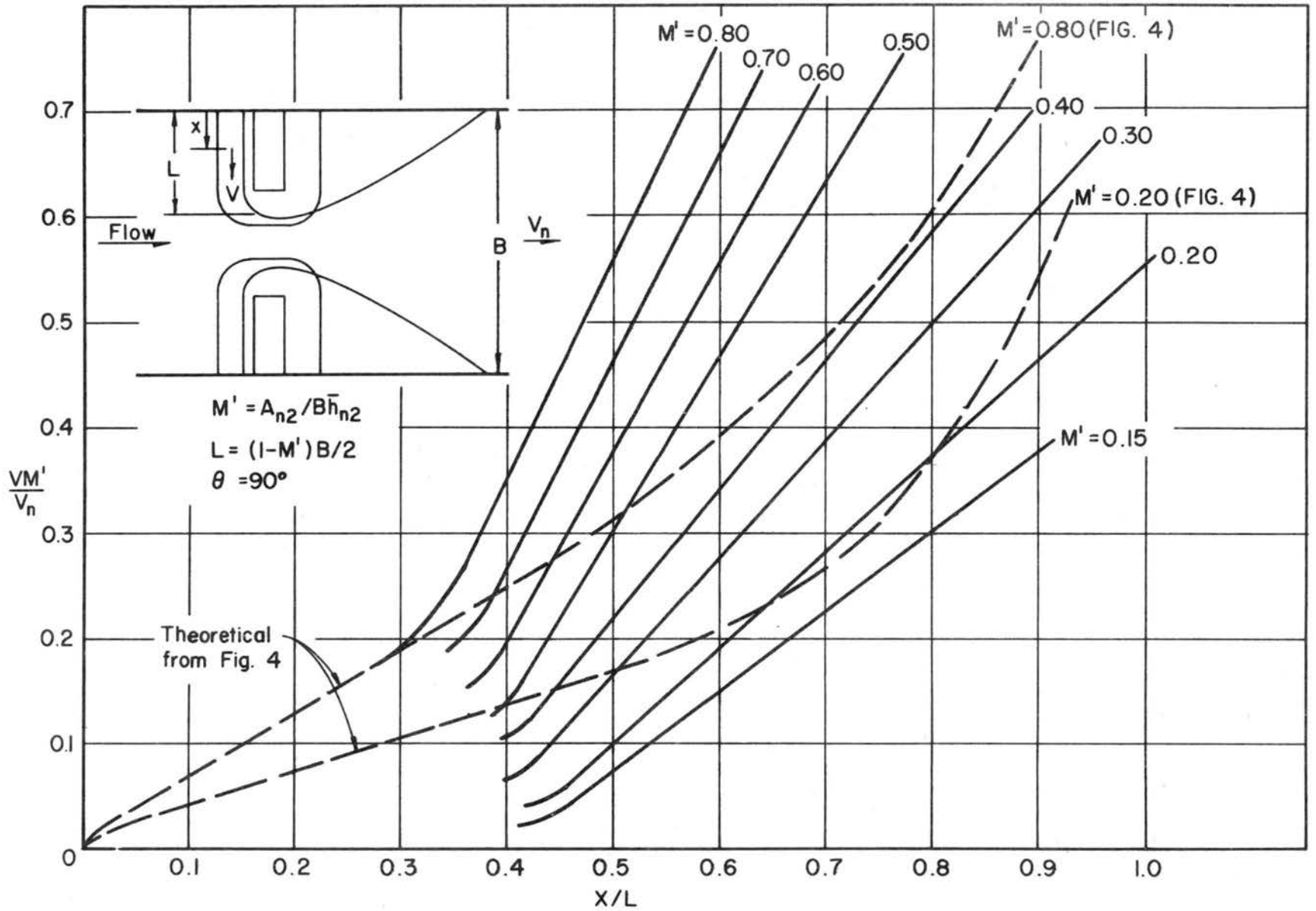

Fig. 35 Variation of Velocity on the Upstream Slopes of Approach Embankments

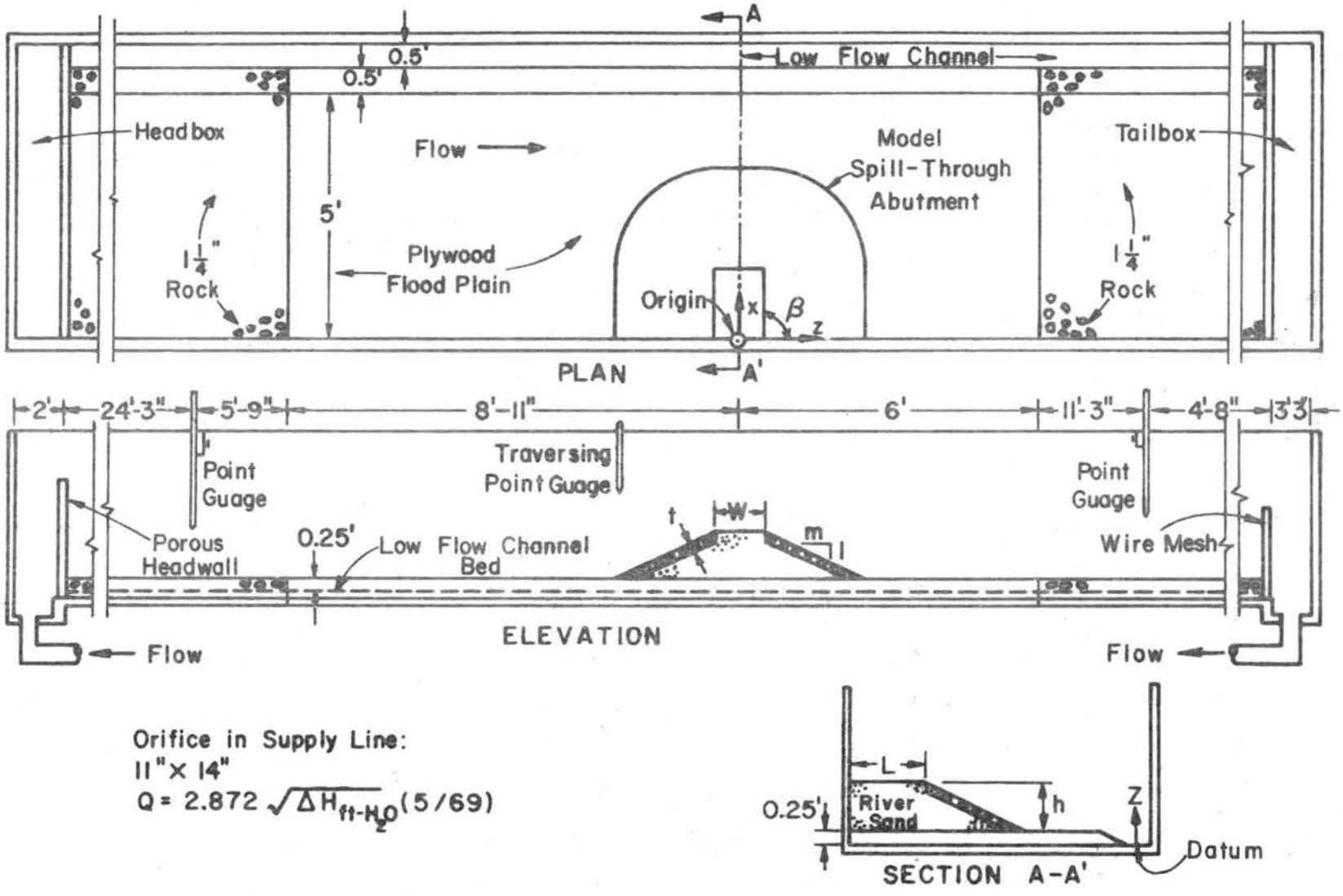

Fig. 36 Six-Foot Wide Flume Detail. Overbank Flow

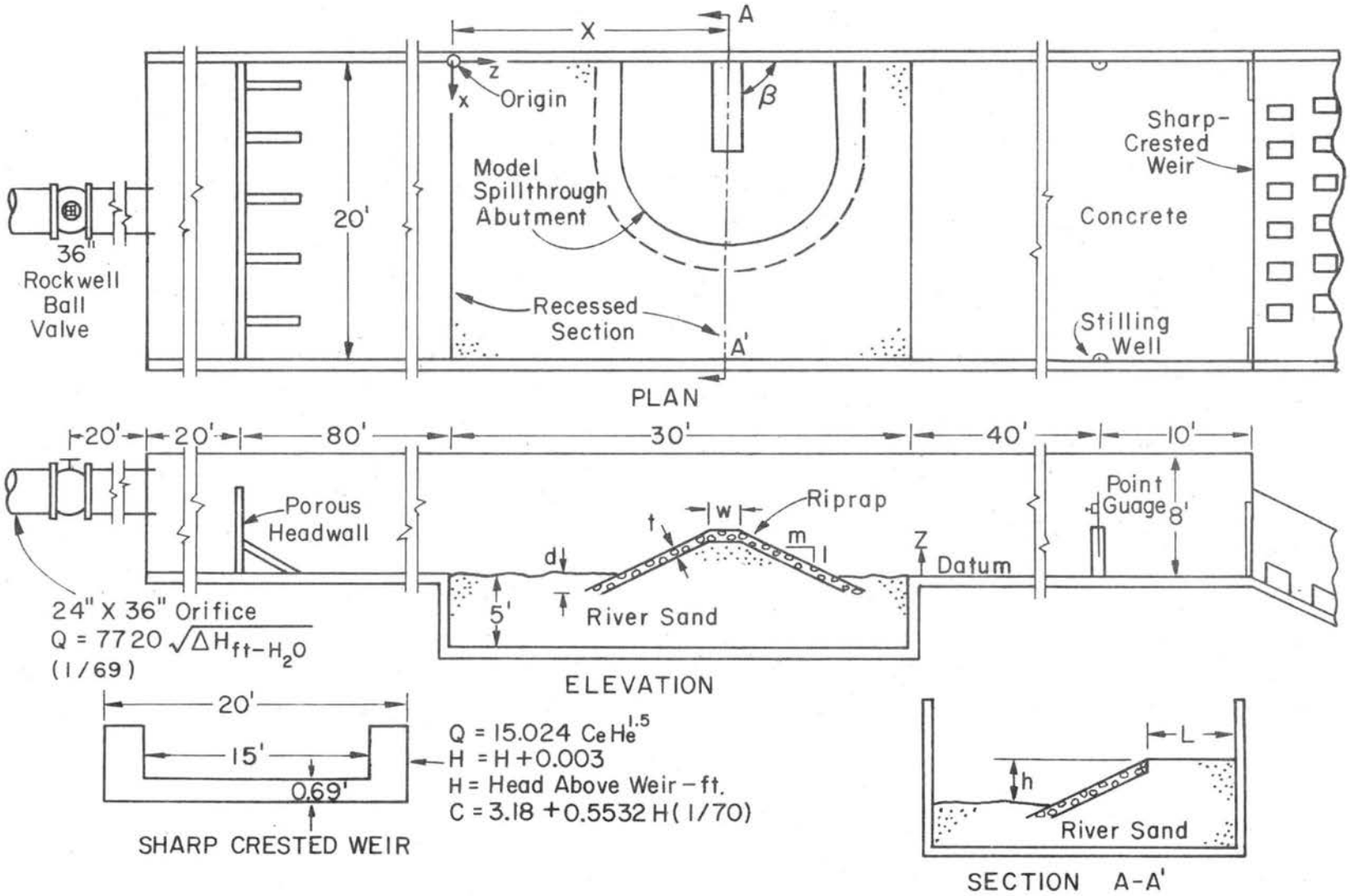

Fig. 37 Twenty-Foot Wide Outdoor-Flume Detail. Wide Channel Flow

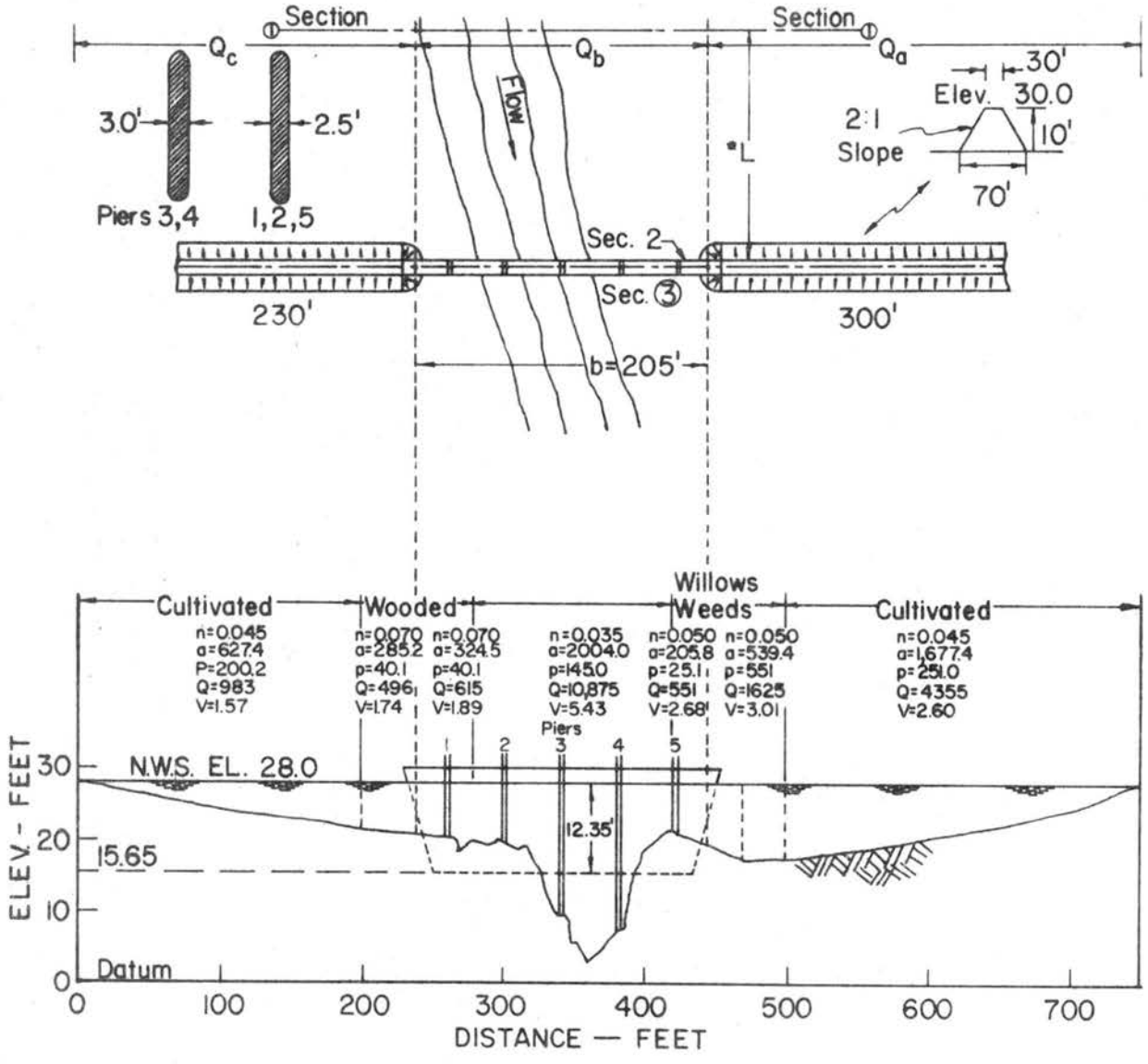

Fig. 38 Plan and Cross Section of Example Crossing, from Bradley (14)

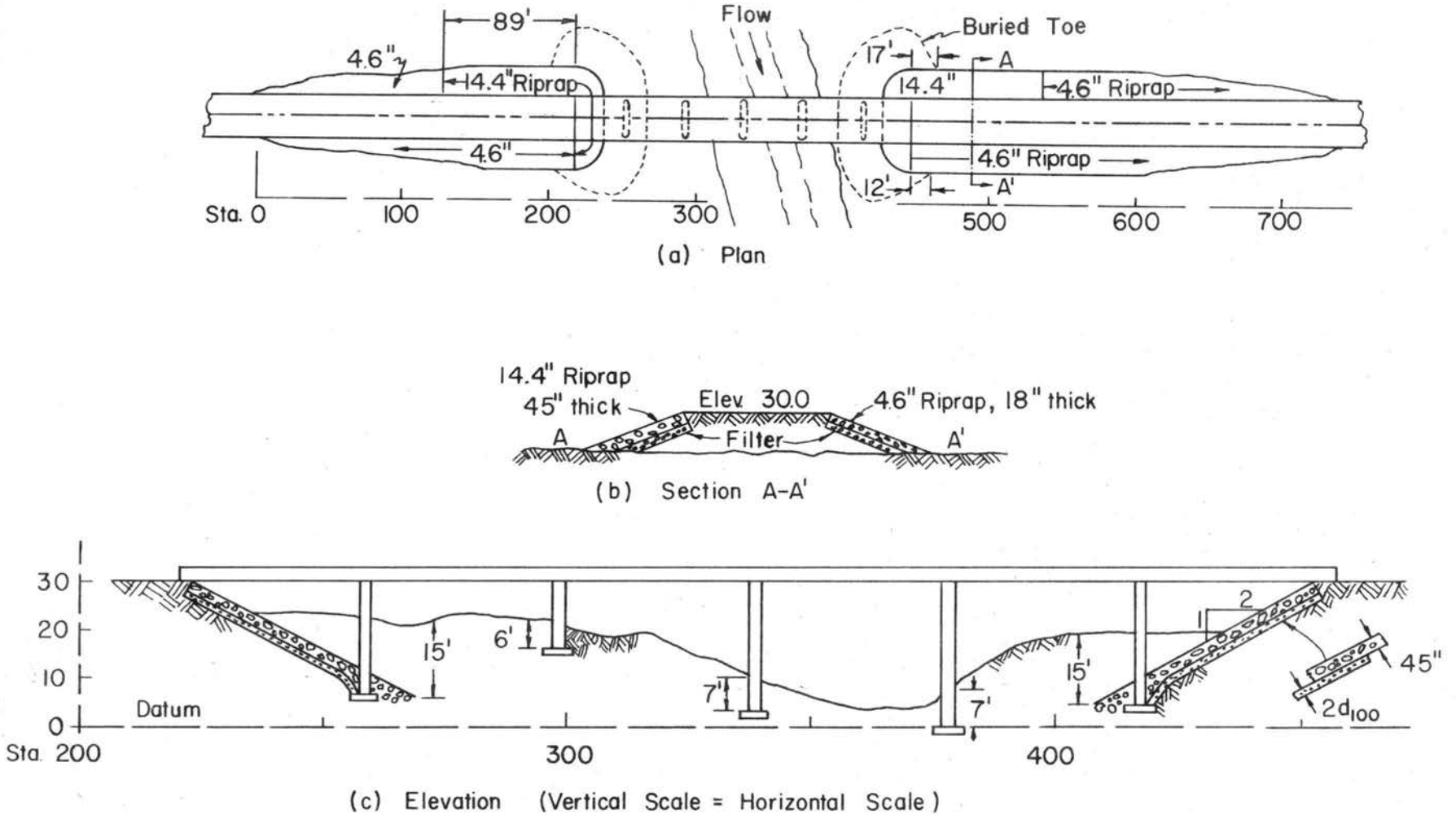

Fig. 39 Summary of Example Design Requirements

APPENDIX B

BACKWATER AND TOTAL WATER SURFACE DROP THROUGH THE ABUTMENTS

COMPUTATION OF BACKWATER AND TOTAL DROP THROUGH THE ABUTMENTS

Methods for computing the backwater and the total drop through the abutments are summarized here from "Hydraulics of Bridge Waterways" (14) for convenience in design. The methods are intended to be used for relatively straight reaches of streams having approximately uniform slope.

There are four types of flow which may be encountered in bridge waterway design. They are as follows:

Type I flow: Subcritical flow (Fig. 1a),

Type IIa flow: Critical flow in the gap (Fig. 1b),

Type IIb flow: Critical flow (Fig. 1c),

Type III flow: Supercritical flow (Fig. 1d), and

Type IV flow: Abnormal flow (Fig. 1e).

Procedures of computing the backwater, h_1^* , and the total drop through the abutments, Δh , for each type of flow under a bridge on a rigid bed are presented in Sections 1 and 2, respectively. Section 3 considers the effect of scour on backwater. Sections 4 and 5 cover the cases of dual bridges and the superstructure partially inundated.

1. Computation of Backwater

a) Type I flow: Subcritical flow (Fig. 1a).

The expression for computation of backwater upstream of a bridge constriction is

$$h_1^* = K^*\alpha_2 \frac{V_{n2}^2}{2g} + \alpha_1 \left[\left(\frac{A_{n2}}{A_{n4}} \right)^2 - \left(\frac{A_{n2}}{A_1} \right)^2 \right] \frac{V_{n2}^2}{2g} \quad , \qquad \text{(B1)}$$

where α_2 is the velocity head coefficient for the constriction, and K^* is the total backwater coefficient. The other symbols are defined in Chapter III and in Figure 1.

To compute backwater, it is necessary to obtain the approximate value of h_1^* by using the first part of Equation B1

$$h_1^* = K^* \alpha_2 \frac{V_{n2}^2}{2g} \quad ,$$

where α_2 can be found from Figure B1 with known M and α_1. The value of A_1 in the second part of Equation B 1 can then be determined, and the total backwater can be computed from Equation B1 if the value of K^* is known.

b) Computation of K^*

Figure B.2 shows the base curves for the backwater coefficient, K_b, plotted with respect to the opening ratio, M, for wingwall and spill-through abutments. In the case of a normal crossing without piers, $K^* = K_b$.

Backwater caused by piers in a bridge constriction may be estimated by adding an incremental backwater coefficient, designated as ΔK_p, to the base curve coefficient, K_b, when piers are present in the waterway. For a normal crossing with piers, the total backwater coefficient becomes

$$K^* = K_b \text{ (Fig. B.2)} + \Delta K_p \text{ (Fig. B.5)} \quad .$$

The magnitude of the incremental backwater coefficient, ΔK_e, accounting for the effect of eccentricity, is shown in Figure B.6. The total backwater coefficient for an extremely eccentric crossing ($e > 0.8$) with wingwall or spill-through abutments and piers is

$$K^* = K_b \text{ (Fig. B.2)} + \Delta K_p \text{ (Fig. B.5)} + \Delta K_e \text{ (Fig. B.6)} \quad .$$

Figure B.7 shows the incremental backwater coefficient, ΔK_s , for the effect of skewness of wingwall and spill-through abutments. The total backwater coefficient for a skewed crossing with piers and abutment faces aligned with the flow would be

$$K^* = K_b \text{ (Fig. B.2)} + \Delta K_p \text{ (Fig. B.5)} + \Delta K_s \text{ (Fig. B.7)} \quad .$$

c) Type II flow: Critical flow (Figs. 1b and 1c).

The curve of Figure B.8 accounts for the contraction ratio only, which is the major factor involved. The effect of piers, eccentricity, and skew, have not been evaluated because of the tentative nature of the curve. The incremental coefficients from Figures B.5, B.6 and B.7 for piers, eccentricity, and skew, are not applicable to Type II flow problems.

The backwater for Type II flow, with no allowance for piers, eccentricity, and skew, is

$$h_1^* = \alpha_2 \frac{V_{2c}^2}{2g} (C_b+1) - \alpha_1 \frac{V_1^2}{2g} + h_{2c} - \bar{h}_{n2} \quad ,$$

where C_b can be found from Figure B.8 with known M , α_2 can be found from Figure B.1, and the other symbols are defined in Chapter III and Figure 1.

d) Type III flow: Supercritical flow (Fig. 1d).

Theoretically, there is no backwater produced by Type III flow. No detailed information is available for supercritical flow occurring both upstream and downstream of a bridge constriction.

e) Type IV flow: Abnormal flow (Fig. 1e and Fig. B.9).

From the laboratory studies, the curves for the base backwater coefficients and the incremental backwater coefficients for Type I flow

(subcritical flow) are reasonably applicable to abnormal stage-discharge conditions. The expression for the computation of backwater for abnormal stage-discharge is

$$h^*_{1A} = K^*\alpha_2 \frac{V_{2A}^2}{2g} ,$$

where

$$K^* = K_b(\text{Fig. B.2}) + \Delta K_p(\text{Fig. B.5}) + \Delta K_e(\text{Fig. B.6}) + \Delta K_s(\text{Fig. B.7}) .$$

The subscript, A , has been added throughout to signify that this is an abnormal case. The symbols are defined in Fig. B.9.

f) Recognition of flow type

Recognition of which type of flow will occur at a proposed bridge site in the field, prior to starting the backwater computations, is difficult. As a suggestion, try the Type I flow approach for computing backwater first. Should the result appear unrealistic, repeat the backwater computation using the Type II approach. If the backwater for the Type II flow results in a lower value than for the Type I computation, the flow definitely will be Type II.

2. Computation of Total Drop Through the Abutments

a) Type I flow: Subcritical flow.

The expression for computation of total drop through the abutments is

$$\Delta h = h_1^* - h_3^* + S_o L_{1-3} ,$$

where h_1^* is the backwater computed by the method described in Section 1, h_3^* is the vertical distance from the water surface on the downstream side of the abutment to the normal water surface (Figs. 1 and B.10), S_o is

the natural slope of the stream, and L_{1-3} is the distance from Section 1 to Section 3 (Fig. 1). The methods of determining h_3^*, L_{1-3}, and Δh are explained as follows:

b) Computation of h_3^*

The differential level ratio, $D_b = h_b^*/(h_b^* + h_3^*)$, is plotted with respect to the opening ratio, M, in Figure B.10. The expression for computation of h_3^* in the case of normal crossings without piers is

$$h_3^* = h_b^* \left(\frac{1}{D_b} - 1 \right) ,$$

where h_b^*, which represents the backwater at a bridge for normal crossings exclusive of pier effect, can be determined by the method of computing backwater (Section 1). With a value of $K^* = K_b$ (Fig. B.2), D_b can be found from Figure B.10.

The effect of piers on the differential level ratio, D_b, is quite small and can be neglected. The expression for computation of h_3^* is

$$h_3^* = h_1^* \left(\frac{1}{D_b} - 1 \right) ,$$

where h_1^* is the computed backwater, including the effect of piers, and D_b can be found from Figure B.10.

For an extremely eccentric crossing with or without piers, the total differential level ratio is

$$D^* = D_b + \Delta D_e ,$$

where ΔD_e is the incremental differential level ratio in Figure B.11, accounting for the effect of eccentricity. The expression for computation of h_3^* is

$$h_3^* = h_1^* \left(\frac{1}{D_b} - 1 \right) ,$$

where h_1^* is the computed backwater, including effects of eccentricity, with or without piers (Section 1).

The incremental differential level ratio, ΔD_s , for the effect of skew has been plotted with respect to M in Figure B.12 for the left bank of wingwall and spill-through abutments. No detailed information is available for the difference in water level along the right bank.

c) Computation of L_{1-3} and Δh

A trial solution is required for determining Δh . Enter Fig. B.13A with appropriate values of $\Delta h/\bar{h}_{n2}$ and $\bar{h}_{n2}$, and obtain the corresponding value of L^*/b , where the distance L^* is defined in Figure B.13, and $\bar{h}_{n2}$ is the mean depth of flow under the bridge, referenced to normal stage (Fig. 1).

Solving for L^* and adding the distance to Section 3 gives the distance L_{1-3} (Fig. B.13B). An estimate for Δh is $h_1^* + h_3^* + S_o L_{1-3}$. If the computed value of Δh differs materially from the value chosen, the above procedure is repeated until assumed and computed values agree.

For eccentric crossings with $e > 0.7$, multiply the L^*/b value from Figure B.13C by ω . For example, assume that $\Delta h/\bar{h}_{n2} = 0.2$, $\bar{h}_{n2} = 10$, and $e = 0.88$. The corrected value would be $L^*/b = 0.84 \times 1.60$, or 1.34.

To obtain the approximate distance to maximum backwater, L^* , and Δh for skewed crossings (Fig. B.4), the same procedure is recommended as for normal crossings except that the ordinate of Figure B.13 is read as L^*/b_s , where b_s is the distance between the skewed abutments (Fig. B.4).

d) Type IV flow: Abnormal flow.

To obtain Δh for abnormal stage-discharge conditions, Figure B.10 is considered approximate but applicable. The method of computation is similar to that explained in Section 2a for normal stage-discharge. The principal differences lie in the manner in which the backwater is computed for abnormal stage conditions. The expression for computation of h_{3A}^* is

$$h_{3A}^* = h_{bA}^* \left(\frac{1}{D_b} - 1 \right) ,$$

where

D_b = differential level ratio from the base curve in Figure B.10 (no adjustment is needed for eccentricity or skew),

h_{bA}^* = backwater above abnormal stage (without piers), and

h_{3A}^* = vertical distance from the water surface to the abnormal stage at Section 3 (Fig. B.9 - this dimension will be the same with or without piers).

3. Effect of Scour on Backwater

Any means of increasing the waterway area under a bridge can be effective in reducing the backwater. To obtain backwater and related information for bridge sites where scour occurs before the flood peak, it is first necessary to compute the backwater and other quantities desired from the method outlined in Sections 1 and 2 for a rigid bed, using the original cross section of the stream at the bridge site. These values are then multiplied by a common coefficient from Figure B.15 as follows:

$$h_{1s}^* = Ch_1^*$$

$$h_{3s}^* = Ch_3^*$$

$$\psi h_s = C\psi h$$

where h_{1s}^* , h_{3s}^* , and ψh_s are defined in Figure B.14A, and A_s is the area of scour measured on the downstream side of the bridge (Figs. B.14B and B.14C).

4. Dual Bridges

The following method for computing backwater and water surface drop through dual bridges is only applicable to Type I flow (subcritical flow).

a) Backwater determination.

The curve in Figure B.17 was established from tests made on normal crossings with and without piers. To determine backwater for dual bridges, it is necessary first to compute the backwater, h_1^* , for a single bridge, as previously outlined in Section 1. The backwater for the dual combination, measured upstream from the first bridge (Fig. B.17) is then

$$h_d^* = h_1^* \eta \quad ,$$

b) Computation of total drop through the abutments.

The water-surface level immediately downstream of the second bridge embankment at Section 3B may be obtained from Figure B.17. Compute h_1^* and h_3^* for the upstream bridge from Sections 1 and 3 and compute $\psi h = h_1^* + h_3^*$ for the single bridge, and $\psi h_{3B} = h_d^* + h_{3B}^*$ for the dual bridge combination. Using the ratio from Figure B.16, the value for h_{3B}^* is computed from

$$\psi h_{3B} = \xi \psi h \quad ,$$

$$\Delta h_{3B} = \psi h_{3B} + S_o L_{1\text{-}3B} \quad ,$$

and

$$h_{3B}^* = \psi h_{3B} - h^*d \quad ,$$

where all the parameters are defined in Figure B.17.

5. Superstructure Partially Inundated (Type I flow only).

Cases arise in which it is desirable to compute either the backwater upstream of a bridge or the discharge under a bridge when flow is in contact with the girders.

a) Case I: Upstream girder in flow (Fig. B.18).

Once flow contacts the upstream girder of a bridge, orifice flow is established. Using a common expression for sluice-gate flow

$$Q = C_d b_N Z \left[2g\left(h_u - \frac{Z}{2} + \alpha_1 \frac{V_1^2}{2g}\right)\right]^{\frac{1}{2}} \quad , \qquad \text{(B2)}$$

where

Q = total discharge (cfs),

C_d = coefficient of discharge,

b_N = net width of waterway excluding piers (ft),

Z and h_u = vertical distances (see sketch in Fig. B.18).

The coefficient of discharge, C_d , is plotted with respect to the parameter h_u/Z in Figure B.18. By substituting values in Equation B2, it is possible to solve by trial and error for either the water surface upstream or the discharge under the bridge, depending on the quantities known. There is a transition zone somewhere between $h_u/Z = 1.0$ and 1.1 where free surface flow changes to orifice flow or vice versa. The type of flow within this range is unpredictable.

The approximate depth of flow, h_3 , can be obtained from Figure B.18 by entering the top scale with the proper value of h_u/Z and

reading down to the upper curve, then over horizontally to the lower curve, and finally down to the lower scale as shown by the arrows. The lower scale gives the ratio of h_u/h_3 .

b) Case II: All girders in contact with flow (Fig. B.19).

To compute the water surface elevation upstream of the bridge, the water surface elevation on the downstream side and the discharge must be known. If the discharge is desired, Δh and the net area under the bridge are required. The experimental points in Figure B.19A, which are for both wingwall and spill-through abutments, show the coefficient of discharge to be essentially constant at 0.8 for the range of conditions tested. The equation recommended for the average bridge with two or four concrete girders is

$$Q = 0.80\ b_N Z(2g\Delta h)^{\frac{1}{2}} \quad .$$

Once Δh is computed from the above equation, the depth of flow upstream, h_u , can be obtained from Figure B.19B.

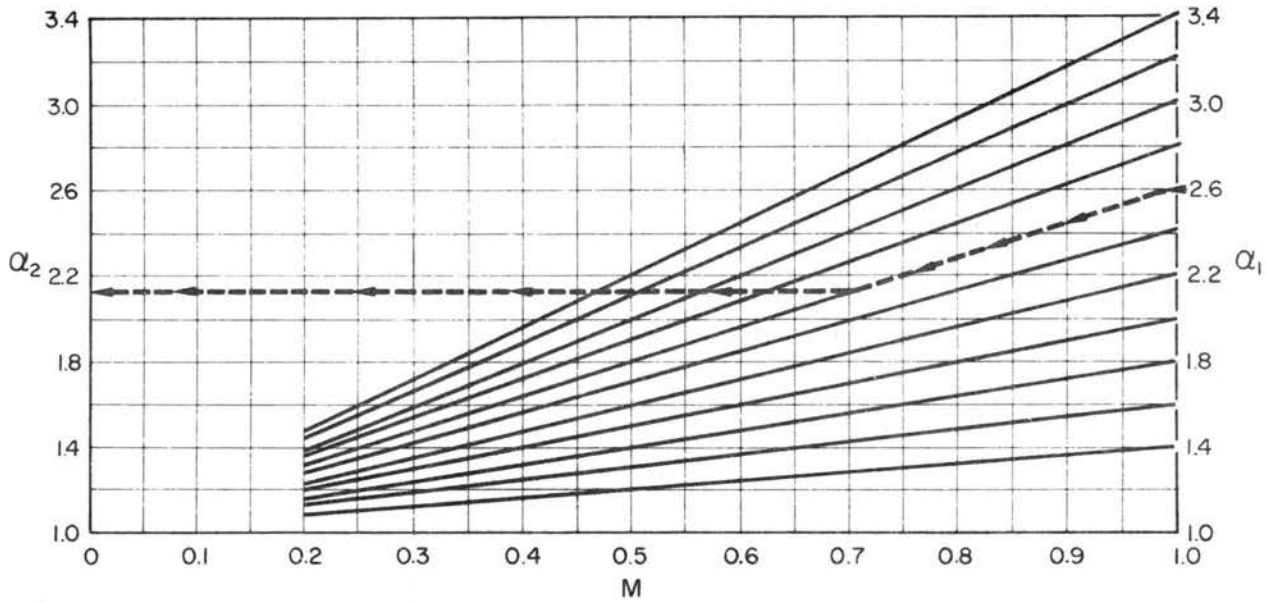

Fig. B.1 Aid for Estimating α_2

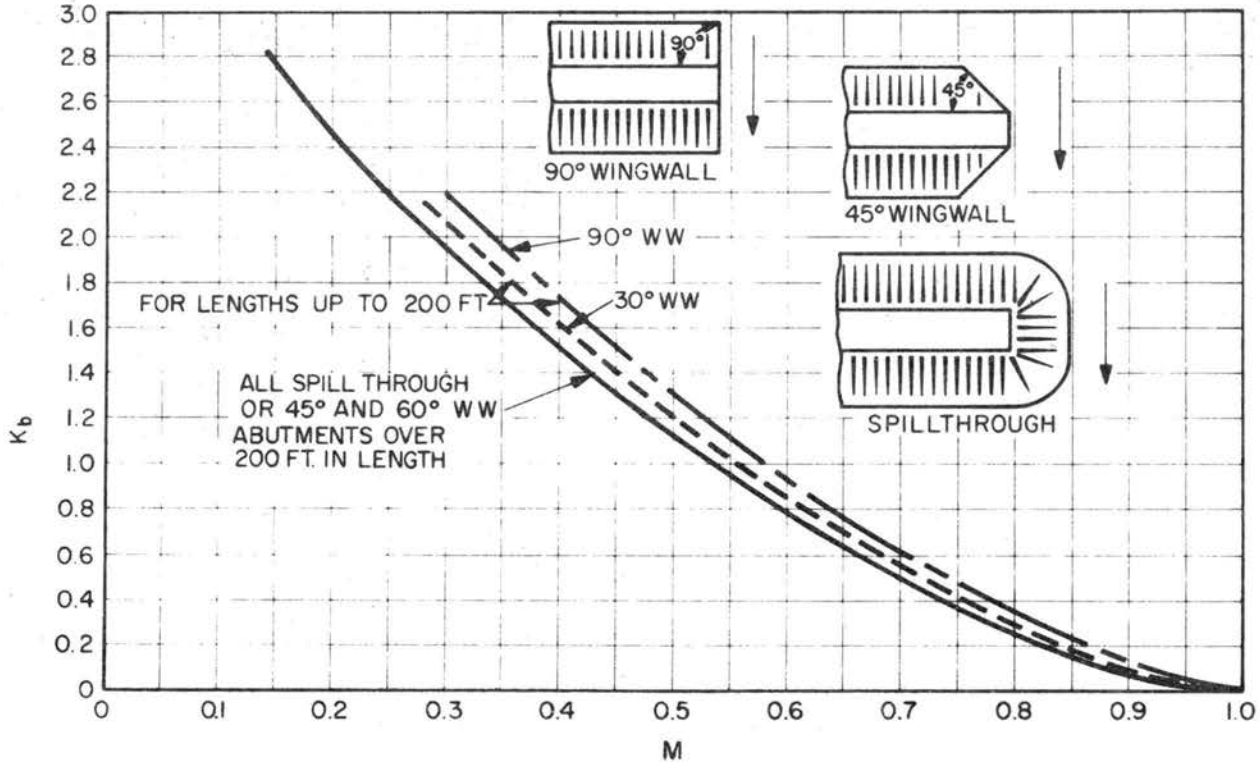

Fig. B.2 Backwater Coefficient Base Curves (Subcritical Flow)

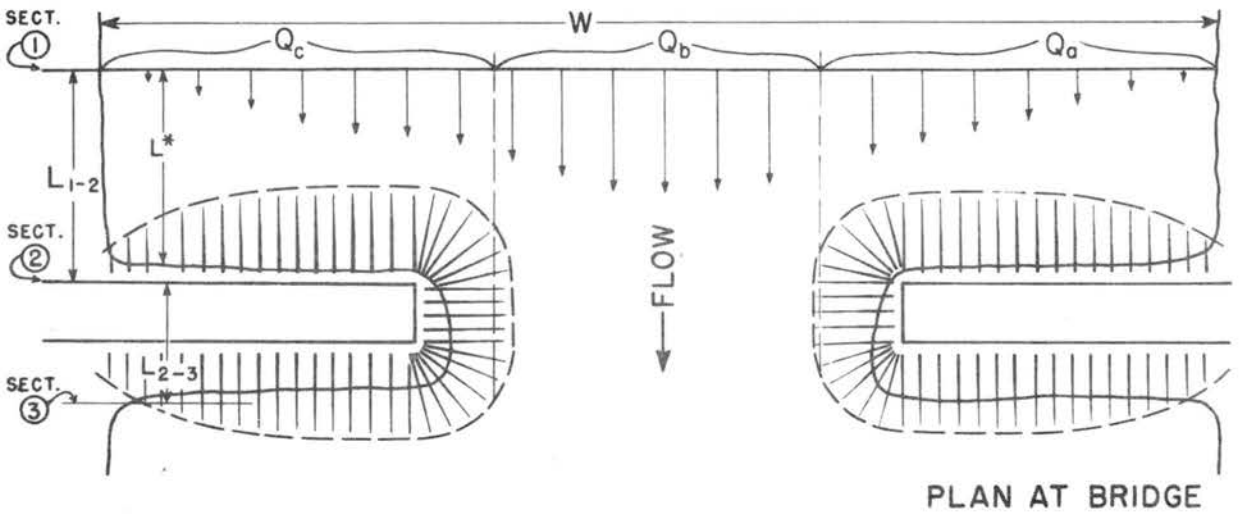

Fig. B.3 Normal Crossings: Spill-through Abutments

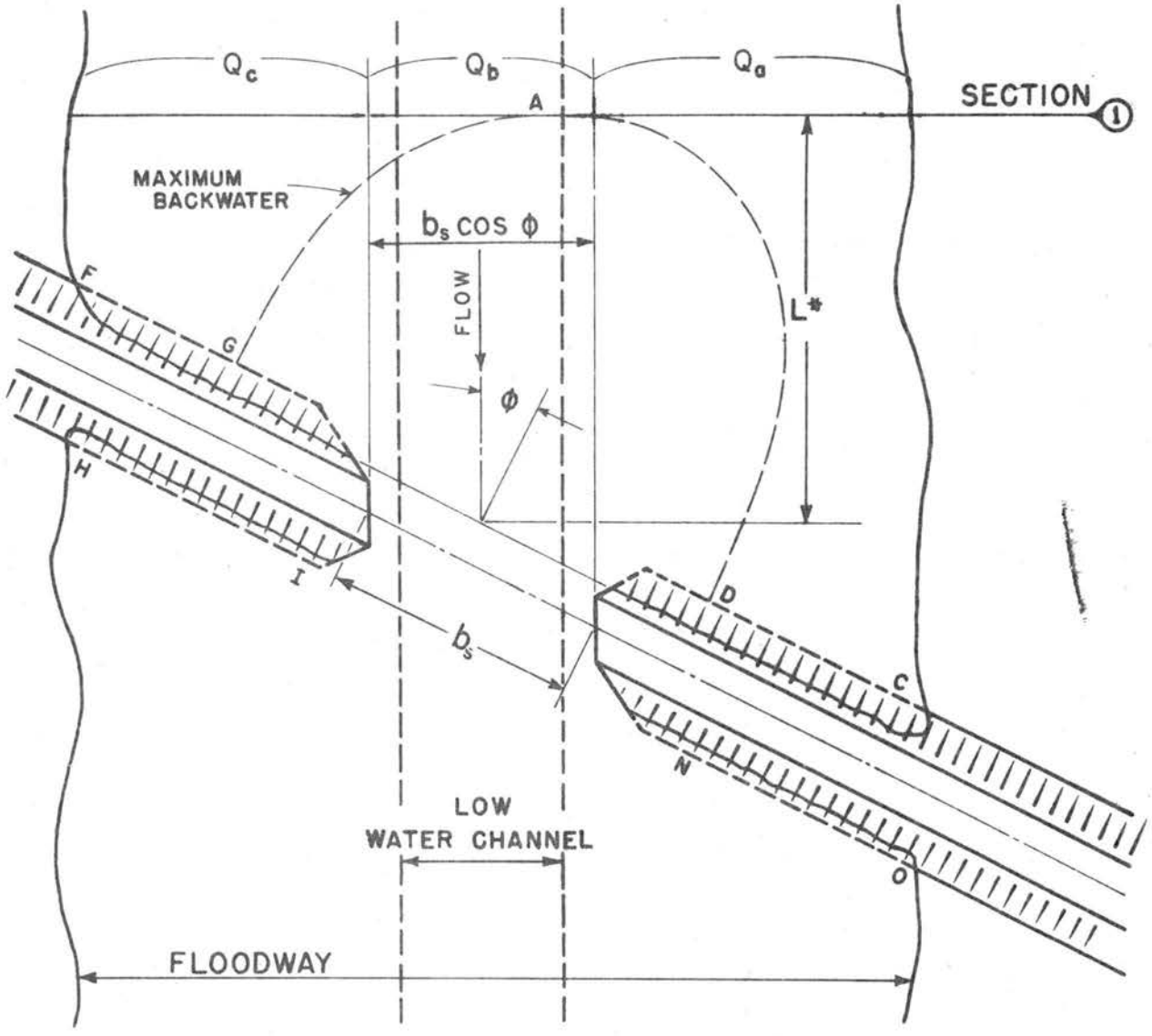

Fig. B.4 Skewed Crossings

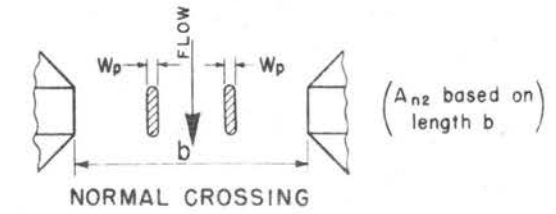

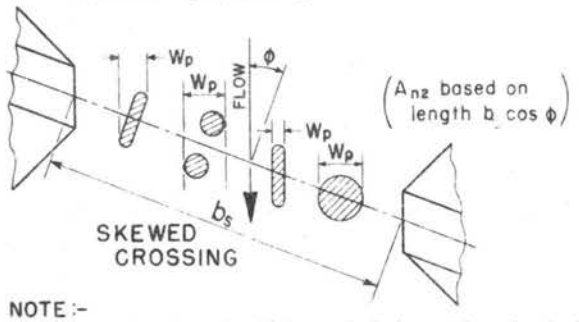

W_p = Width of pier normal to flow — feet

h_{n2} = Height of pier exposed to flow — feet

N = Number of piers

$A_p = \Sigma^N W_p h_{n2}$ = total projected area of piers normal to flow — square feet

A_{n2} = Gross water cross section in constriction based on normal water surface. (Use projected bridge length normal to flow for skew crossings)

$J = \frac{A_p}{A_{n2}}$

NOTE :-
Sway bracing should be included in width of pile bents.

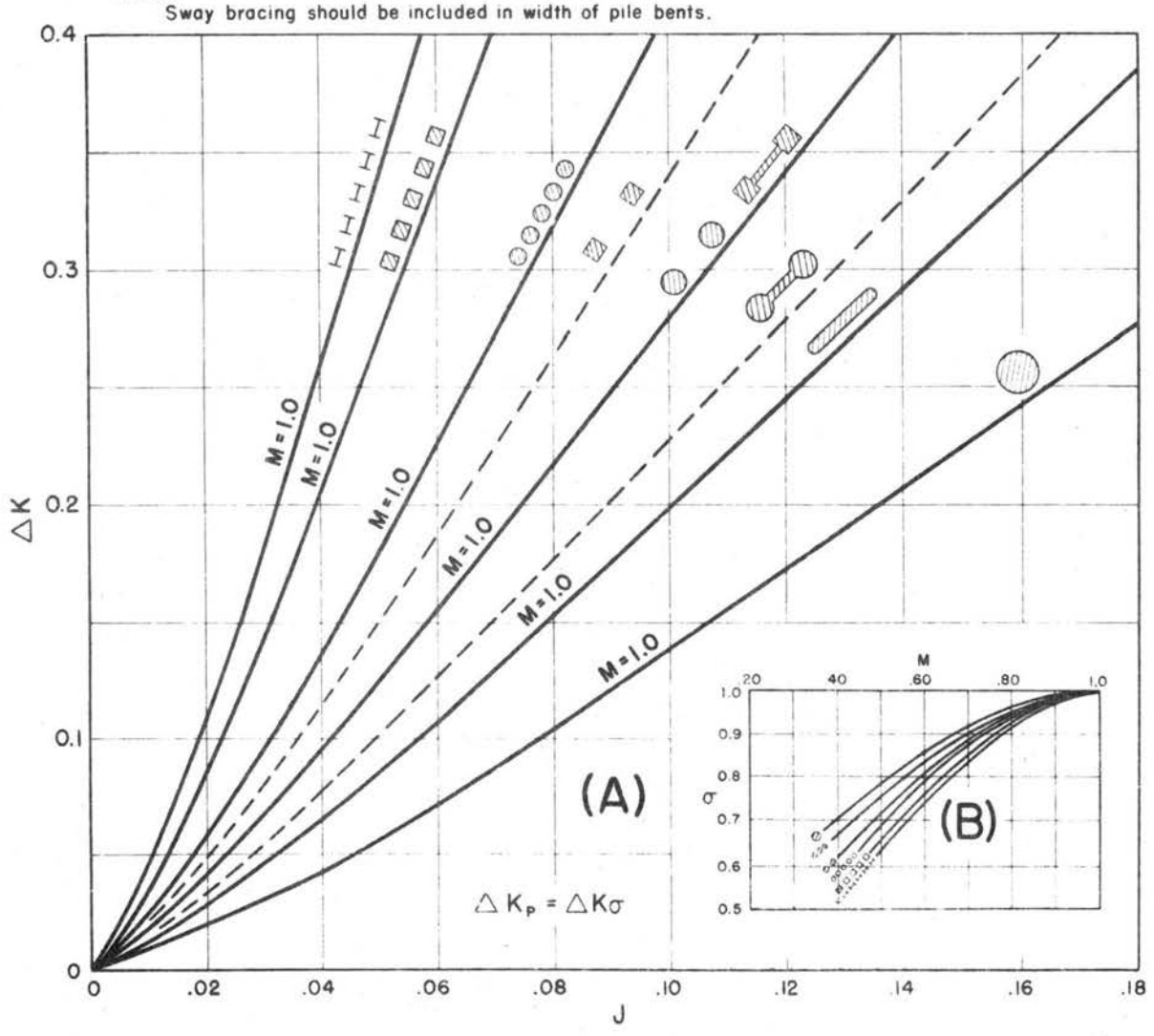

Fig. B.5 Incremental Backwater Coefficient for Piers

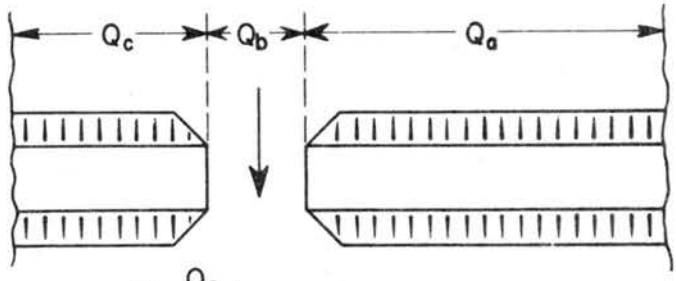

$$e = (1 - \frac{Q_c}{Q_a}) \quad \text{where} \quad Q_c < Q_a \quad \text{or}$$

$$e = (1 - \frac{Q_a}{Q_c}) \quad \text{where} \quad Q_a < Q_c$$

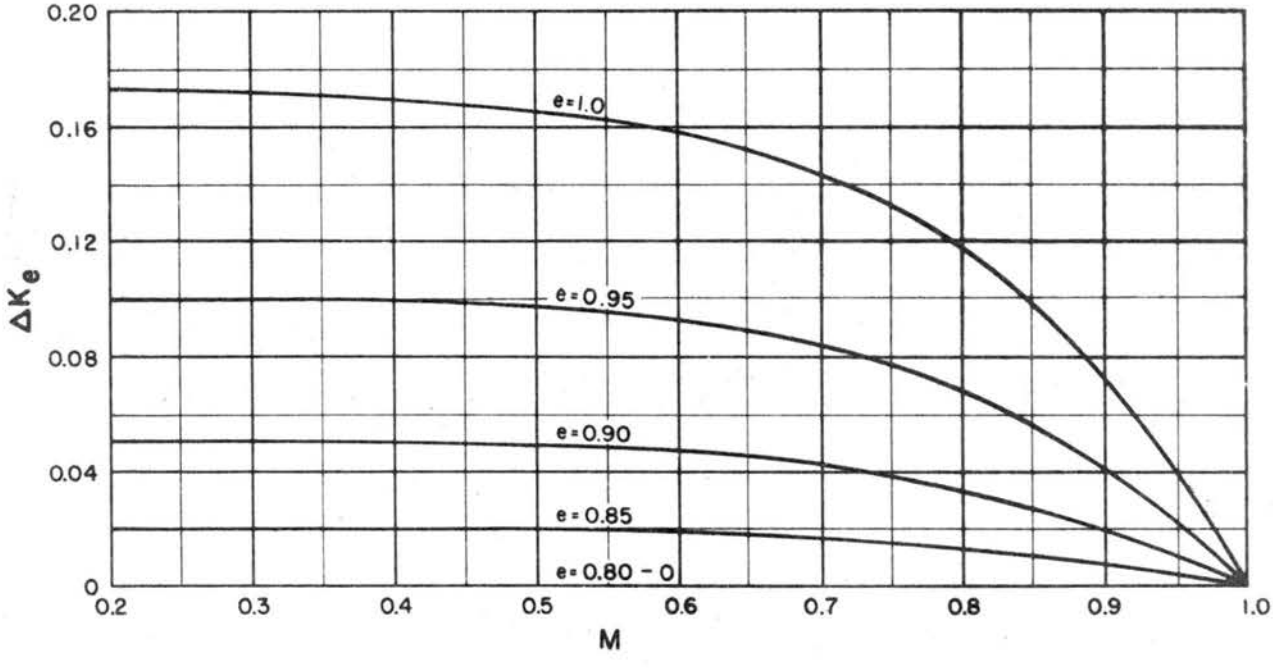

Fig. B.6 Incremental Backwater Coefficient for Eccentricity

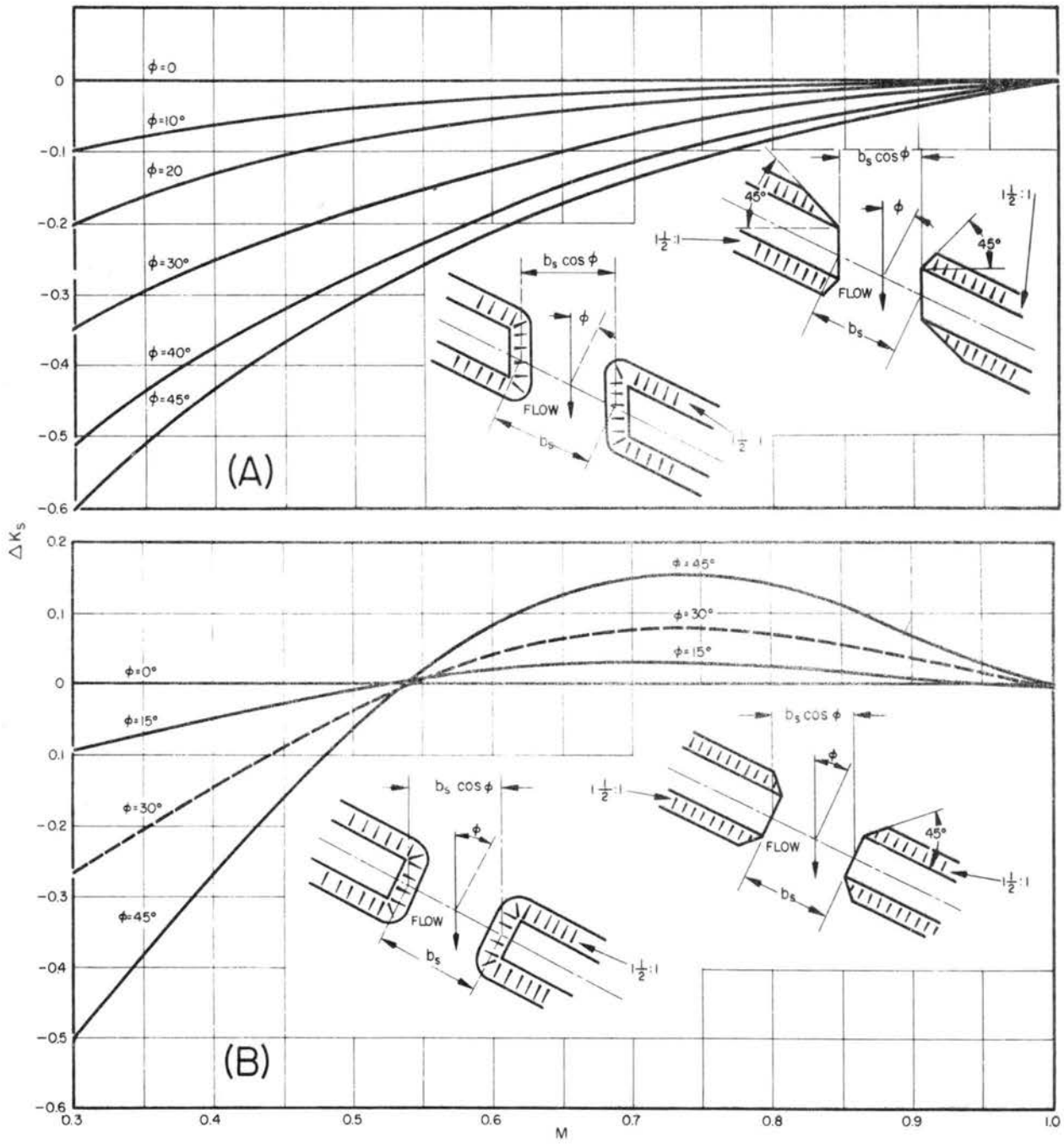

Fig. B.7 Incremental Backwater Coefficient for Skew

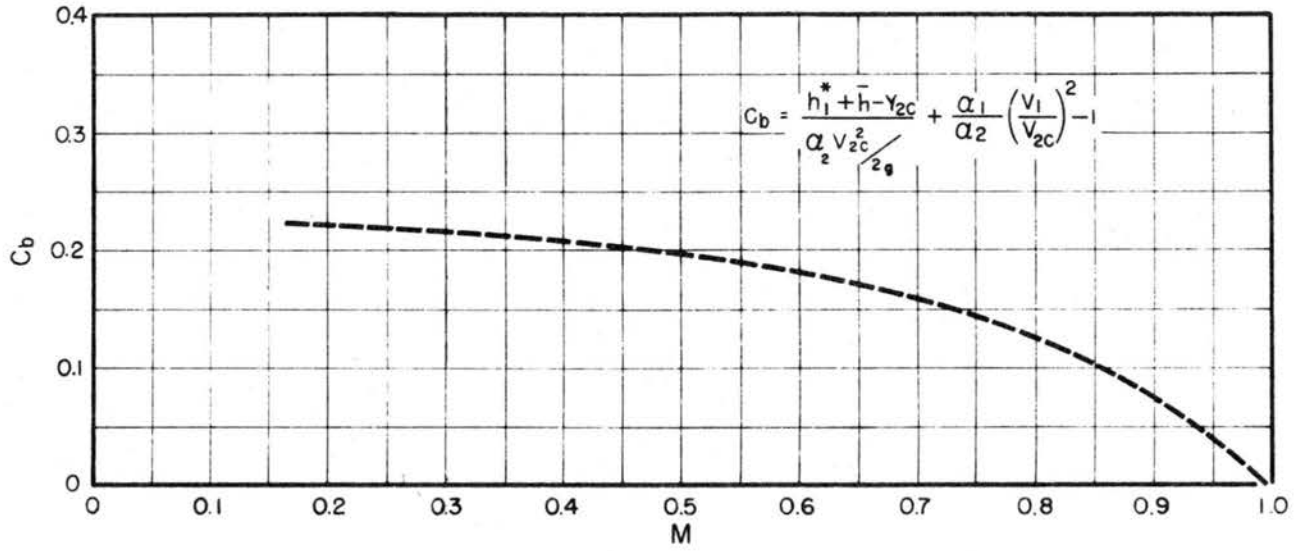

Fig. B.8 Tentative Backwater Coefficient Curve for Type II Flow

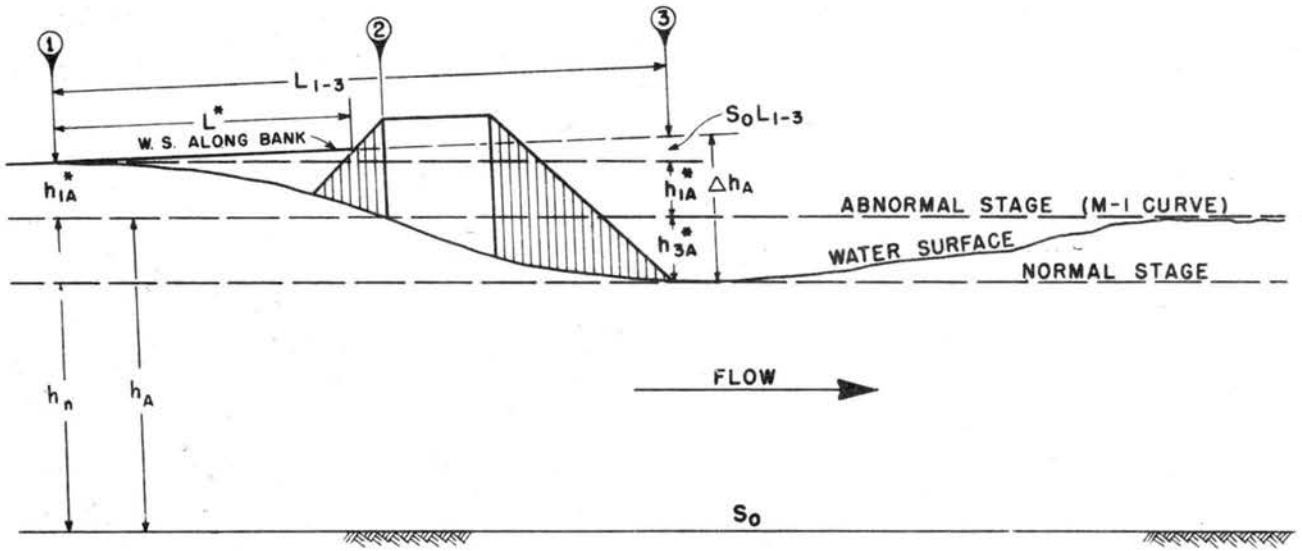

Fig. B.9 Backwater with Abnormal Stage-discharge Condition

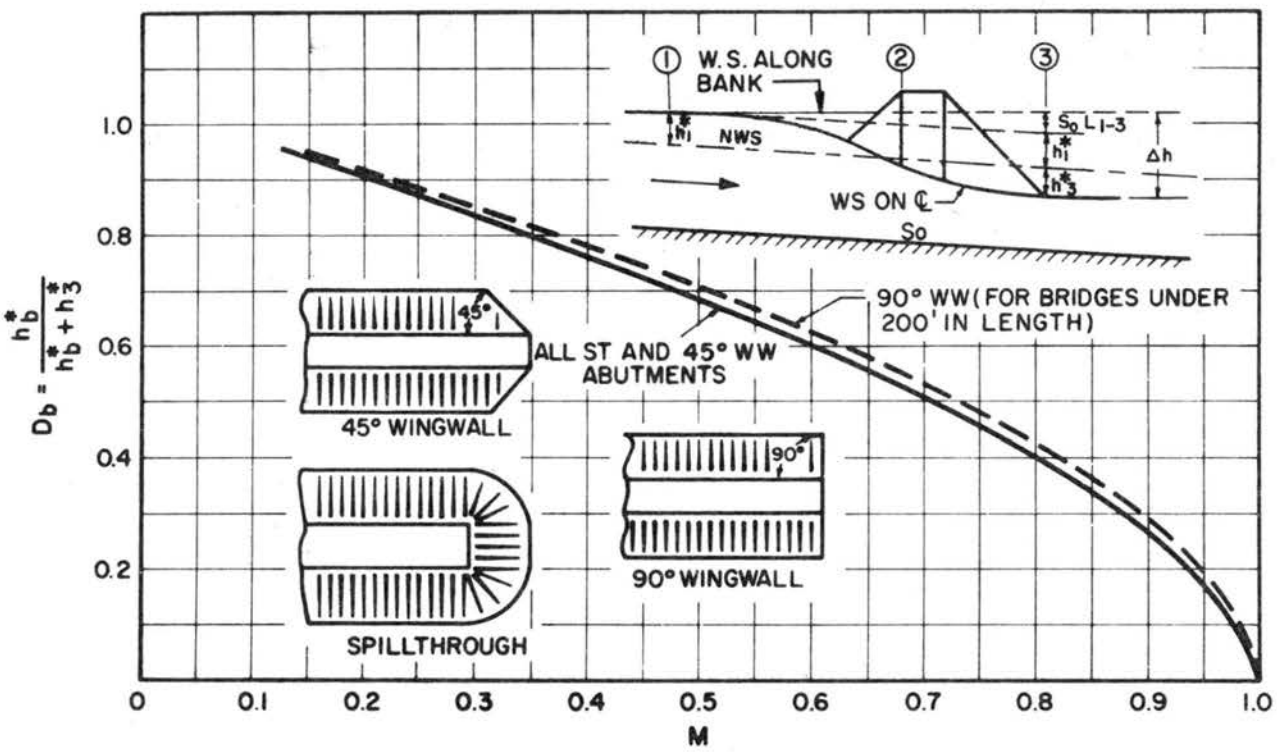

Fig. B.10 Differential Water Level Ratio Base Curves

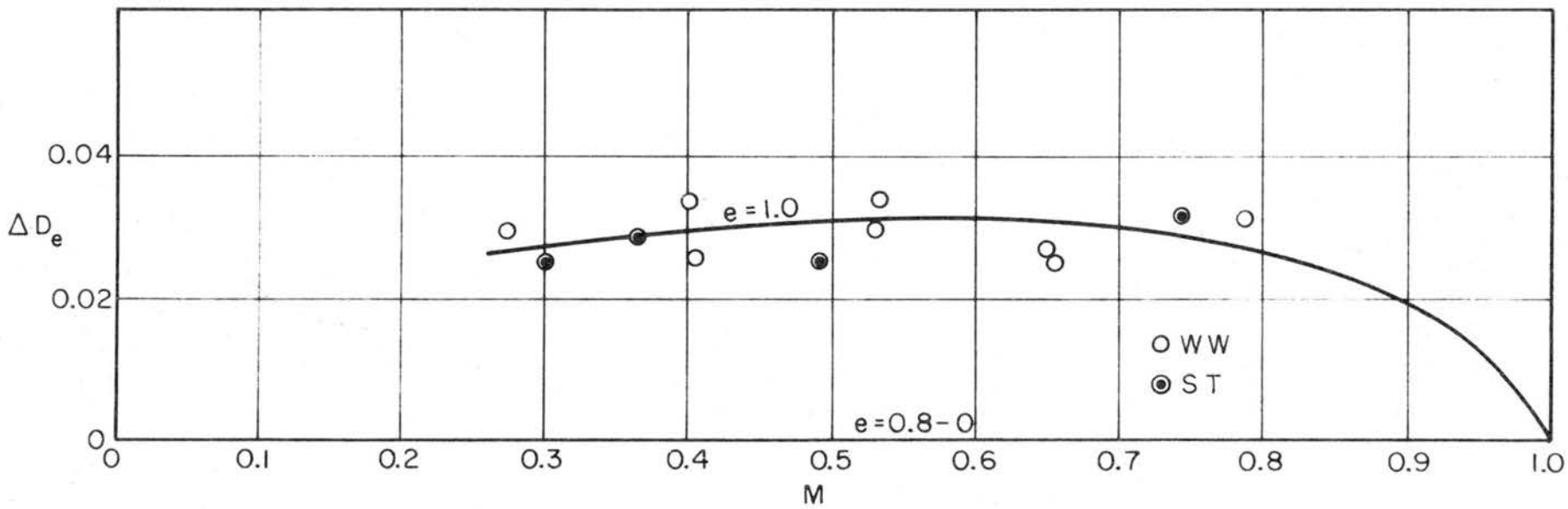

Fig. B.11 Incremental Differential Level Ratio ΔD_e for Eccentric Crossing and Wing-wall and Spill-through Abutments

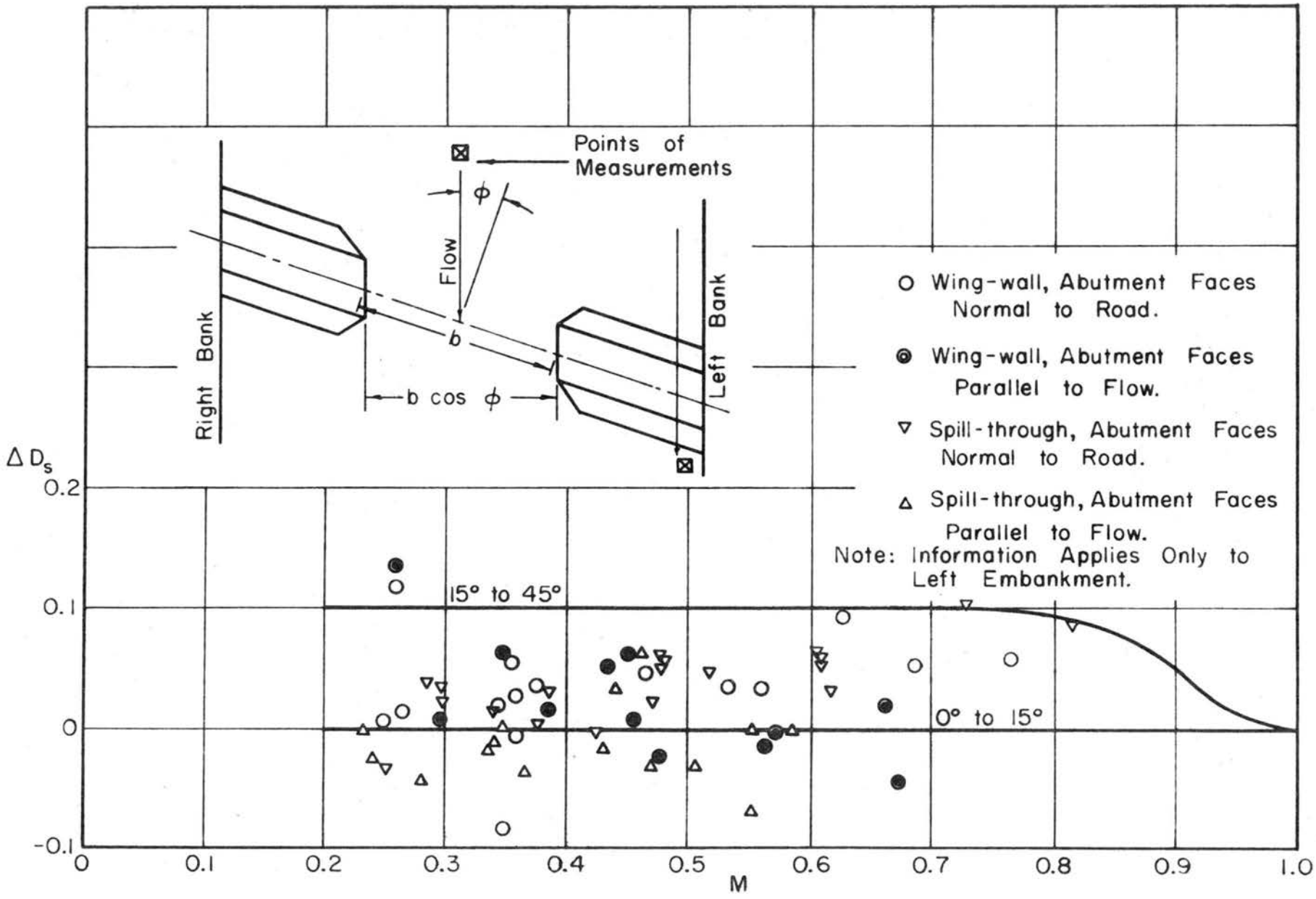

Fig. B.12 Incremental Differential Level Ratio ΔD_s for Wing-wall and Spill-through Abutments

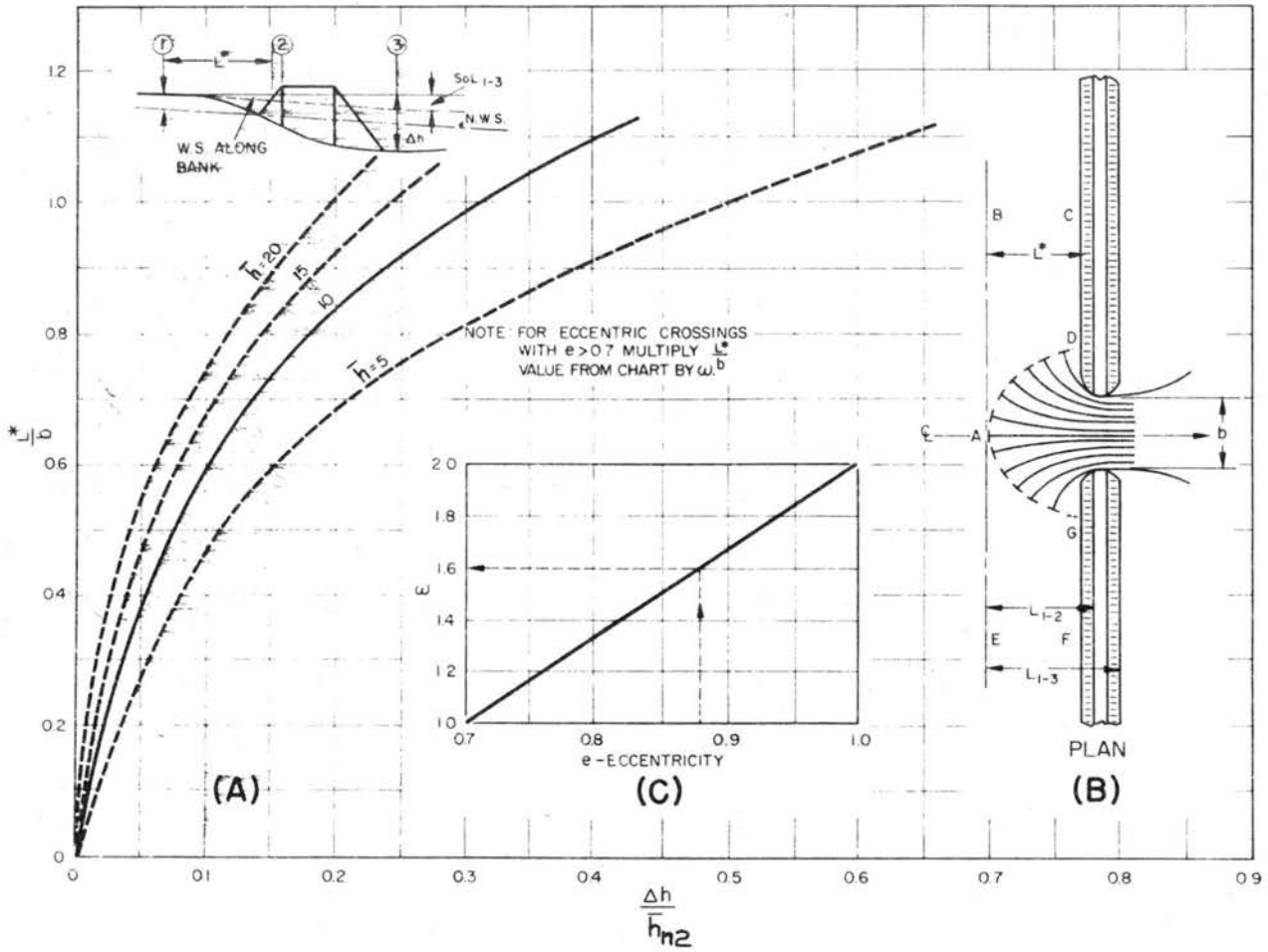

Fig. B.13 Distance to Maximum Backwater

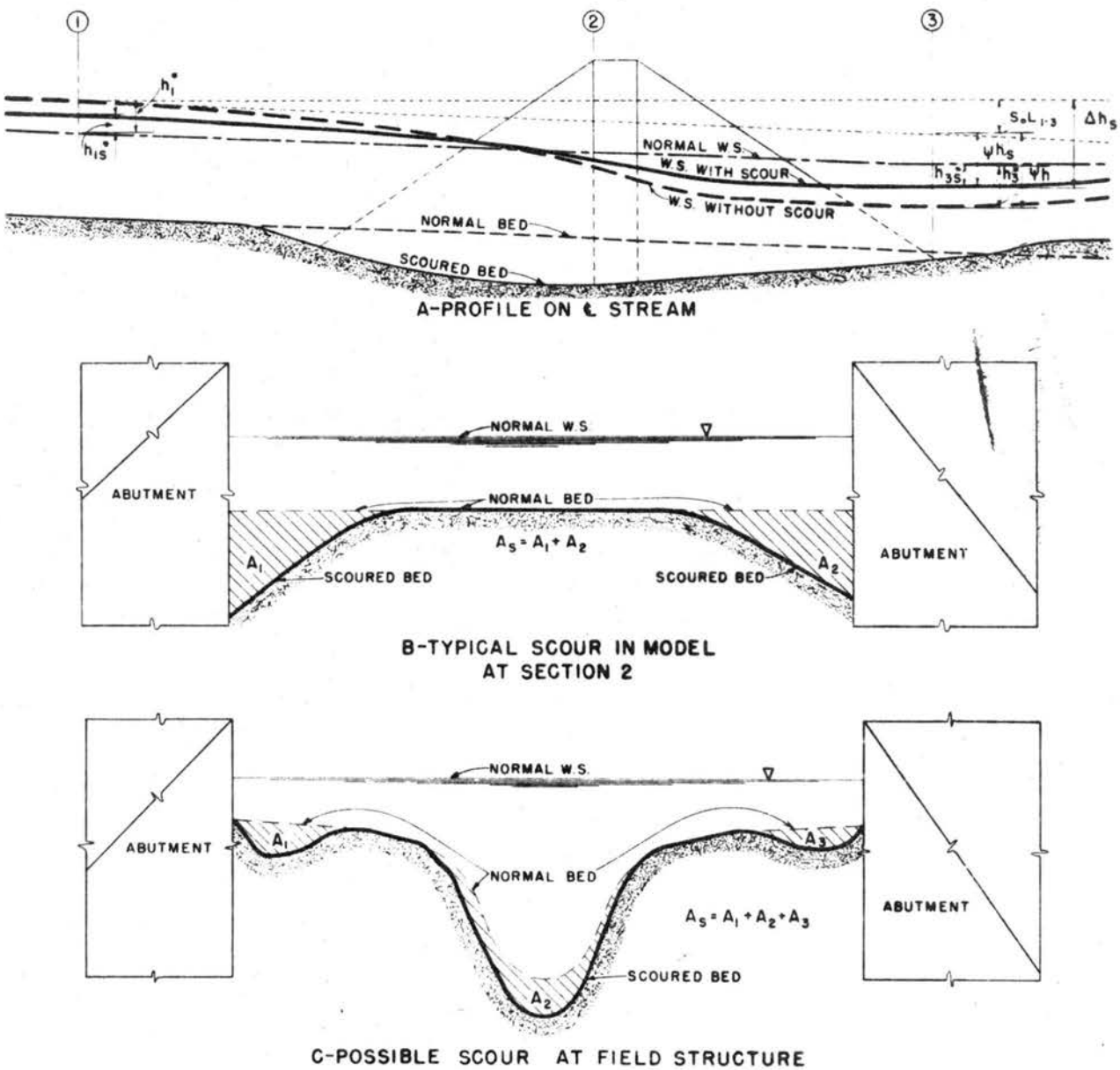

Fig. B.14 Effect of Scour on Bridge Backwater

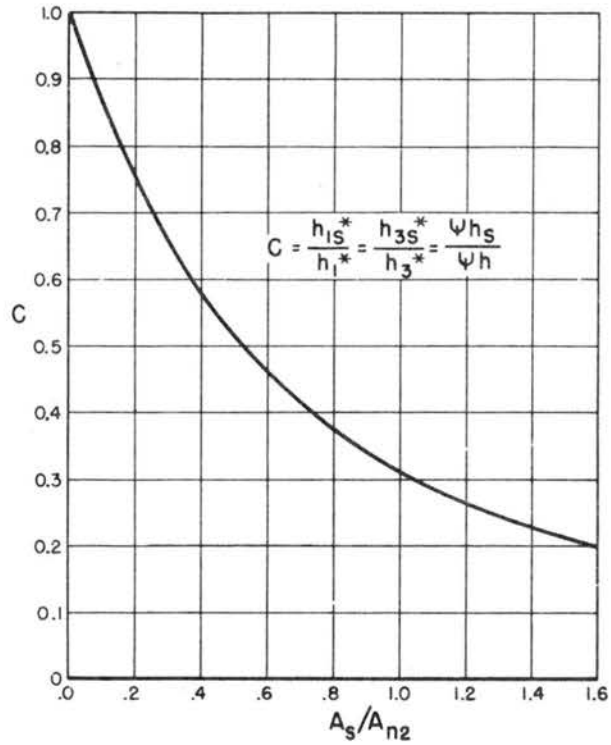

Fig. B.15 Correction Factor for Backwater with Scour

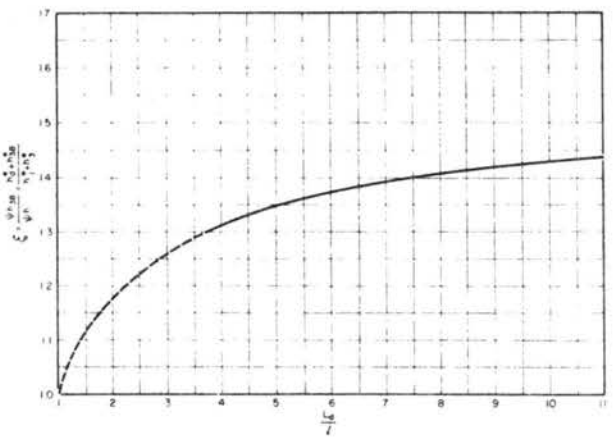

Fig. B.16 Differential Level Multiplication Factor for Dual Parallel Bridges

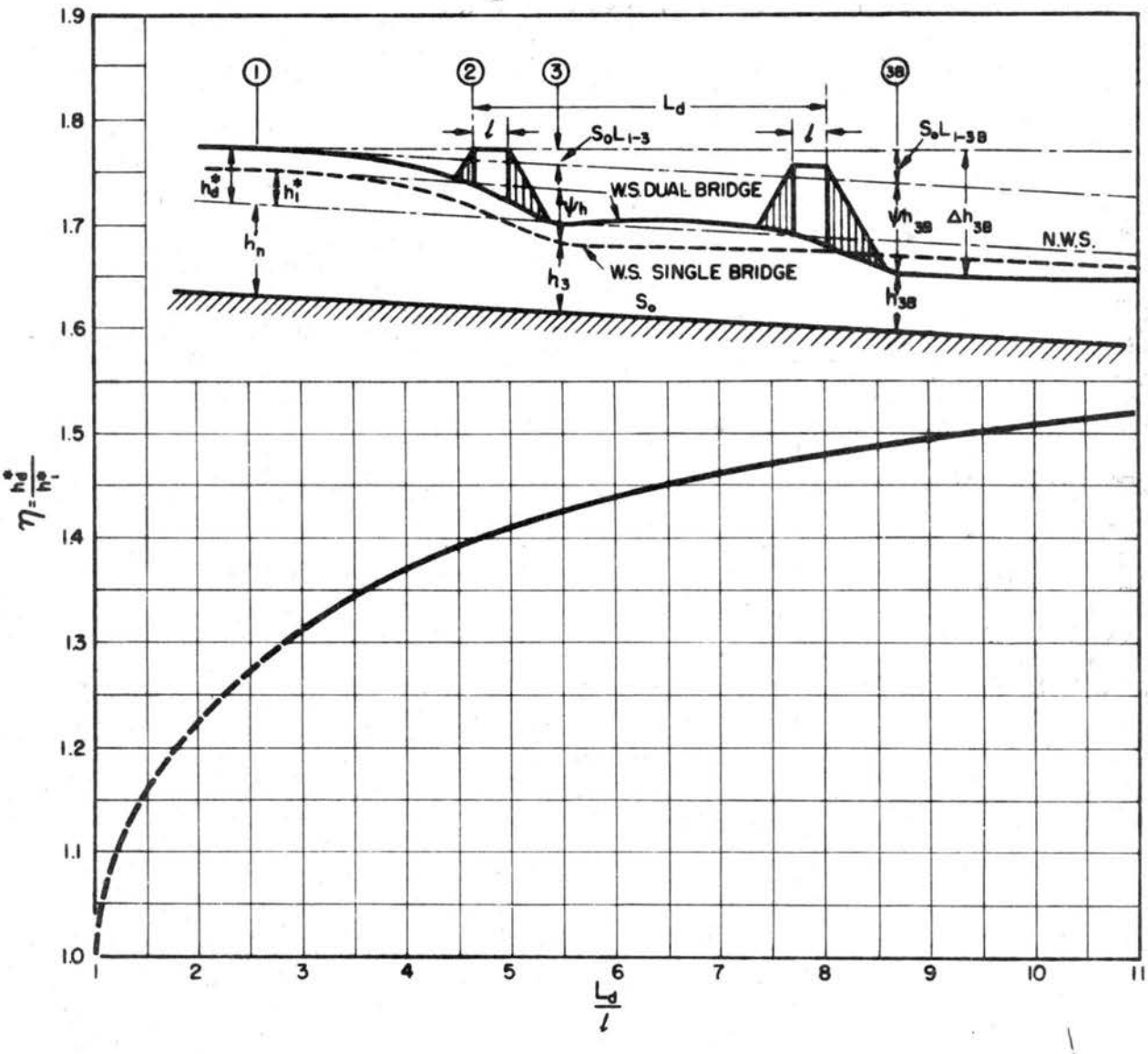

Fig. B.17 Backwater Multiplication Factor for Dual Bridges

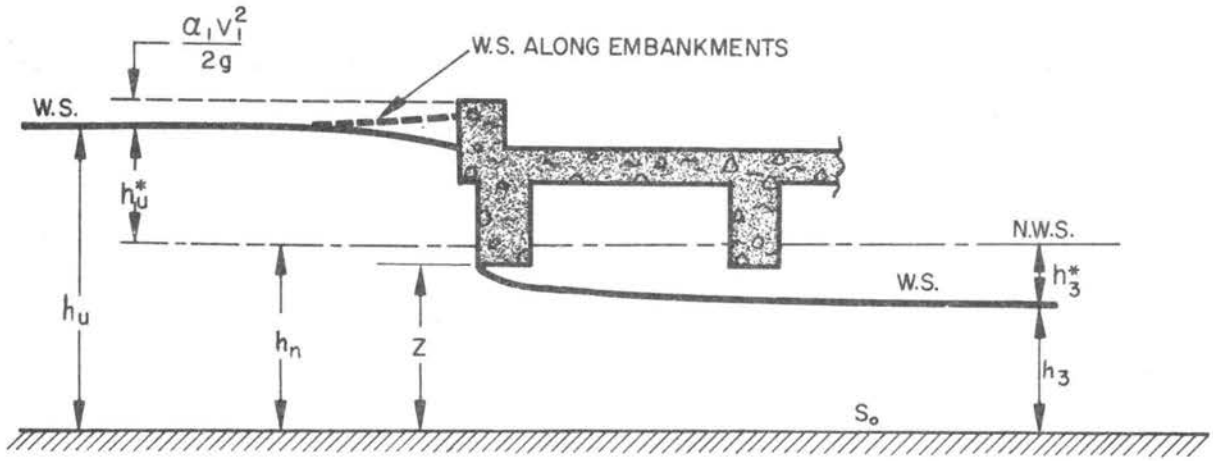

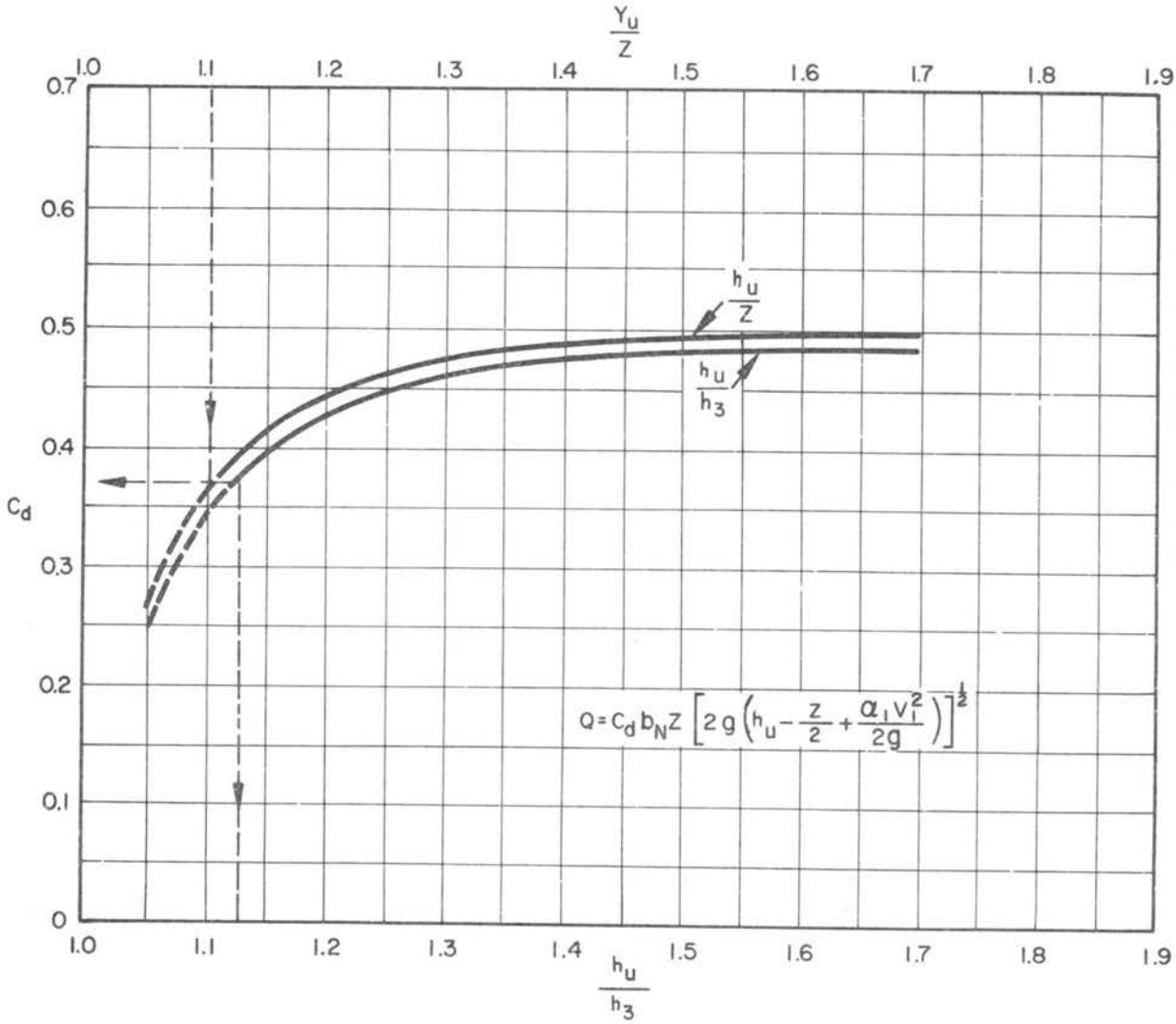

Fig. B.18 Discharge Coefficients for Upstream Girder in Flow (Case I)

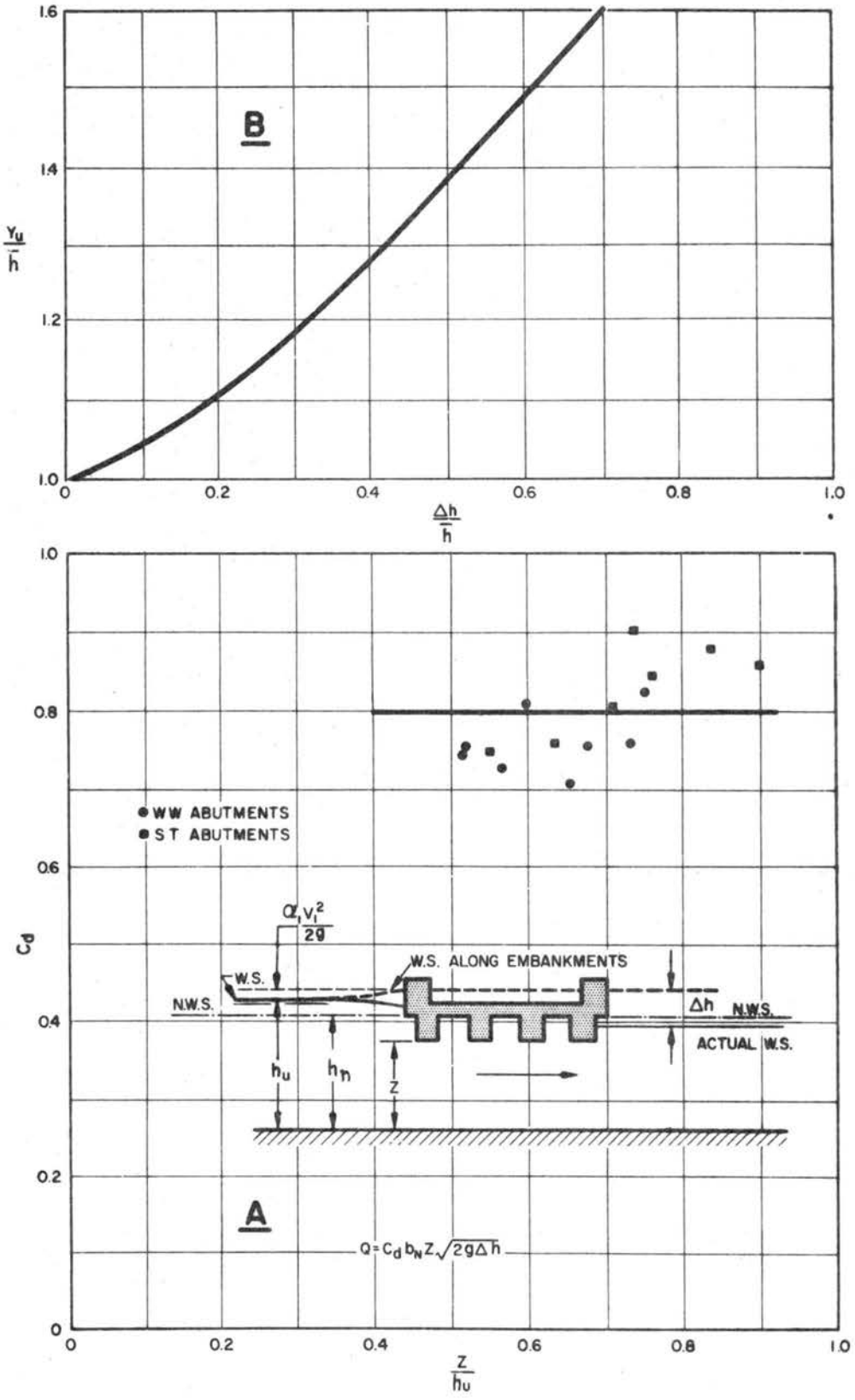

Fig. B.19 Discharge Coefficient for all Girders in Flow (Case II)